Upper limb prostheses control based on user's body compensations

Mathilde Legrand

Sorbonne Université

École doctorale n°391
Sciences Mécaniques Acoustiques Electroniques et Robotiques (SMAER)

Institut des Systèmes Intelligents et de Robotique – AGATHE

Upper limb prostheses control based on user's body compensations

Par Mathilde Legrand

Thèse de Doctorat de Robotique

Présentée et soutenue publiquement le 29/03/2021

Devant un jury composé de :

Véronique Marchand-Pauvert Directrice de Recherche, LIB (UMR 1146) Sorbonne Université	Présidente
Christine Chevallereau Directrice de Recherche, LS2N (UMR 6004) Université de Nantes	Rapportrice
Jean-Louis Vercher Directeur de Recherche, ISM (UMR 7287) Aix-Marseille Université	Rapporteur
Hélène Pillet Maître de Conférence, IBH Georges Charpak Ecole Nationale Supérieure des Arts et Métiers	Examinatrice
Antonio Bicchi Professeur, Research Center E. Piaggio Italian Institute of Technology	Examinateur
Christophe Huchet Membre affilié, ISIR (UMR7222) Sorbonne Université	Invité
Guillaume Morel Professeur, ISIR (UMR7222) Sorbonne Université	Directeur de thèse
Nathanaël Jarrassé Chargé de recherche, ISIR (UMR7222) Sorbonne Université	Co-encadrant de thèse

A Aurorou

Résumé étendu

Afin de redonner de la mobilité et une certaine autonomie aux personnes ayant subi une amputation, différents types de prothèses sont disponibles. En fonction de leurs besoins et de leurs projets de vie, les personnes amputées peuvent choisir entre des prothèses cosmétiques (complètement passives), des prothèses mécaniques (actionnées par des câbles) et des prothèses robotiques (actionnées par des moteurs). Ces dernières suscitent beaucoup d'intérêt : elles pourraient offrir une plus grande autonomie grâce aux nombreuses possibilités de mouvement qu'elles rendent possibles. Véritables bijoux technologiques, elles sont néanmoins limitées par le contrôle qu'en a l'utilisateur : capter l'intention motrice du porteur de prothèse pour actionner cette dernière est encore à ce jour un problème non entièrement résolu. Cette question du contrôle est particulièrement importante pour les prothèses de membre supérieure, qui ont de nombreux degrés de liberté disponibles. Plusieurs pistes ont été explorées pour y répondre mais aucune ne remporte une adhésion massive de la part des utilisateurs.
L'approche la plus répandue enregistre un signal auxiliaire, i.e. indépendant du mouvement du sujet nécessaire pour effectuer la tâche, qui code directement pour un mouvement de la prothèse. Le signal majoritairement utilisé est un signal musculaire (électromyogrammes, dans le contrôle myoélectrique); la contraction d'un muscle (ou d'un groupe de muscles) code pour le mouvement d'une articulation prothétique. Efficace pour un degré de liberté, cette technique est vite limitée lorsque le nombre d'articulations à contrôler augmente, car les muscles disponibles sont souvent peu nombreux. De plus, en séparant le mouvement de la prothèse de celui du sujet, elle crée une double tâche pour l'utilisateur (contrôler son mouvement et contrôler la prothèse), amplifiant la charge cognitive. Une deuxième approche propose d'éviter cette double tâche en prédisant le mouvement de la prothèse à partir du mouvement du membre résiduel du sujet, grâce aux synergies articulaires. Une fois modélisées, ces relations prédictibles entre le mouvement de différentes articulations permettent en effet de compléter le mouvement de l'utilisateur avec celui de sa prothèse. Il suffit au sujet d'initier le mouvement pour que la prothèse bouge en accord. Cependant, les synergies dépendent de la tâche. Pour donner un nombre suffisant de mouvements, essentiel à un minimum d'autonomie, un contrôle basé sur les synergies nécessiteraient donc une architecture d'algorithmes complexe, non exemptée de problèmes de précision, et inadaptée à la multiplicité des mouvements du membre supérieur.

Partant du constat que toutes les approches existantes sont en boucle ouverte pour la prothèse, i.e. qu'aucune étape dans le contrôle ne vérifie si le mouvement de l'appareil correspond à celui

souhaité par l'utilisateur, nous proposons dans cette thèse de construire un mode de contrôle en boucle fermée. Cela permettra de décharger l'utilisateur de l'attention permanente qu'il doit porter à la position de sa prothèse et de la correction éventuelle à apporter. Pour se faire, il est tout d'abord nécessaire de définir un signal d'erreur, qui ne peut être, dans un environnement domestique, ni sur la tâche ni sur la position de la main prothétique, toutes les deux inconnues *a priori*. Un message d'erreur accessible semble être celui que donne l'utilisateur par le biais des mouvements de compensations. Lorsque la position de la prothèse doit être corrigée, on remarque en effet que la personne amputée a tendance à faire appel à ses articulations fonctionnelles pour terminer le mouvement, plutôt qu'à envoyer un nouveau signal de contrôle. La correction est ainsi plus rapide et le mouvement plus fluide. Bien connues du corps médical, ces compensations sont souvent considérées comme devant être évitées car elles peuvent entraîner des troubles musculo-squelettiques. Le concept développé dans cette thèse est de détecter ces mouvements de compensation puis d'actionner la prothèse de sorte à les éliminer; un couplage cinématique est ainsi créé entre l'utilisateur et sa prothèse. Avec ce mode de contrôle, baptisé Contrôle par Suppression de Compensations (ou CCC pour Compensations Cancellation Control en anglais) le sujet humain est responsable de la bonne position de la main prothétique, pendant que la prothèse est responsable de la bonne posture de l'utilisateur. Il reste important de noter qu'un tel contrôle est applicable aux articulations intermédiaires (poignet, coude, épaule) mais pas à la main, puisque la saisie ne peut être compensée par aucune autre articulation.
De nombreux travaux ayant déjà caractérisé les mouvements compensatoires pour le poignet (pronosupination), il nous semblait tout d'abord nécessaire de complétér cette connaissance par la caractérisation des mouvements compensatoires pour le coude (flexion/extension), avant de pouvoir étudier CCC en détails. Une première preuve de concept a ensuite été réalisée pour le contrôle d'un poignet prothétique, avec des sujets sains portant un dispositif adapté puis avec des personnes amputées transradiales portant leur propre prothèse. Nous avons ainsi montré (i) que le couplage cinématique créé entre l'utilisateur et sa prothèse, via les mouvements compensatoires, permet de corriger ces derniers pendant que le sujet réalise une tâche; (ii) que CCC est indépendant de la tâche à accomplir, autorisant ainsi une grande possibilité d'utilisation.

Suite à ces premiers résultats encourageants, nous proposons une formulation générale de CCC, à partir de laquelle pourront être déclinés tous contrôles de prothèse de bras, quelque soit leur nombre d'articulations intermédiaires. Nous menons ensuite une étude théorique de CCC, afin de mieux analyser le couplage cinématique et de déterminer les valeurs des paramètres de la loi de contrôle nécessaires à l'établissement d'un système stable. L'humain étant particulièrement complexe à modéliser, nous avons choisi de considérer pour cette étude un système linéaire composé d'un robot proximal et d'un robot distal (contrôlé avec CCC à partir du robot proximal). Deux exemples développés en simulation permettent de confirmer l'intérêt du couplage tout en soulignant l'importance du réglage du gain de la loi de contrôle de CCC pour avoir un système stable. Cette observation est complétée par une étude de stabilité du système robotique considéré, aboutissant à

un critère sur le gain, qu'on veille à respecter par la suite.
Afin de valider les conclusions de l'étude théorique sur un système réel homme-prothèse, un ensemble de trois expériences complémentaires est mené, dans lequel CCC est implémenté pour contrôler un coude prothétique. Les deux premières expèriences sont réalisées avec des sujets sains portant une prothèse adaptée, la troisième avec une personne amputée transhumérale portant sa prothèse. Le premier volet valide le critère de stabilité sur le gain de la loi de contrôle avec un sujet; le deuxième vérifie que ce critère est indépendant de l'utilisateur et il analyse à quel point CCC peut être maîtrisé par ce dernier sans aucune connaissance sur son fonctionnement. Nous montrons ainsi que, puisque les mouvements de compensation sont une réaction naturelle du sujet humain à une mobilité réduite, les utiliser comme entrée du contrôleur de la prothèse permet une prise en main de CCC sans apprentissage particulier. Ceci est un bénéfice notable en comparaison des modes de contrôle avec un signal auxiliaire, et du contrôle myoélectrique en particulier, qui demandent jusqu'à plusieurs mois d'entraînement avant d'être maîtrisés. Le troisième volet valide ces conclusions avec une personne amputée.
De par sa formulation générique, CCC peut théoriquement être implémenté pour contrôler plusieurs degrés de liberté simultanément. La dernière expèrience présentée dans cette thèse, dans laquelle CCC est utilisé par une personne amputée transhumérale pour contrôler la pronosupination du poignet et la flexion/extension du coude, permet de confirmer cette affirmation. La charge cognitive mobilisée par CCC est également évaluée par la réalisation d'une double tâche de calcul et par un questionnaire. Pour le sujet participant à l'expèrience, cette charge n'est pas plus importante que celle demandée par un contrôle myoélectrique pour un seul degré de liberté.

Le travail effectué au cours de cette thèse pose les fondements d'un nouveau concept de contrôle pour les prothèses robotiques de membre supérieur. Celui-ci présente d'importants avantages : une prise en main facile, une formulation indépendante de la tâche et de l'utilisateur ou encore un contrôle simultané de plusieurs articulations. De nombreux aspects demandent maintenant à être approfondis pour s'approcher d'une implémentation réaliste au quotidien, comme la caractérisation de l'absence de mouvement compensatoire ou la possibilité d'utiliser uniquement des capteurs embarqués pour mesurer la posture du sujet. Enfin, ce schéma de contrôle semble être transposable à d'autres dispositifs robotiques de réhabilitation, tel que les exosquelettes ou les robots d'assistance, ouvrant ainsi de multiples perspectives d'application.

Abstract

In recent years, the development of advanced mechatronics for upper-limb prostheses has led to technological improvements such as a better fixation system to the body with osseointegration or a larger number of degrees of freedom. However, providing these devices with a natural and efficient control is still a major challenge.

Current approaches, such as myoelectric control, all show limitations, that can lead prosthetic users to abandon the active dimension of the device, use it as a rigid tool and perform the desired task with body compensations. To avoid such a behavior, we propose in this PhD thesis to employ body compensatory motions as an error signal to control the prosthetic device. With this concept, the human subject is in charge of the end-effector task, while the prosthesis is in charge of its users posture.

This proposition is implemented and tested to control prosthetic wrist and elbow joints, first individually and then simultaneously. A theoretical study completes this work and analyzes in details the human-robot coupling created. The presented experiments first confirm that using body compensations as controller input does not enhance them. They then show the easy learning of the control scheme by naive subjects, its task-versatility and its scalability. The foundations thus laid open exciting perspectives for a natural prosthesis control.

Acknowledgments

Vivre et travailler au même endroit pendant plus de trois ans fut un luxe que je n'avais pas eu depuis longtemps. Nombre de personnes sont venues peupler cette période, en y passant quelques mois ou en l'habitant de son début jusqu'à sa fin. Les quelques mots qui suivent sont là pour les remercier.

Il m'est impossible de ne pas commencer par mes deux encadrants, Guillaume et Nathanaël. Vous m'avez fait confiance avant même le début de ma thèse, en acceptant de déposer un dossier de bourse seulement 15 jours après mon arrivée à l'ISIR, puis tout au long de ces années, malgré (ou peut-être à cause de) mes questionnements fréquents et mes quelques entêtements. Guillaume, merci de croire autant en notre travail, cela m'a reboostée lors de mes baisses de motivation. Merci de nous avoir proposé d'ajouter une composante théorique à ma thèse, lui donnant ainsi de multiples facettes, ce qui m'a beaucoup plu ! Nat, merci pour ton investissement sans faille et ta disponibilité à toutes heures du jour et de la nuit. Merci d'avoir aussi joyeusement accepté que je parte en congé maternité 3 mois avant la fin présumée de ma thèse, ce qui témoigne de ta profonde humanité pour tes doctorants. N'oublie pas de prendre soin de toi !

Je remercie l'ensemble des membres du jury d'avoir pris le temps de relire avec tant d'attention les pages qui suivent, ainsi que pour les échanges que nous avons eus lors de ma soutenance. J'espère avoir un jour l'occasion de rencontrer en personne celle et ceux qui ont participé à distance.

J'adresse un merci tout spécial à Christophe Huchet, membre invité de ce jury, notre pilote du Cybathlon et testeur officiel de nos manips. Merci de nous avoir rejoints pour cette aventure du Cybathlon et surtout, merci d'être resté ensuite avec nous. Tes conseils et retours d'expérience ont été (et sont) extrêmement précieux. Ta patience et ta bonne humeur lors de nos essais m'ont aussi permis de dédramatiser ces séances expérimentales ... ! Je ne crois pas me tromper en disant que notre collaboration s'est peu à peu changée en amitié, dynamique souvent observée en équipe AGATHE.

En effet, qu'auraient été ces trois années de thèse sans la bonne ambiance de l'équipe ! Merci aux permanents: Ludo, MAV, Wael, Fabien, Jérôme, Agnès, Emmanuel, Nat et Guillaume, d'être les gardiens temporels de l'atmosphère si particulièrement agréable de l'équipe. Merci à ceux qui lui ont donné sa couleur non-permanente 2017-2021, mes collègues et compères doctorant(e)s et ingénieur(e)s : Eléonore, Clémence, Josh, Jimmy, Jésus, Félix, Etienne, Alexis, Delphine, Lucas. Vous avez chacun(e) apporté la touche unique de votre personnalité pour créer une petite tribu qu'on rejoint en chantant chaque matin. Les différents confinements et autres télétravaux ont fait ressortir, par contraste, le bonheur d'être avec vous. Je retiendrai longtemps les mots fléchés, les

footings aux Tuileries suivis d'un kebab, les repas de Noël et les petites bières aux Sciences, même si ma présence n'y était que ponctuelle. Ceux qui ne se sont pas vus cités jusqu'alors doivent savoir qu'ils ont une place un peu spéciale pour moi dans cette tribu. Tout d'abord, Etienne et Charlotte, sans qui ma thèse n'aurait pu avoir lieu, tant votre support technique mais aussi humain m'ont portée. Etienne, merci pour ton caractère si posé et pour l'ambiance cosy et musicale que tu donnais à ton repaire de la salle Agathe. J'avais toujours un refrain de Renaud qui me venait en tête en passant la porte, même bien après ton départ du labo. Charlotte, c'est toujours détendant de travailler avec toi, tu respires la quiétude. Mes bonjours banals de chaque matin cachaient un véritable plaisir à te retrouver. Merci d'avoir été mon bras droit pour mes manips et merci de nous avoir fait découvrir le Takenoko ! Restent les "Vieux", ou les "Sages" : Rémi, Omar, Mario, Angelina et Mégane. Un petit groupe bien hétéroclite mais tellement complémentaire ...! A la fois langues de vipère, peaux de vache, bisounours, adorables. Merci pour votre soutien sans faille les jours où je mettais ma capuche, pour les Skype puis Zoom pendant les différents épisodes de confinement, pour ces petites réunions au sommet en J08. J'ose espérer que nos chemins n'auront pas fait que se croiser.

Je tiens à remercier aussi toute l'équipe du Service Technique et Administratif de l'ISIR. En particulier Adela, qui a supporté nos nombreuses missions de dernière minute à Nancy; Awatef et Sylvie, qui m'ont rendu si simples toutes les démarches pour mon congé maternité et autres changements de contrat, merci pour votre accueil si chaleureux à chaque fois qu'on frappe à votre porte; Philippe qui m'a laissé emprunter tant de fois l'appareil photo; David pour ton expertise OptiTrack; Laurent pour ta bonne humeur permanente et les nombreux dispositifs expérimentaux que tu m'as construits et Flo, pour toutes ces heures patiemment passées à m'aider à débugger mon code et à faire fonctionner le proto.

Merci à toute l'équipe médicale de l'IRR de Nancy: Amélie, Isabelle, Marie-Agnès, le Dr Martinet, de nous avoir donné ces occasions de venir tester nos travaux avec vos patients; et merci à eux de s'être prêtés au jeu de nos manips, avec toujours beaucoup d'enthousiasme.

Vient désormais le temps de remercier mes amis et ma famille, pour leur soutien inconditionnel depuis toutes ces années. J'adresserais une pensée particulière à la bande des copaaaaains : Amaury, Gabriela, Léa, Quentin, Mathieu, Sophie, Romain, Sophie, Sylvain et Maxence. Ça a parfois été relou de vous entendre parler de recherche et de publis pendant des dîners censés nous détendre, mais je sais que ce n'est que l'expression de votre passion et, au fond, ça m'a inspiré... Merci aux basketteurs : Jérôme et Elsa, Luca et Francesca, Ruty, Marti, Emile et Camille. Des docteurs qui ne se prennent pas la tête, c'est bien ! Merci à Pauline et Guillaume, Laure, Hermine, Pauline, Pierrot, et tant d'autres, pour tous ces bons moments partagés pendant ces trois ans et qui ont participé à me rendre la vie douce. Vivement les prochains ! J'ose mettre enfin quelques mots pour remercier mes parents et mes frères et soeur, qui parviennent à me supporter encore. Je ne vous ai pas spontanément beaucoup parlé de mon travail, ce qui ne vous a pas empêché de sentir quand j'avais besoin que vous soyez à mes côtés, et d'y être, tout simplement.

Merci à tous ceux qui ont assisté à ma soutenance, devant leur écran, et qui se sont laissés

intéresser par cette thèse. Vous m'avez permis de partager mon travail, ce qui est tellement plus sympathique que de le garder pour soi !

Last but not least, mon William. Tu te doutes des lignes qui vont suivre mais il faudrait que tu puisses venir dans ma tête pour te rendre compte de la profondeur de ma pensée. Merci de m'avoir parfois poussée dans mes retranchements pour me permettre de donner le meilleur de moi-même dans cette thèse et de ne pas faire les choses qu'à moitié. Merci de croire en moi pour moi et de m'apprendre à voir le positif avant tout. Nous croyons en un même idéal, alors vivons-le !

Contents

List of Abbreviations

ASC	Auxiliary Signal Control.
BDM	Bayesian Decision Making.
CCC	Compensations Cancellation Control.
CI	Confidence Interval.
CNS	Central Nervous System.
COWAT	Controlled Oral Word Association Test.
DOF	Degrees of Freedom.
EEG	Electroencephalograms.
EMG	Electromyograms.
GMM	Gaussian Mixture Model.
GMR	Gaussian Mixture Regression.
IMU	Inertial Measurement Units.
IRR	Institut Régional de Réhabilitation.
LL	Lower-Limb.
MCC	Motion Completion Control.
MLP	Multi-Layer Perceptron.
OLC	Open-Loop Control.
PCA	Principal Components Analysis.
RBFN	Radial Basis Functions Network.
ROM	Range of Motion.
SVM	Support Vector Machine.
TMR	Targeted Muscle Reinnervation.
UL	Upper-Limb.

Chapter 1

Limb losses and amputation

Limb loss dramatically affects the quality of life, since it severely reduces one's autonomy. To help amputated people to recover some limb functionality, engineering – especially mechatronics and robotics – develops technical aids, which range from simple mechanical tools to advanced bionic replacement limbs.
This chapter briefly reviews the etiology and some important figures of Lower-Limb (LL) and Upper-Limb (UL) amputation, before focusing on UL prostheses equipment and issues, starting point of this research.

1.1 General information on amputation

To have a quantitative idea of number of people affected by a limb loss, they were almost 1.6 million in the US in 2005, and this number will more than double by 2050 [1]. Affected population and causes differ between LL and UL losses, and are detailed in this section. It is important to keep in mind that precise figures are difficult to obtain[1], which explains that most known studies rely on estimations and that some of them date from more than ten years.

1.1.1 Overview of amputations

Among the approximate 1.6 million people living with a limb loss in the US in 2005, around 65% underwent **LL amputation** ($\approx$ 1 million). In occidental countries, men are usually more affected than women, since the men-to-women ratio is 2:1 [2, 3]. The majority of affected people are 60 years and above, which can be explained by the fact that the first cause of LL loss is vascular diseases (more than 50% of LL amputations), especially diabete. The two main other causes are trauma and tumors [1–4]. Twelve different levels of LL amputation are identified [2, 5]: 4 for the foot, 1 for the ankle, transtibial, 2 around the knee, transfemoral (2 levels) and 2 for the hip (see Figure 1.1(a)). The three most common ones are toe disarticulation, transtibial and transfemoral [2, 3, 6].

UL loss is less common. It affected only an estimated 41.000 people in the US in 2005 [7], which approximately represents 14 UL amputees per 100.000 inhabitants. This is more or less the proportion in european countries since it was 11.6 per 100.000 inhabitants in Norway in 2010 [8]. Among them, 0.1% are congenital amputees (born without a limb) [9]. Like LL loss, men are more affected than women. On the contrary, the population mainly affected by UL loss is not the elderly but the young people (mean age between 20 and 36 years [8]), since the main cause is trauma (from occupational or traffic accidents). Other prevailing factors are cancer (especially for high-level amputations) and vascular diseases [6, 8, 9]. There are seven levels of UL amputation [5, 7]: partial amputation of the hand, disarticulation of hand and wrist, transradial amputation, disarticulation of the elbow, transhumeral amputation, disarticulation of the shoulder and forequarter amputation (see Figure 1.1(b)). Apart from partial amputation of the hand, the most common UL amputations

[1] This lack of data is mainly due to a limited follow-up of amputated people, who are little monitored by Healthcare systems once leaving hospital with their initial prosthetic prescription.

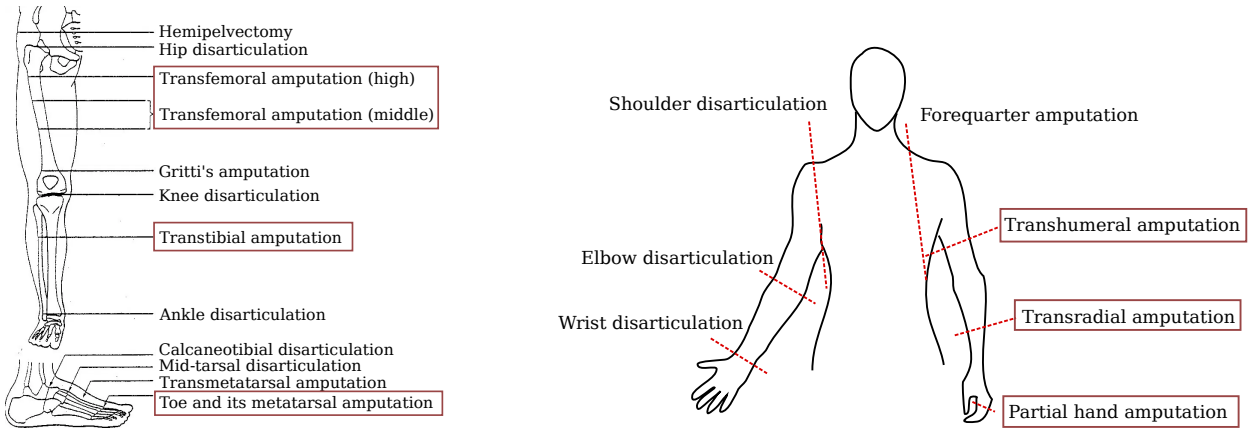

(a) The 12 levels of LL amputation (inspired from [5]).

(b) The 7 levels of UL amputation.

Figure 1.1: Levels of amputation for LL and UL losses; the most common ones are indicated with a brown rectangle

are transhumeral and transradial [7–10].
LL and UL losses are similar in their consequences on daily life: psychological aftereffects of the amputation, decrease of the quality of life and the autonomy, remaining pain, etc. [11]. They are thus sometimes gathered in what could be called the *amputation issue*. However, their etiology and the affected population differ, as well as the limb function lost. LL amputation affects walking functions, essential to be independent to move around, while UL amputation affects prehension abilities, which may be considered as a less severe impairment. This distinction greatly influences both how amputated people view the need for prosthesis wear and the research works related to either disability.
This PhD thesis focuses on upper limb amputation. The rest of the manuscript will therefore only detail this case and its dedicated prosthetic technology.

1.1.2 From amputation to prosthesis wear

Be it for LL or UL amputation, the path from surgery to homecoming follows the same stages [10, 12]. A pre-surgical step consists in deciding the level of amputation, usually together with the patient, depending on the medical situation, but also on his/her life plan [10, 12]. It can be decided to amputate at a higher level than necessary to allow the wear of a prosthesis. Once the surgical operation is performed, a period of healing and post-operative care is obviously required. This time is necessary for stump stabilization, muscle strenghtening (through exercise), pain management and also for psychological monitoring, to help the patient to conceive his/her life after the surgery. If the patient wants to wear a prosthesis, this post-operative phase is useful to prepare the stump for this purpose; the socket is molded at the end, when the stump is completely healed and its volume stable. All these surgical and recovery processes finish with rehabilitation: the patient works with occupational therapists to learn personnalized tricks to get back some autonomy, with or without the help of a prosthesis, and to adapt his/her home or work environment accordingly.
While it is hardly conceivable not to wear a LL prosthesis – because of the impossibility to stand without –, the **question of prosthesis wear** is much more discussed for the UL. Some amputated people deliberately choose not to wear one, from the beginning, while others abandon it because it does not suit them [10, 13–15]. For example, among the 486 UL amputees questioned in [13] and [14], there were 20% of abandon and 20% of non-wear. According to [15], 30 to 80% of all prosthesis users worldwide end rejecting their device. Device abandonment is not homogeneous among the UL amputated population; predisposing factors are the level of limb loss (abandon is more common for high-level amputees), the origin of limb absence (congenital amputees tend not to wear prostheses

compared to people with acquired limb absence) and the gender (female are more likely to reject their prosthesis) [13]. The causes of UL prosthesis rejection are thus diverse; they also depend on the type of device used.

1.2 Different types of upper-limb prostheses

UL prostheses are composed of two main parts: the physical interface between the user and the device, which can be a socket held by straps and/or harness or an implanted fixture (see Section 1.4.1 for more details), and the artificial limb, which can be more or less sophisticated. In the following, I will often use the term prosthesis to refer to the artifical limb only.
Three types of artifical limbs are available: motionless, body-powered and active. UL amputees commonly own at least two prostheses, generally of two different types, since their use can be complementary. The choice depends on the life plan and the needs of each person.

1.2.1 Motionless

Motionless is not traditionally employed in UL prosthesis terminology. I use it here to gather all prostheses that are rigid structures and have no joints to move; they can be cosmetic or functional. Cosmetic prostheses are gloves of silicon or PVC [16], put on to hide the limb absence (see Figure 1.2(a)). Their main purpose is esthetics but they can also be used as a tool to help the contralateral arm. In a questionnaire study performed in Norway in 2007-2008, cosmetic prostheses were chosen by 23% of users as their first device, and by 20% as alternative device [14]. Their rejection rate is high because of the discomfort (gloves easily cause sweating), the artifical appearance and the advent of active devices [7, 17]. The motionless but functional prostheses have an end-effector specifically designed to perform a given task, such as holder for cuttlery or universal holder (see Figure 1.2(b)) [18, 19]. They date back to the end of World War I and are more considered as tools; they are thus anecdotal and hardly considered in studies. However, motionless but functional prostheses are undergoing a renewal in sport, with an end-effector specifically designed to suit one activity [20].

(a) Examples of cosmetic UL prostheses (from [21]).

(b) Examples of functional but motionless prostheses (from [19]).

Figure 1.2: Examples of motionless UL prostheses

1.2.2 Body-powered

Body-powered prostheses were some of the first movable prostheses to exist [22]. Their joints can be moved: the end-effector can open and close, the wrist can rotate or the elbow can flex for instance. They are controlled with a system of cables and harness, tensioned via body motions (see Figure 1.3) [10, 18]. In the questionnaire study of [14], they represent 30% of the first device chosen by UL amputees and 28.6% of the alternative one.
Body-powered prostheses bring new opportunities with the possible activation of the joints. They are reported to be very reliable and give a good feedback on prosthetic joints positions, with the

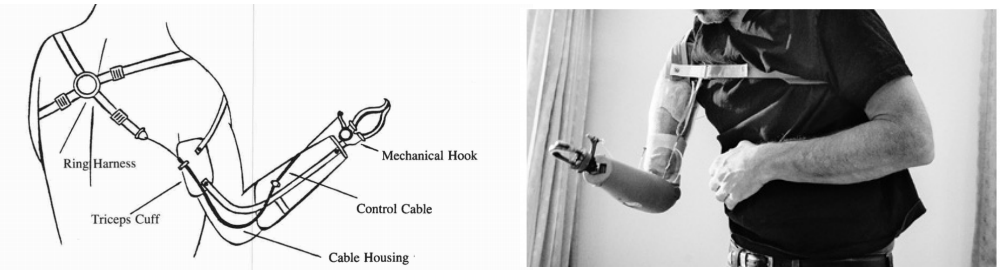

Figure 1.3: Example of body-powered prostheses (from [23] and [24]). Prosthetic joints can be moved by tensioning the cables with body motions

prosthetic forces applied back by the harness onto the body of users [13, 17, 25]. The harness yet quickly becomes uncomfortable and the user has to expend high energy to control the prosthetic joints with his/her body. Moreover, functions are restricted by the number of cables that can be actuated with body motions (the hand is often the only movable joint). Body-powered prostheses users also complain about the appearance of the device, not very esthetic with the apparent cables, and the abrasion of clothes it causes [7, 17, 25].

1.2.3 Active

In active (or externally-powered) prostheses, cables and harness are replaced by electric motors with an embedded power source; the assistive devices become true robotic tools (see Figure 1.4)[10, 18]. Motors can be controlled by different means as detailed in Chapter 2. While 34% of prosthesis users of the study in [14] select them as their first device, only 11.4% select them as their alternative one. Indeed, controlling these devices is not innate and they become worthwhile only when used regularly. Compared to body-powered prostheses, it is easier to grasp heavy objects, since the grasping force does not depend on body motions but on the motors that can be more powerful. The removal of the cables is also a great benefit [13, 17, 25]. Yet, three drawbacks still prevent a more extensive use of active prostheses: the weight of the devices, increased by the motors, their cost, which goes up due to the addition of electronic components and sensors, and the robustness of their control, which will be discussed in the next chapter.

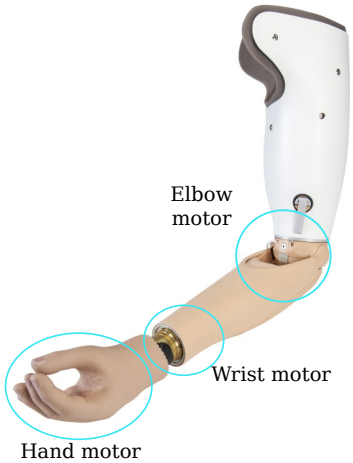

Figure 1.4: Example of active prosthesis (from [21]). Prosthetic joints are activated with electric motors

1.3 Different types of active upper-limb prostheses

Active devices have known considerable progresses since their emergence: they are more and more anthropomorphic, have more Degrees of Freedom (DOF) and have become absolute gem of technology with a well advanced mechatronics.

1.3.1 From tool to anthropomorphic prosthetic arm

(a) Examples of prosthetic hooks and grippers. From left to right: Hosmer 5A hook [26], RSL Steeper Carbon Gripper [19] and Ottobock Axon hook [21]

(b) Examples of human-like active devices. From left to right: body-powered Steeper VO Hand [19] and active Ottobock MyoFacil hand [21]

Figure 1.5: Towards anthropomorphic UL prostheses

For a long time, UL prostheses were considered as tools, with an utilitarian function only; the end-effector was thus a simple hook or a gripper (see Figure 1.5(a)). These kinds of devices are often associated to body-powered prostheses, that have limited DOF, but some are also offered as externally-powered devices (like the Axon hook and the Electric greifer from Ottobock [21]). Despite their simplicity, these kinds of tools are sometimes more adapted than more refined devices for what they are used for (e.g.,farming). The prosthesis-tool is also featured in recreational activities, where convenience and efficiency are more important than anthropomorphism [20]. The desire for a more natural appearance, which participates to a better integration of the prosthesis into users' body image [23], then led to the development of more human-like devices (see Figure 1.5(b)). The choice between function and esthetics now depends on individual needs [16]. Surprisingly, hiding the prosthesis under an anthropomorphic appearance (e.g., with a hand-like silicon glove) has become less common with the advent of fine robotic arms; more and more amputated people are proud of showing their cyborg limb.

Besides the esthetic goal, drawing inspiration from human limb is also a way to efficiently increase the number of feasible motions. Active devices indeed offer possibilities to go beyond the limit of one DOF of body-powered prostheses. For the hand for instance, the latter is often restricted to one grasp (power grip), whereas able-bodied subjects frequently use 3 or 4 different types of grasp [16, 29]. With the development of individually powered digits, some active prostheses can move fingers separately and thus perform multiple grasps (power grip, tripod, tip pinch, lateral grip, etc., see Figure 1.6(a)) [16, 30]. Users now have the choice between simple open/close hand (Speed Hand from Ottobock for instance) and individual mobile fingers (Michelangelo and BeBionic from Ottobock or I-limb Quantum and I-limb Ultra from Össur) [7]. Some of these devices are shown Figure 1.6(b).
The increase of active DOF is also visible on the other prosthetic joints: 2-DOF wrist (prono-supination and flexion) [31, 32], motorized elbow (like the Utah) [33, 34] and full mobile arm with powered shoulder, elbow and wrist [35, 36] are now available. Hardware for high level amputation (upper-arm and shoulder) yet remains little developed compared to the multitude of propositions for prosthetic end-effectors (hands or hooks). Only three prosthetic elbows are commercialized (Dynamic Arm from Ottobock, the Utah and LTI Boston, see Figure 1.7) and have not greatly evolved since the 1980s. As for whole arm devices, only the Luke Arm has been recently commercialized

(a) Four commonly used types of grasps (from [27])

(b) Examples of available hands, from simple open/close to individual mobile fingers. From left to right: Speed Hand, Michelangelo (from [21]) and I-limb Ultra (from [28])

Figure 1.6: Towards more mobile prosthetic hands

[37]; the other devices are still in development in research laboratories. The complex control of more than one DOF indeed limits the real use of active upper-arm devices, which can sometimes be more disabling than helpful.
Theoretically beneficial to prosthesis mobility and thus users' autonomy, a large number of DOF will not be practically worthwhile while the control and the device's weight will remain an issue.

Figure 1.7: Commercialized elbow prostheses. From left to right: Utah Arm (from [38]), Boston Arm (from [39]) and Dynamic Arm (from [21])

1.3.2 From rigid to compliant joints

The addition of motors to increase the number of DOF of UL prostheses increases also the weight of the device. To have a fine control of each finger, the user has to accept a more expensive and heavier device. For example, a Michelangelo hand (2 actuators) weighs 420g, whereas a BeBionic hand (5 actuators, one by finger) weighs 500g [7]. This difference is enough to be felt and to affect the user. For comparison, a human hand is around 400g, but it is even recommended that an artificial limb should be lighter than the human limb, because of the discomfort caused by suspension and the binding system [16, 40]. Moreover, a growing number of motors makes the prosthesis more rigid, whereas the human hand and arm are compliant; hitting a hard surface with a rigid device can indeed be painful and damage the device. An increasing number of works thus focus on designing more compliant or flexible prosthetic joints. A well-known example in the UL prosthetics community is the PISA/IIT SoftHand [41, 42], a compliant hand with an adaptive grip

(i.e. its fingers conform to the object's shape). Its actuation is inspired from muscular synergies and human tendons repartition and allows to move all digits with only one motor. In the same vein, some flexible wrists are developed, like the flexible AxonWrist from Ottobock and the ones proposed in [32] and [43].
Various active devices are thus proposed to UL amputees. It can be noticed that the advent of sophisticated prostheses has not evicted basic ones, which are reported to be as appreciated [25, 44]. Indeed, the offer must correspond to the needs of amputated people, which are diverse.

1.3.3 Towards democratization of active prostheses?

Figure 1.8: Examples of personnalized 3D-printed UL prostheses, from [40], body-powered (left) and esthetic (right)

As pointed out above, active UL prostheses are much more expensive than cosmetic or even body-powered devices, due to the associated mechatronics and electronics. When a cosmetic prosthesis costs between 3.000$ and 5.000$, a body-powered around 10.000$, active prostheses available on the market range from 20.000$ to 100.000$, depending on the amputation level and the included technology (number of motors, grasping sensors, etc.) [40, 45, 46]. To democratize the access to UL prostheses, a do-it-yourself community has grown, around 3D-printed devices [40, 47]. Besides a lower price (between 5$ and 500$ when the only cost is the material and maximum 3.000$ for an active prosthesis to be sold by a company), making or buying a 3D-printed prosthesis gives access to a community, and allows a wide freedom of design, leading to very personnalized prostheses (see Figure 1.8). 3D-printing is not employed only to build active devices but also cosmetic and body-powered since the price is well decreased for all. When actuated, the majority have two basic grasps available but some have adaptive grip, which allows more possibilities.
In spite of its attractive benefits, the following criticisms are addressed to 3D-printed prostheses [40]. As 3D-printing has a weak accuracy when shaping a device, there can be material shrinkage, which degrades the overall quality of the prostheses. As the mechanical properties of the devices are hard to predict correctly, it is also difficult to rely on their robustness and to know the force they can apply. Poor mechanical transmission also makes the actuation of 3D-printed prostheses complex. Note that, until now, these kinds of device have mainly been designed for hand and forearm amputation. They still require some improvements but open new perspectives for a broader and easier access to UL prostheses.

1.4 Current issues of active upper-limb prostheses

A large panel of active UL prostheses exists, from basic to more sophisticated. Even if weight and cost sometimes still raise problems, the mechatronics can now offer many motion possibilities, very close to the human arm. However, three key issues prevent a really convenient and effortless usage of these devices: socket, sensory feedback and control.

1.4.1 Socket

(a) Examples of traditional socket for transradial amputation (left, from [48]) and transhumeral amputation (right)

(b) Example of osseointegration for transhumeral amputation (from [48])

Figure 1.9: Interfacing human body and UL prostheses: traditional sockets and osseointegration

The socket is the binding system, i.e. the physical interface between the remaining limb and the prosthesis (see Figure 1.9(a)). It is actually crucial for comfort and for the integration of the device by the user. A prosthesis can be a perfect copy of the human arm, with a natural control, it would be useless if the socket was not appropriate.
Socket technology evolution has truly begun one century ago. First, improvement was realized on the design and the materials (from wood and leather to aluminium, laminates and now thermoplastic); then, through the specialization of the socket makers, the ortho-prosthetists, who became skilled experts [49]. Albeit valuable ameliorations, socket remains a persistent issue. It causes sweat, skin irritation and thus discomfort [50]; it restricts the range of motions of the remaining limb [49]; and the distribution of forces is not equally spread, which induces pain [49, 51, 52]. The existing socket techniques are also still inappropriate when the stump is short [53]. To improve comfort, some works propose adaptive sockets, that automatically adjust the distribution of internal forces, either with pressure-adjustable chambers [54] or with a soft robotic actuator driven by temperature changes [51]. Yet, none of them are advanced enough to be clinically used.
A noteworthy alternative to traditional socket is osseointegration, which allows a direct rigid fixation of the prosthesis on human body, without a socket, via implantation of a titanium fixture into the bone (see Figure 1.9(b)) [55]. Currently available for partial hand, transradial and transhumeral amputations, it removes the need for hand cover or harness and thus improves comfort. The arm motion amplitude is well increased because there is no thermoplastic cover blocking it. Osseointegration also allows some sensory feedback on prosthesis motion through osseoperception [55–57], and does not encounter problems if the stump is short, since there is no need for a socket to be fitted. It yet has to be cautiously considered: clinically approved less than ten years ago, studies about long term use and possible complications are still lacking. Indeed, choosing osseointegration is not mild; the fixing of the implant requires two surgery procedures and the integration of a foreign object into the human body.

1.4.2 Sensory feedback

Integration of the prosthesis by UL amputees can be enhanced by the physical interface but also by the feedback the device gives to the user. A significant difference between a human and a prosthetic arm is indeed the sensory feedback one gets from it. When human arm has the sense of touch – which informs about the shape of an object, its roughness, the temperature, the grip force, etc. – and proprioception – the ability to know self-movements and body position without vision –, prosthetic arm only transmits information through its mechanical components. To perceive the

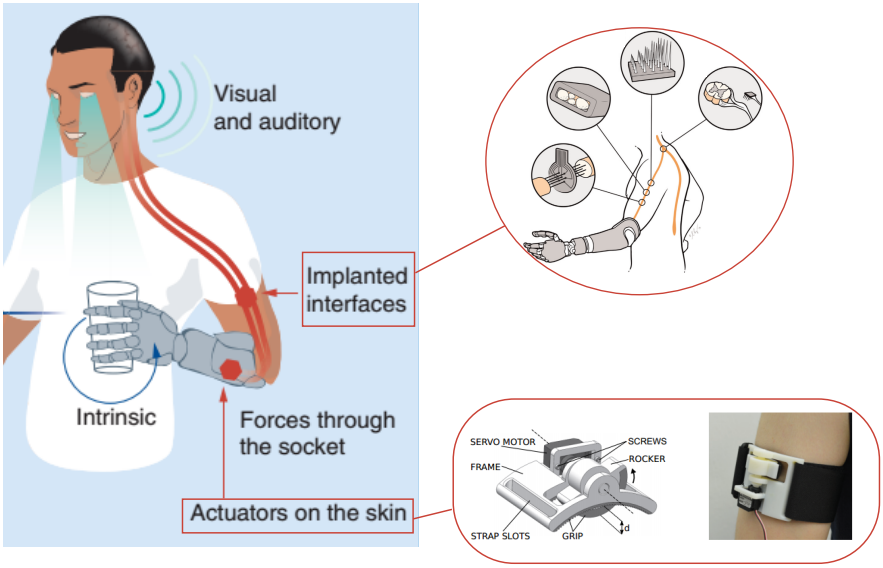

Figure 1.10: The different feedback information pathways (inspired from [58], [59] and [60]). In navy blue, the intrinsic feedback within the prosthesis; in light green, sensory information directly fed back to the Central Nervous System (CNS); in red, sensory information sent to the sensory motor system either invasively (examples of implanted electrodes) or noninvasively (example of skin stretch feedback)

surrounding in contact with their prosthesis, amputated people only rely on vision, sounds emitted by the device and socket pressure (or osseoperception). Research studies are thus conducted to develop prosthetic sensory feedback. Making the device *feeling* its surroundings is not that difficult with pressure, force or temperature sensors; the challenging part is to transmit these information to the wearer. Two alternatives exist: mimicking physiological sensory input or using sensory substitution (see [58] for a review). The first one aims at litterally repairing human and being as natural as possible, to avoid learning and cognitive charge. It communicates touch and position via electrical signals that directly stimulate the nerves, through implanted electrodes [61–63]. Yet, despite the use of natural pathways, this technique is not a straightforward sensory rehabilitation: nerves stimulation creates new feelings that have to be decrypted by the user and this decoding has to be learnt. As the signal to send to restore touch and proprioception is not known in advance, multiple trials can be required before finding the correct one [64]. The second alternative is easier to implement since it does not need any implant. Touch and position information from the prosthetic hand are transformed into vibrations, skin stretch or mechanical pressure performed on the user's skin (see [65] for a review). The latter has thus to learn a new language to interpret the signals sent by the device. Figure 1.10 shows an overview of the available sensory information a user can receive.
Although prosthetic sensory feedback could seem to be a great advance, its benefits are still being debated. While some promote it, arguing a real need, in particular to perform delicate grasping and to control slippage, and a better embodiment [66, 67], others draw attention on excessive amount of information given to users [53]. Explicit feedback (nerves stimulation or sensory substitution) may not be more efficient than implicit feedback (force applied on the stump, sounds of prosthesis' motors) to transmit touch and prosthesis position [68–70]. This could be subject to change with improvement of explicit feedback technology.

1.4.3 Control

The last important issue, and one of the main concern of UL amputees [13, 44], is the control of active prosthetic devices. While passive prostheses do not have any movable part (thus do not need any control interface) and while the DOF of body-powered are actuated through cables tensioned

with body motions, the control of externally-powered prostheses is not fully solved yet. Indeed, how to drive all their DOF in a simple, robust and natural way? How to collect, decode and transfer the motion intention of the user to the device? Transforming UL prostheses into limbs implies to find a way to properly control them, so that active devices have a real asset over body-powered ones. The main challenge of UL prostheses control is that arm motions are plentiful, difficult to predict from antecedent motions, and varying; they are thus hard to automatize, contrary to LL motions. The most widespread method is myoelectric control (with muscular signals), which can take different forms, but other techniques are also explored. Their functioning, pros and cons are described in-depth in the next chapter, since **UL prosthetic control is the area of interest of this PhD**.

1.5 Chapter summary

The loss of a limb highly modifies the autonomy and quality of life of affected people. In addition to surgery improvements, mechatronics, electronics and robotics have brought piece of solutions in more efficient prostheses design. In this chapter, after a quick insight into amputation problematics, be it for LL or UL, focus was made on UL prostheses, field this PhD falls within. The three available types of UL prostheses (passive, body-powered and active) were depicted, and the evolution of active devices were discussed in more details. Finally, the three major challenges that prevent externally-powered prostheses to be broadly used were discussed, including control which is the one tackled in this work. While many research studies focus on prosthetic hands, be it for more advanced devices or grasping control, I will focus here on intermediate joints for high amputation level (wrist and elbow), which are little covered in prosthetics research.

Chapter 2

Controlling an upper-limb prosthesis: trick or treat?

Among the main challenges to improve UL prosthetics – and thus amputated people's quality of life – , control is the focus of many studies and research works. Indeed, the benefits of active UL prostheses are annihilated if their user cannot properly control them.
In this chapter, existing control schemes, either available on commercialized prostheses or still under development in research laboratories, are described in detail, to allow a deep understanding of the prosthetic control challenge and of how the proposition of this PhD, exposed in Chapter 3, fits in. I chose to classify the existing control schemes into three categories, depending on the role they give to the user, and finally explain why none of them currently manage to meet amputees' expectations and what can be missing to build a robust and efficient UL prosthesis control.

2.1 Auxiliary Signal Control

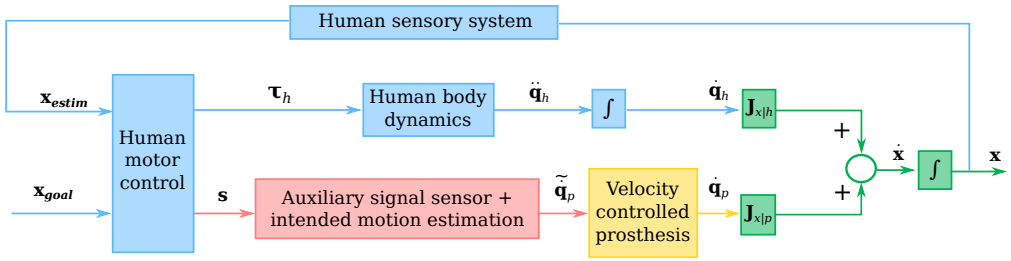

Figure 2.1: Auxiliary Signal Control scheme. x, x_{goal} and x_{estim} are the real end-effector position, the desired one and the one estimated by the human sensory system, respectively; $\dot{x}$ is the end-effector velocity. s is an auxiliary signal generated by the human, measured through a sensor. $\tilde{\dot{q}}_p$ and $\dot{q}_p$ are the command and the actual prosthesis joint velocity respectively. τ_h is the torque of the human joints (for simplicity, dynamic coupling between human body and prosthetic joints is not modeled). $\ddot{q}_h$ and $\dot{q}_h$ are the acceleration and velocity of the human joints respectively. $\mathbf{J}_{x|h}$ and $\mathbf{J}_{x|p}$ are the jacobian matrices of the human and the prosthesis part respectively

Before introducing the dominant approach, let us first consider the scheme presented on Figure 2.1 and detail how human user must adapt to prosthesis wear.
When performing a task with a prosthesis, the first important point to take into account is the **serial character of the human-and-device kinematics** (green path on Figure 2.1). Arm and hand motions of the prosthetic side indeed depend on both human and prosthesis movements. When the latter is passive ($\dot{q}_p = 0$), the end-effector motion is the result of human movement only (blue path on Figure 2.1); the prosthesis user compensates the acquired mobility loss with residual functional joints. S/he takes advantage of body redundancy – that makes possible the realization of a same task in different ways – and achieves the desired task with, e.g., trunk or shoulder, that substitute motionless wrist or elbow [8, 71, 72]. When the prosthesis is active, human and device

joint velocities add up and participate altogether to the end-effector motion:

$$\dot{\mathbf{x}} = \mathbf{J}_{x|h}\dot{\mathbf{q}}_h + \mathbf{J}_{x|p}\dot{\mathbf{q}}_p \tag{2.1}$$

with $\dot{\mathbf{x}}$ the end-effector velocity, $\dot{\mathbf{q}}_h$ and $\dot{\mathbf{q}}_p$ the human and prosthesis joint velocity vector respectively, $\mathbf{J}_{x|h}$ and $\mathbf{J}_{x|p}$ the jacobian matrices mapping the human and the prosthesis joint movements into end-effector movements. Upper-arm prostheses are mainly controlled in speed (yellow path on Figure 2.1), since it allows multiple prosthesis positions with binary signal inputs, easier precision and is less noisy than control in position [73–75].

To control the prosthesis joint velocities, the most widespread approach consists in creating a direct connection between an auxiliary signal, generated by the user, and the motion of the device (red path on Figure 2.1). Auxiliary means here that the generation of the signal does not naturally contribute to the intended task. Signals may be of various kinds but they are all independent of the control of user's healthy body motions required for the upper-limb task. **The control of the prosthesis and the control of human kinematics are totally decoupled.** Auxiliary Signal Control (ASC) approaches actually create a double task for the user: (i) controlling the prosthetic joints (red path on Figure 2.1) and (ii) controlling his/her functional joints (blue path on Figure 2.1). These approaches yet assume that, after a learning phase, the generation of the auxiliary signal becomes fully integrated into the user's motor control scheme, which is far from being obvious [76, 77].
Auxiliary signals currently in use and examples of connection between these generated signals and the prosthesis motions are detailed below.

2.1.1 Auxiliary signal with individual contractions of remaining muscles

Healthy motions are produced by muscle contractions. To control an UL prosthesis, it thus seems appropriate to exploit this natural source of information and link remaining muscle activity to prosthetic motions. In conventional myoelectric control, muscular activity is captured through Electromyograms (EMG), whose amplitude is extracted and used as input of the prosthetic controller. This approach was developped at the very beginning of active UL prostheses in the 1960s (see [78] for instance, or [77, 79] for a short review) and is still predominant nowadays.
Most of the time, EMG are measured with surface electrodes located on two antagonistic muscles [80], each controlling one of the two opposite motions of a same prosthetic DOF, such as hand opening and hand closing. This pair of muscles is typically composed of the wrist flexor and the wrist extensor for transradial amputees and the biceps and triceps for transhumeral amputees. Two control options can be considered: on/off and proportional [73, 80].
On/off control is a simple threshold detection: as soon as the EMG amplitude of one muscle exceeds a predefined threshold, the corresponding motion of the DOF is activated, with a constant velocity. For example, when the wrist flexor amplitude is higher than its threshold, the hand opens and when the wrist extensor amplitude exceeds its threshold, the hand closes, with the same speed whatever the level of contraction. **Proportional control** proposes a finer solution since, once the threshold is exceeded, the velocity of the prosthetic joint motion is proportional to the EMG amplitude. It allows to perform both slow and fast motions, depending on the tasks and situations. The speed of hand closing can thus be fast at the beginning and then slower to grasp objects cautiously. When there are more than one prosthetic DOF to control (which happens frequently in high UL amputation levels), the same pair of muscles is used for all of them. A finite state machine is thus required, with each DOF corresponding to a different state [81]. The DOF are individually controlled as explained above (with on/off or proportional law) and, to switch from one to another, the amputated user has to perform a co-contraction, i.e. to contract both muscles, higher than their thresholds, at the same time (see Figure 2.2(a)) [67, 80]. Sometimes, the amputation surgery outcomes do not allow to have access to two muscles but only one. In this case, on/off control with more than one threshold is implemented: the activated DOF and its motion depend on the level of

muscular activation [79, 80]. For instance, when the EMG amplitude is lower than all the thresholds, the prosthesis does not move; when the first threshold is exceeded, the hand closes and when the second is exceeded, the hand opens. The user must produce a contraction that stays into the range corresponding to the desired motion (see Figure 2.2(b)). To add more controllable motions or DOF, more thresholds should be defined. However, the number of thresholds reasonably manageable by the user, and thus the number of prosthesis functions, is limited to two according to [82].

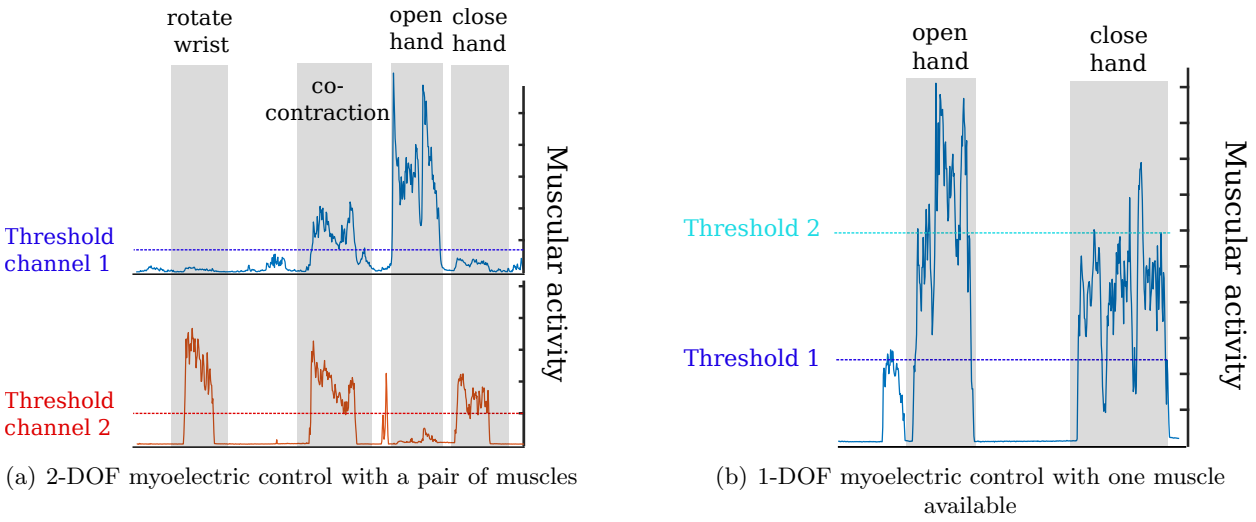

(a) 2-DOF myoelectric control with a pair of muscles

(b) 1-DOF myoelectric control with one muscle available

Figure 2.2: Illustration of on/off myoelectric control (with EMG signals recorded during our experiments in the lab)

If conventional myoelectric control remains the most common approach for active UL prostheses, it is mainly due to its **robustness** and its easy functioning: the user contracts his/her muscle, the prosthesis moves as expected. The implementation is also straightforward as there is no surgery required and the electrodes are placed once and for all in the socket of the subject. Its natural character is also claimed for transradial amputees since the employed muscles (wrist flexor and extensor) are the ones that are responsible for wrist and some hand motions in able-bodied subjects [80]. For transhumeral amputees, though, biceps and triceps are not naturally linked to wrist and hand motions, which removes this benefit. Moreover, as soon as there is more than one DOF to control, it quickly becomes a burden to perform a motion because of the co-contraction switching between joints, which is cumbersome and creates a slow and sequential global prosthetic movement [77, 79, 80].
Conventional myoelectric approach is, indeed, easy to understand but not as easy to handle. Individual muscle contractions are not natural nor intuitive, in the sense that a **long and heavy training** of several months is necessary to master the prosthesis control [12, 80], training that can be a factor of device abandonment [13, 79]. The robustness is earned with great efforts. The permanent use of only two muscles also leads to muscular fatigue, which affects muscle activity and make more difficult to reach the defined thresholds [76]. Eventually, EMG signals depend on the skin impedance, which is modified by sweat (generated by the socket), and on electrodes placement with respect to the considered muscles (even if the electrodes are placed once and for all in the socket, the positioning of the socket relatively to the stump can vary). These dependances can alter the signals and modify the benchmarks of the user [76].

2.1.2 Auxiliary signal with electromyograms: recent evolutions

To increase the natural character of more-than-one-DOF control and remove the need for co-contraction switching, pattern recognition-based methods are proposed. They rely on the observation that each natural motion is characterized by a specific activation pattern of the muscles

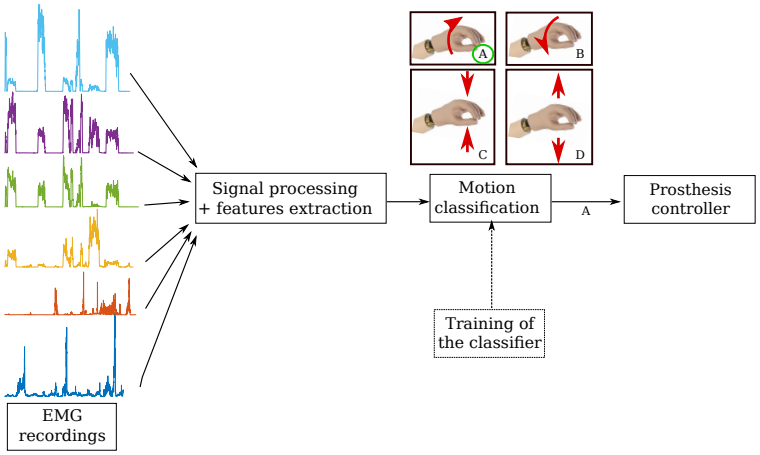

(a) Classification

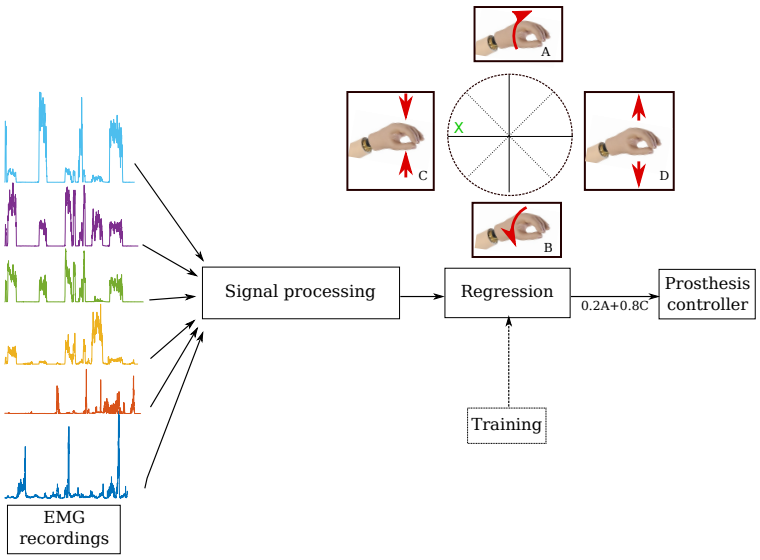

(b) Regression

Figure 2.3: Illustration of pattern recognition-based myoelectric control functioning. (a) Classification algorithms interpret time and frequency EMG features to send a motion class to the prosthesis. (b) Regression algorithms take continuous muscular signal as input and send a weighted combination of motion to the prosthesis

involved. Machine learning algorithms are developed to recognize these patterns from EMG measurements of amputees' remaining muscles and identify the corresponding intended motion. This motion is then performed by the prosthesis [80, 81]. Two main types of algorithms are employed: classification [83, 84] (see also [80, 81] for a review) and regression [73, 85, 86] (see Figure 2.3).
Classification generally differentiates the patterns with time and frequency features of EMG, such as mean, variance or zero crossings, while **regression** takes continuous signals as input, such as the EMG envelopes. Both techniques are supervised, meaning that the algorithms need to be trained before being used in real time, in order to know which pattern is associated to which motion. This training can be performed with data from movements of the sound limb or from phantom movements with bilateral mirroring [73, 85]. The algorithms can thus only recognize the motions they were trained for. The number of motions that can be identified is limited, for two main reasons: a high number (i) leads to a complex and less robust algorithm and (ii) requires more EMG information and thus more recording sites (i.e. more electrodes). Depending on the number of motions to identify, it requires from 4 [87] to 16 [80] electrodes, which applies only if the subject has enough residual functional muscles. This is often a problem for transhumeral amputees, who can then be

proposed Targeted Muscle Reinnervation (TMR), a surgery that reroutes the nerves of arm muscles to the chest, which can increase the number of recording sites [88, 89] (see Figure 2.4). This asks for a heavy surgical operation though.

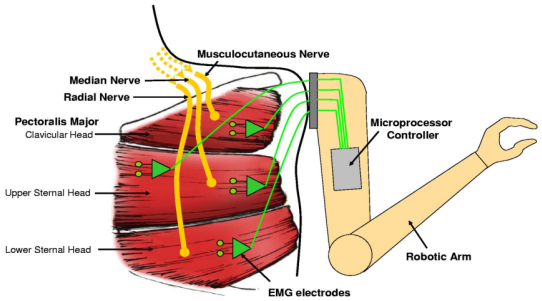

Figure 2.4: Illustration of TMR for prosthetic control in high-level amputation [89]

Besides the removal of inter-DOF switching, pattern recognition-based approaches allow for a **more natural control** since the user does not have to learn to contract his/her muscles individually. Indeed, it is the natural muscular activity, generated by the user when s/he intends to perform a motion, that is considered. Moreover, simultaneous motions of different prosthetic DOF can be performed: with regression, since it allows a combination of the movements used for training [85, 86], but also with classification, if a 2-DOF motion class is defined [90, 91]. Pattern recognition thus seems more appropriate for UL prosthetic control. However, even if this approach has been explored since the 1960s (see [84, 92] for instance), it was lately commercialized and in two devices only (MyoPlus from Ottobock [21] and CoApt [93]). This is due to many shortcomings that are not solved yet, such as identification of an efficient electrodes placement or good accuracy of the classification algorithms.
Indeed, in addition to the increase of required recording sites and the limited number of recognized motions, a major issue is the **low robustness** of the algorithms. Muscular activation patterns depend on many factors, such as limb position, electrodes placement and muscular fatigue [15, 67], that vary in everyday life, while algorithm training is often performed with EMG data recorded in static conditions. The robustness is also altered by muscle redundancy, the fact that one movement can be obtained with numerous muscle contraction patterns. Moreover, lots of works analyze the performance of the algorithms with classification accuracy whereas a proper accuracy does not necessarily go hand in hand with a good prosthesis usability [77, 94, 95]. The variation of EMG across time and subjects is rarely taken into account during algorithms evaluation. Pattern recognition developments **lack clinical studies**, where the conditions are closer to the daily-life ones with non-ideal muscle contractions, possible fatigue of the subject and electrodes repositioning [67].

Algorithms optimization and sensor fusion
To face this question of robustness, a lot of work is being done to optimize the algorithms and gain a few percent accuracy: from Linear Discriminant Analysis to Multi-Layer Perceptron, via Artificial Neural Networks, fuzzy logic or evidence accumulation (see [81] for an extensive review). Some algorithms are also built to be robust to limb position or electrodes shift, or to be easily adapted to individual subjects, in particular with deep-learning methods [96–98]. Hybrid approaches are also becoming more and more popular. Myoelectric signals have been combined with kinematics data –obtained with Inertial Measurement Units (IMU) [87, 99–101], goniometers [102] or motion capture systems [103]–, with vision [104] or with Electroencephalograms (EEG) [105], in order to decrease the number of required electrodes while improving the accuracy (see [106] for a review on hybrid myoelectric control systems). Yet, too many of these works are still offline studies or realized in the monitored environment of the labs. In this race for a few percent optimization, the ***hot coffee problem*** (as named in [81]) may be raised: if an algorithm succeeds in 99% of the cases, but the time when it fails causes the slipping of a hot coffee cup (or another annoying disaster), will

this high accuracy be considered as satisfactory? Or will prosthesis users find the slightest error of motion recognition unacceptable and abandon their device? If so, can 100% accuracy be reached, whatever the techniques and the data combination?

Beyond surface EMG
In parallel to algorithm optimization, complementary works are performed on the muscular signals employed. Indeed, EMG recorded with surface electrodes are of low quality: the resulting signal largely depends on skin impedance (that varies across time and subjects), on electrodes shift, muscular fatigue, sweat, etc. and crosstalks (interference between the measures) are common when electrodes are too close [15, 77, 95]. To improve the capture of motion intention through muscular activity, other characteristic signals and other recording techniques are explored:

- implanted electrodes [18, 107], an invasive solution to measure EMG without the skin impedance or electrode shift issues;
- sonomyography, which measures the actual movement of the muscles with ultrasound (see [15, 66, 80] for brief reviews), but the current instrumentation cannot be integrated in a prosthesis;
- myokinemetry, which detects the displacement of the superficial tendons and muscle bulge, induced by muscle contractions [15, 73, 108]. This measure can be obtained with pressure differential [109] or Hall effect [110]. There is no clinical outcomes yet;
- myokinesy, or force myography, which measures the change of pressure distribution produced at the skin surface by the muscle contraction [111–113];
- and mechanomyography, which measures the vibrations generated at the skin surface by muscle fibers activation, with accelerometers or microphones [114–116].

However, none have proven to be efficient and pratical enough to really supplant surface EMG for a daily application.

2.1.3 Non-muscular auxiliary signals

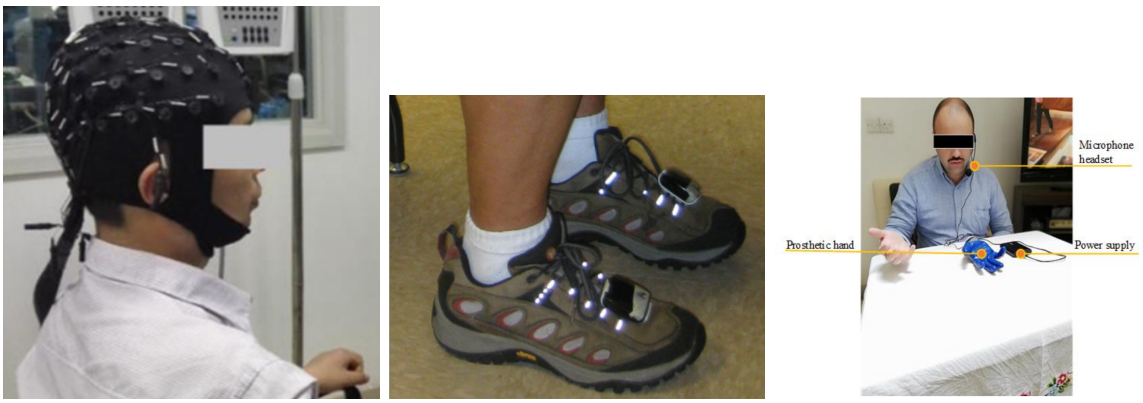

(a) EEG, from [105] (b) Joint-to-joint, from [36]. (c) Speech recognition, from [117]

Figure 2.5: Examples of auxiliary signal other than EMG. (a) EEG, recorded with surface electrodes. (b) Joint-to-joint linkage, with foot motions recorded with an IMU on the shoe. (c) Speech recognition, with the voice recorded by a microphone

Muscular signals, and surface EMG in particular, are by far the most employed and studied auxiliary signal in the search for improvement of UL prostheses control, despite the previously mentioned drawbacks. Some works are still looking for another signal, independent from the user's own motion, that could be a transmitter of the movement intention and control UL prostheses.

We can first cite **EEG**, which have been employed alone [118–121] or combined with other data, like EMG or eye-tracking [105, 122]. The use of EEG was brought about by the same reasoning as EMG: in the natural process of movement generation, the main contributors are the brain, that sends the command, and the muscles, that execute it. With EEG, the idea is to go to the source and directly use brain activity to detect the motion intention; it would allow a natural and very intuitive control, the prosthesis would move only by *thinking* to the desired motions. Theoretically, this is flawless but again, signal recording and processing in real life are not that plain. Existing methods only allow to decode very simple cerebral states, which imposes a discrete prosthetic control with few motion states. Moreover, the redundancy issue is greater than with muscles, since there are many ways to generate a "thought". Accessing EEG is also cumbersome for the user, since s/he has to permanently wear a headset with many electrodes (see Figure 2.5(a)) or to accept to be implanted with intracranial electrodes. This solution thus still requires sensoring and signal processing developments to be more appropriate.
Another explored solution is **joint-to-joint** control, where a linkage is created between an healthy joint, that does not take part in the arm motions, and the prosthetic joints. For instance, the foot motions have been linked to elbow, wrist or hand motions in [36] and [123] (see Figure 2.5(b)). We can also imagine to link the head motions with the prosthesis ones, as proposed in [124] with a robot arm for tetraplegic people. Two drawbacks limit this approach: the need for learning (nobody is used to coordinate feet and arm motions to reach or grasp an object), and the linkage itself that prevents independent motions of the healthy joint. This last issue can be avoided by adding a switch that turns on and off the direct connection between functional and prosthetic joint motions, but this reduces the movement fluency.
Incidentally, **speech recognition** has been tested for UL prostheses control in [117] (coupled with foot linkage). This could be relevant in a very quiet place but it is quickly limited in a noisy environment. More importantly, using voice commands to move the prosthesis not only leads to a high delay between the motion intention of the user and the realization by the prosthesis, but also increases the cognitive load required from the user.

The sub-optimality of Auxiliary Signal Control approaches

Whatever the auxiliary signal and the algorithms exploited, every ASC approaches follow the scheme of Figure 2.1: the user is entirely in charge of the prosthetic control and transmits his/her motion intention via the auxiliary signal. This signal generally codes for one joint motion at a time, except with some pattern recognition algorithms.
ASC approaches create a double task for the user: (i) generating the auxiliary signal, independent of the human arm kinematics, and (ii) moving his/her functional joints. This disconnection between the signal generation and the body kinematics of the user tends to forget the yet obvious fact that the motion of the human-prosthesis system is the result of the combination of both human and device kinematics (as expressed in Equation 2.1). To perform an efficient motion with such a human-robot combination, the two participating kinematics must be equally easy to control. Yet, as controlling prosthetic motions with the previously described techniques is much slower and cumbersome than controlling one's proper body motions, and because the redundancy of the human-prosthesis system often gives the user the possibility to perform a desired task with his/her own functional joints only, human kinematics tends to be preferentially employed at the detriment of prosthetic one. Indeed, as the CNS is known to adopt a slacking behaviour – it continuously attempts to reduce efforts – [125], prosthesis users will choose the easiest and fastest way and perform the intented task with his/her body only. The device motion possiblities are thus often neglected, while the prosthesis, albeit motorized, is used as a rigid tool. When the task is not feasible with human joints only, robotic DOF are mobilized by the user but, in that case, an asynchronous

sequence is often observed: a joint-by-joint reconfiguration of the prosthesis, followed by a mobilization of human joints inducing postural compensatory motions [126, 127].

2.2 Partially automatic control

To ease and speed up the control of the prosthesis and unburden the user, some works propose to partly automate joint motions: the amputee does not have to send an individual signal for every prosthetic joints. Both alternatives presented below are also classified as ASC approaches, since a signal, parallel to the human kinematics, must be generated. The control of the prosthesis is yet facilitated, thanks to the partial automation, which reduces the double task signal generation + human kinematics.

2.2.1 Eye-tracking

It is very rare to reach and grasp an object without looking at it. Moreover, the size and the shape of the object condition the orientation of the hand and the type of grasping. Eye-tracking thus proposes to collect all these visual information to automatize part of the UL prosthesis control. Thanks to cameras that follow the prosthesis user eye motions, the object s/he is looking at, its shape and its position in 3D space can be identified and the appropriate prosthesis motion computed. The cameras can be in-hand or worn by the subject on glasses (see Figure 2.6). This technique has particularly been explored for automatic grasping [128–130] and semi-automatic [131] or fully automatic hand orientation [132–134]. The other prosthetic joints motions and the possible corrections of eye-tracking algorithms errors are the responsibility of the user.
Eye-tracking solutions have only recently been studied thanks to progress on sensors and vision recognition algorithms. Now, they are still not very effective, especially to measure the vision depth [135]. When these sensors and algorithms will be fully capable, the benefits of eye-tracking-based control will have to be balanced against the discomfort of permanently wearing cameras-mounted glasses or the inconvenience to have in-hand cameras, and against the effort to lock one's gaze on the target before it is finally reached.

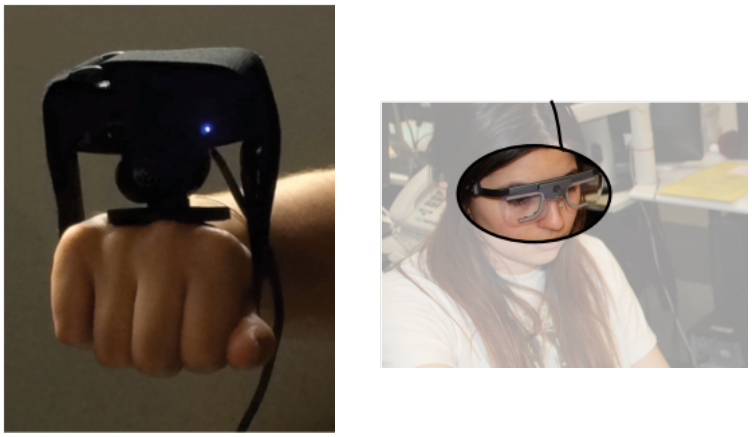

Figure 2.6: Examples of in-hand camera, from [134] (left) and cameras on glasses, from [104] (right)

2.2.2 Endpoint control

In healthy subjects, the coordination of joints is learnt in such a way that it becomes natural and unconscious. Subjects focus on their hand position or motion rather than on the movement of their individual joints. With a robotic device, it seems impossible to learn and control such

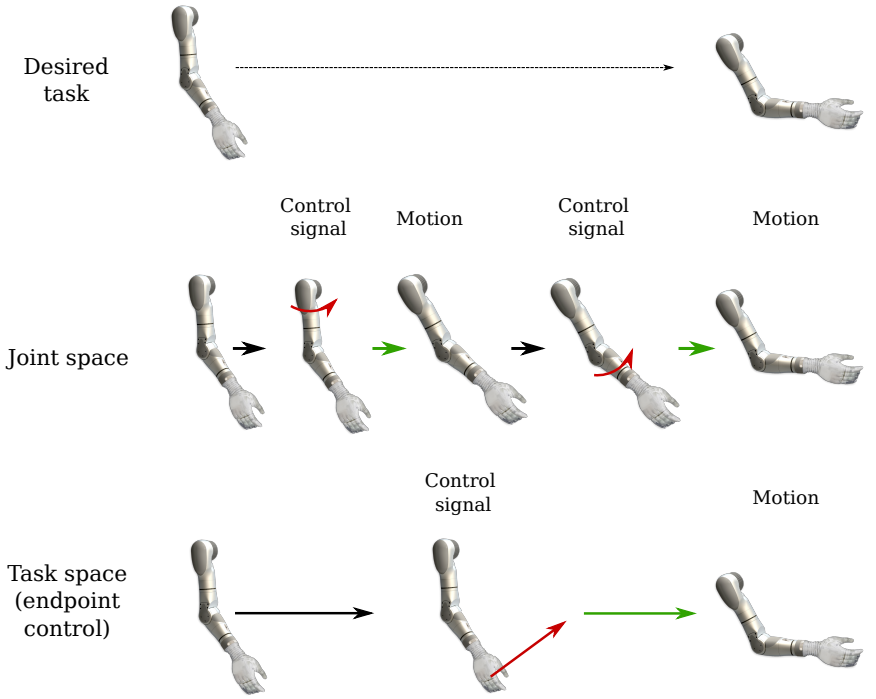

Figure 2.7: Illustration and comparison of joint control and endpoint control approaches

coordinations by using joint control auxiliary inputs. For this reason, researchers have proposed to rather use endpoint control inputs (see Figure 2.7).
This proposition has been formulated for a long time [136] but is not as simple to achieve. To control a robotic system in task-space (endpoint control), inverse kinematics of the system is used to compute the motions of each joint that allow to realize the desired end-effector motion (displacement and orientation). For a human-prosthesis system, the end-effector (i.e. the prosthetic hand) motion is a combination of human and prosthesis motions. The inverse kinematics of the system can be known, appropriate joint motions computed, the prosthetic joints can be moved according to this computation but it is impossible to be sure that the human will also move his/her joints accordingly. If the human motion does not correspond to the computation with inverse kinematics, the prosthesis command is useless since the state of the system has changed. That's why endpoint control has been developed only for entire prosthetic arm, with active shoulder, elbow, wrist and hand [36, 137–139], when there is no human joints in the motion loop. Moreover, this approach aims to generate human-like motions with a redundant system, which is an inverse kinematics problem with an infinite number of solutions.
With endpoint control, the user has to focus on the position and orientation of the hand only and does not have to decompose the end-effector movement into intermediate joint sub-motions. This is directly performed by the prosthesis controller, which reduces a lot the cognitive charge. By nature, endpoint also allows simultaneous motions of prosthetic joints, which is a property highly desired by amputated people [7].
To control the end-effector, several propositions of inputs have been made:

- with a joystick in the contralateral hand [137]. Very few studies exist, since constraining the functional arm is not convenient at all in everyday life;
- with a joystick on the shoulder stump [138];
- with a joystick activated by a healthy limb that does not take part in the arm motion, like the foot [36];
- with eye-tracking that gives the 3D position and orientation of the object to reach and thus the corresponding position and orientation of the hand [139] (preliminary study).

Endpoint control has thus many benefits but is limited to shoulder disarticulation prostheses.

A limited enthusiasm for (partial) automatic control approaches

Eye-tracking and endpoint control are ASC approaches that both aims at reducing the double task between prosthesis control and human body motion. They bring new perspectives for an easier UL prosthesis command, by automating some prosthetic motions. Compared to the previous approaches presented in Section 2.1, for which the user is in charge of every individual joint motions, they reduce the user's burden by reducing the dimension of his/her control space: either the hand or the intermediate joint motions are automatized. They are inspired by the natural human motor control: eye-tracking considers the gaze, signal embedded into the natural realization of the task, and endpoint control lets the user focusing on the end-effector only. However, these prosthesis control schemes are still constraining, either because the user has to fix the gaze on the object s/he wants to grasp, or because s/he has to control a joystick with movements unrelated to the prosthesis desired motion. Gaze jumps and approximate arm models can also be source of errors, whose correction has to be performed by the user. Last, it can be beneficial for some tasks to have a separate control of individual joints – in particular when the computed prosthetic motion is not achievable because of environment constraints –, which is not possible with (partial) automatic approaches.

2.3 Motion Completion Control

In the search towards a more appropriate UL prosthesis control, some approaches propose to unburden the user by taking his/her natural body motion as source of information, which removes the double task present in ASC.
Contrary to EMG- and EEG-based schemes which collect the motion intention signals from the root, Motion Completion Control (MCC) opts for considering the last level in the motion chain, claiming, among others, for a simpler signal acquisition and processing. Note that, except for partial hand amputation, it is exclusively applied to the control of the intermediate prosthetic joints (i.e. shoulder, elbow, wrist). As reaching and grasping are two very different tasks, MCC approaches chose to separate the two; they control the intermediate joints but keep myoelectric control for grasping. Indeed, while reaching results from a combination of the intermediate joint motions, grasping results from the hand motions only, and is rarely related to the other joints.
MCC has emerged in the last decades, in order to bring solutions to some significant shortcomings of ASC approaches (in particular those using EMG). Besides a less problematic signal acquisition and processing, it removes the need for an auxiliary signal which does not contribute effectively to the task; the **input of the prosthetic controller is now the healthy body motions, naturally generated to realize the task**. Figure 2.8 shows the corresponding block diagram: it is clear that there is no double task, the prosthesis motion is directly infered from its user natural motion. Moreover, while it is difficult for a person to know which muscle or which cerebral area s/he is exactly activating, or where s/he is precisely looking at, proprioception allows a perfect knowledge of the motions performed. Mastering the prosthesis control is thus straightforward. To link the prosthesis and its wearer motions appropriately, the main approach uses healthy joint motions with models of joint synergies (detailed in the next Section). Some studies also employ residual bone motions: in [140], wrist pronosupination for transradial osseointegrated amputees is deduced from the percutaneous portions of the implants, while in [141], Li et al. propose to deduce arm rotation from the humerus motion, with a magnet implanted into the bone.

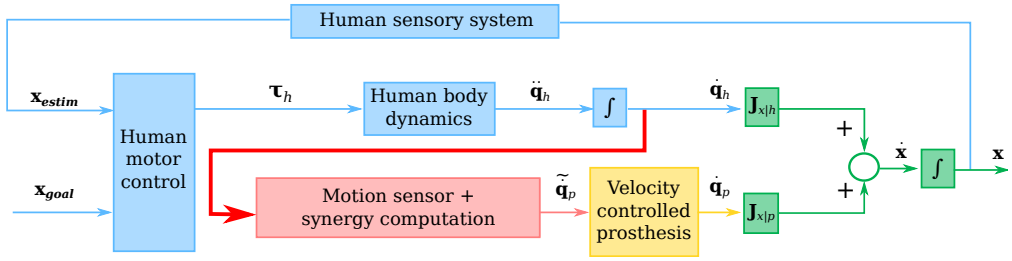

Figure 2.8: Motion Completion Control scheme. The red bold arrow indicates the difference with ASC scheme

2.3.1 Modeling joint synergies

The most widespread MCC approach takes advantage of joint synergies, specific coordinations between human joints, established by the CNS.
The human body is redundant, which means that there are more DOF than the 6 DOF of space (3 for translation and 3 for rotation). To perform a movement, there is thus not a single but an infinite number of possibilities. To deal with this redundancy, the CNS combines together the motions of some joints in synergies, coordinations which are constant across different performances of a same motion (see Figure 2.9). These coordinations can be visible with joints positions [142–145], angular velocities [143, 144] or angular accelerations [146]. For the UL, shoulder-elbow [143, 147], shoulder-wrist [142, 144] and elbow-wrist [144] coordinations can be found. Synergies are invariant characteristics of the human motions and are similar between individuals [142–145, 147]. For these reasons, they can be modeled, i.e. the relationship which links the joint kinematics can be analytically or numerically expressed: $k_1 = f(k_2)$, with $k_{1,2}$ the position, angular velocity or acceleration of the considered joints and f, the function that models the synergy. With such a model, it is possible to compute a joint position, angular velocity or acceleration (k_1), if those of the coordinated joint(s) (k_2) are known. This is the fundamental principle of joint synergy-based MCC: **modelling UL synergies allows to obtain prosthetic joint motions from human residual joint motions**. With a model of the shoulder-elbow coordination for instance, prosthetic elbow motions can be infered from user's shoulder motions [148]: prosthetic intermediate joint motions automatically complete a natural body action.

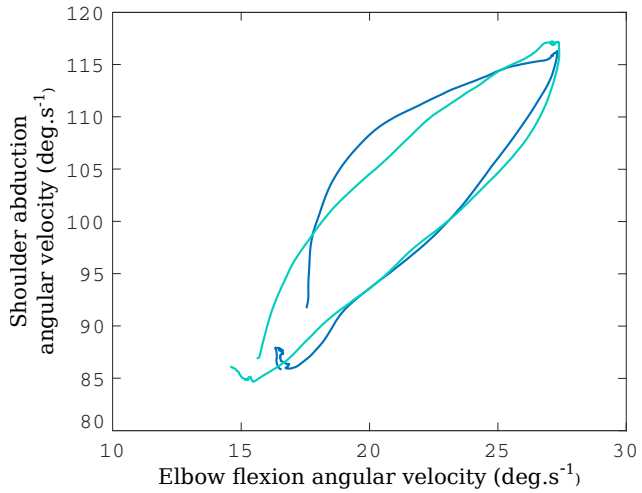

Figure 2.9: Illustration of shoulder-elbow synergy. The coordination of these two joints motions is visible through an invariant law that connects the shoulder abduction and elbow flexion angular velocities. The two colors corresponds to two different performances of the same motion

The concept of synergies for prosthetic control may yet define different realities, since it is widely employed to refer to a coordination between joints, in a general way. The implemented models are thus very diverse, and do not necessarily reflect the accurate joints relationship. The most simple mapping is a proportional law between the angular velocity of a human functional joint and the one of the prosthetic joint to control [149, 150]. It is easy to understand for the prosthesis user but does not correspond to the real synergies, which are a bit more complex. It creates a systematic link between a functional and a prosthetic joint, which prevents any independent motion of the first one. In [149] for instance, the angular velocity of the prosthesis elbow joint is proportional to the angular velocity of the human upper-arm. Moving the upper-arm only is thus impossible since the slightest motion makes the prosthetic elbow moving. To model joint synergies with more accuracy and avoid such a systematic linkage, many studies have developed supervised machine learning algorithms such as regression with Principal Components Analysis (PCA) [145], Multi-Layer Perceptron (MLP) [151, 152] or Radial Basis Functions Network (RBFN) [146, 153, 154]. The two last methods have been tested for the purpose of prosthetic elbow control, via shoulder-elbow synergy.

The main benefit of MCC is the **absence of learning** on the subject's side: motions of the intermediate prosthetic joints and of the user's joints are coordinated like those of able-bodied subjects. The amputee initiates the movement with his/her residual joints (e.g., shoulder), as able-bodied would do, and the prosthetic joints complete it. However, the development of synergy-based approach is restrained by two issues. First, building a synergy model requires to train the algorithm with data from all involved joints. For instance, shoulder and elbow motions must be known to then derive the coordination law that links them. This is, obviously, only feasible with able-bodied motions or with motions of the contralateral arm of an amputated subject. Yet, although similar, synergies between individuals – especially between able-bodied and amputated people – and between the two arms of a same person, are not exactly identical [155–157]. The difference in dynamics and mass repartition between a prosthetic and a human arm also affects the amputated limb motions, which can change from natural motions. These variations prevent to have a very accurate human-prosthesis joints coordination and can limit the user's satisfaction. Indeed, recursively missing the intended target by a few centimeters is an understandable cause of prosthesis rejection. Second, synergies are task-dependent; they can even depend on the direction and distance of targets to reach [142, 145]. These two points call for the addition of supplementary layers in the algorithm, that would deal with model **personalization** and **task versatility**.
Garcia Rosas et al. have recently explored the model personalization part [158, 159]. Their studies first confirm the subject-dependence of the synergies. Starting from an algorithm trained with other subjects data, they then propose to add an online training of the algorithm parameters for individuals, with an optimization scheme, which was tested in virtual reality environment for elbow joint control.

2.3.2 Versatility: an illustrative study

Task versatility of synergy-based MCC is a different type of problem. While the personalization is a parallel step performed once and for all, versatility must be a permanent stage embedded into the control algorithm. The first logical question to ask is whether different tasks can be processed by the same model. Yes, synergies are task-dependent but can several of them be modeled by one function? As explained in Section 2.3.1, the regression algorithms employed to build synergy model need to be trained before being used for prosthetic control. Training consists in identifying the algorithm parameters from example input-output pairs, before using this now identified mapping to compute output from new input data. We could imagine to build a global model, able to manage different synergies, by taking a training data set with various movements.
A short illustration study was realized to see if state-of-the-art algorithms could permit that. RBFN and Gaussian Mixture Regression (GMR) [160] were implemented to model shoulder-elbow synergy (see Appendix A for some details on these implementations). They were trained and tested on

different data sets from able-bodied subjects. Figure 2.10 shows typical results. On Figure 2.10(a), the two algorithms are trained and tested with data from the same task, composed of one synergy; on Figure 2.10(b), training and testing data sets come from two tasks, composed of one common and one different synergy; on Figure 2.10(c), training data set gathers a group of different tasks, which contains the one of the testing data set.

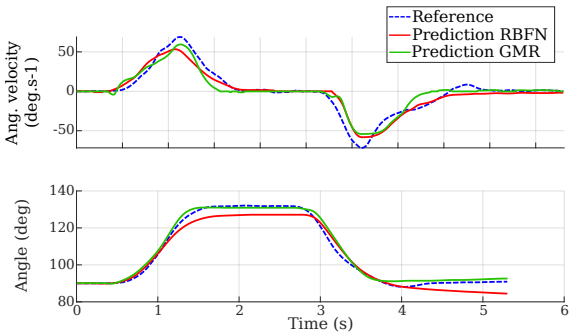

(a) Training and testing data set coming from the same task.

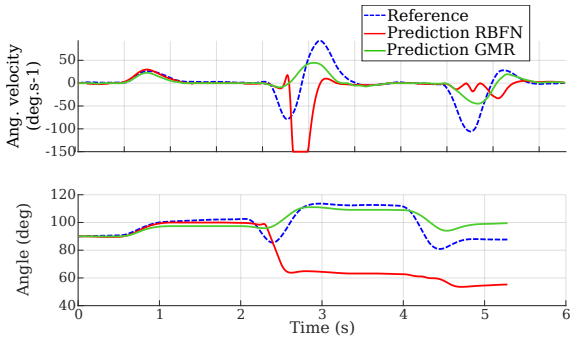

(b) Training and testing sets coming from two different tasks

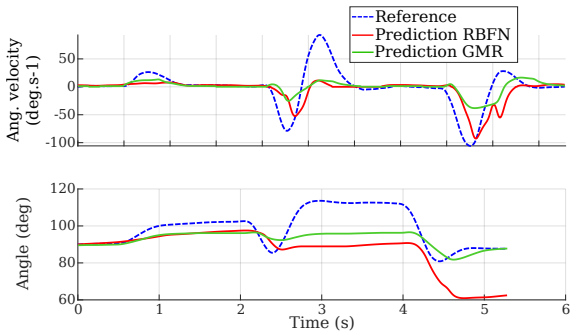

(c) Training data set containing various tasks, including the one of the testing data set.

Figure 2.10: Results of RBFN and GMR modeling, with different training and testing data set. For each figure, upper graph is elbow angular velocity output, lower graph is the reconstructed elbow flexion angle. The blue dotted line corresponds to the true elbow motion (reference to which compares the models output), red and green lines correspond to RBFN and GMR output respectively

We see on Figure 2.10(a) that the output of the model corresponds to the true elbow motion. A single synergy is thus well modeled by RBFN and GMR. On Figure 2.10(b), the beginning of the sequence is well predicted (which corresponds to the common synergy, included in the training data set), but the models diverge from the second sub-movement, whose corresponding synergy is not in the training set. This confirms that a model trained on one synergy cannot be extended to another one. Figure 2.10(c) shows that a global model is also not feasible with the two considered algorithms. The task (and thus the synergies) of the testing set may be included into the training set, the outputs of the models do not coincide with the expected elbow motion. Indeed, training an algorithm on too many various synergies might build a mixture model, that does not correspond to any natural synergy.

Versatility thus requires to consider a new algorithm structure: a high-level classification layer to select the appropriate synergy model among an index, and a lower-level layer to execute the selected model and command the prosthesis motion (as proposed in [161, 162] for instance). Figure 2.11 illustrates the difference between a simple one-layer (as implemented in most of current studies) and a two-layers algorithm, that could be more appropriate for a versatile MCC.

To explore the possibility to add a classification layer for prosthetic elbow control, with shoulder-

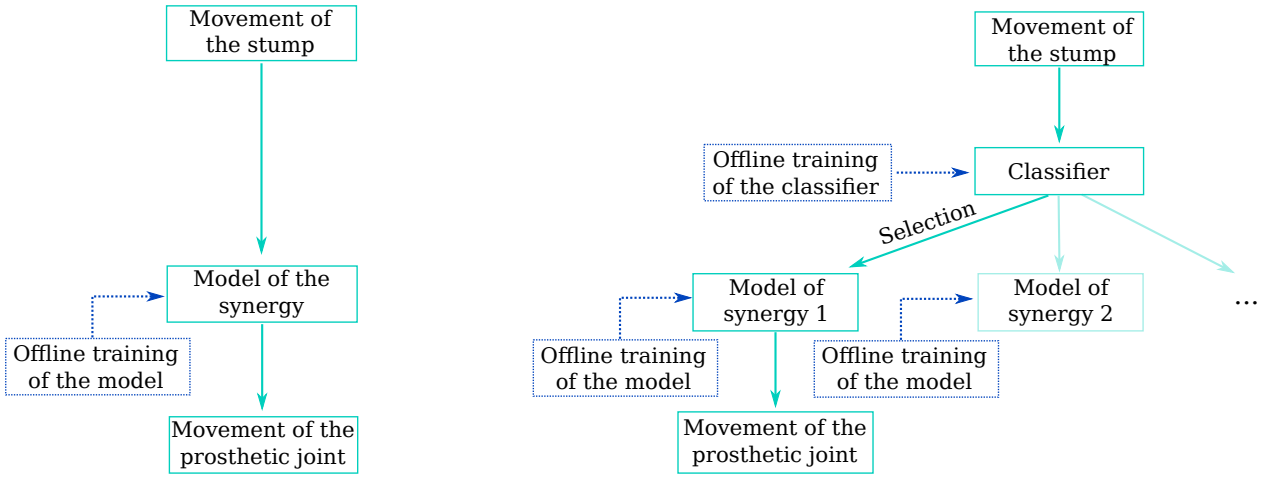

(a) One-layer algorithm for synergy-based MCC

(b) Two-layers algorithm for synergy-based MCC

Figure 2.11: Illustration of possible algorithm structures for synergy-based MCC. (a) One-layer algorithm. (b) Two-layers algorithm, that could be more appropriate for a versatile control. The first layer is for task recognition with classification; the second for motion execution with the proper loaded model

elbow synergies, I conducted a short feasibility study (see Appendix B for details on the set-up, data collection and features definition). A data set from one able-bodied subject performing various tasks was collected and two state-of-the-art classification algorithms were considered: Bayesian Decision Making (BDM) and Support Vector Machine (SVM) [163] (see Appendix A for some details on the algorithms and their implementation). They were implemented on Matlab Mathworks®, which was also used to study the classification results. Four motion classes were defined by hand: reaching, return, change height and bring-to-mouth; the features were computed in a sliding window of 100ms or 500ms, with an increment time of 10ms.

Size of sliding window	$t_w = 100$ms	$t_w = 500$ms
BDM	45.2%	62.8%
SVM	61.1%	60.2%

Table 2.1: Mean classification accuracy of BDM and SVM, with two different sizes of sliding window, t_w.

Table 2.1 shows the mean classification accuracy (percentage of correct outputs) for both classification algorithms, with two sizes of sliding window. A brief study of the results shows that increasing the size of the sliding window improves the performance for BDM and that BDM with a 500ms window and SVM have similar accuracies. Results are in acceptable range, compared to similar works [164, 165], but we are still far from 100%.

Multiple options can be explored to get improvements – changing the choice of features or the windowing techniques, optimizing some algorithm settings, automatically identifying motion classes with an other algorithm, using a more suitable algorithm [164, 166] – but too many questions are raised to rush headlong into this. Indeed, even if it seems logical to build a two-layers algorithm, is it really appropriate? Adding a classification layer first increases the computation time, which creates an additional delay between user's intention and prosthesis motion (classification time is usually around few 100ms, depending on the selected algorithm and its corresponding parameters, see [90] for instance). Then, even if few percents of accuracy can be earned by optimizing the algorithms,

the same *hot coffee problem* as raised in Section 2.1.2, remains. Can we, one day, achieve 100% of correct output: (i) whatever the situation, also on impredictable actions for which no data could be collected? (ii) in everyday life environnement and without a precise measure with a motion capture system (which is restricted to the laboratories)? If some classification errors can still occur, they will be added to the potential errors of the regression algorithms which model the synergy. By accumulating layers, we accumulate errors and the overall benefit can then be questioned. Finally, to have enough data to correctly train classification algorithms, data from different subjects may be required and the same issue of personalization as the one of the synergy models arrises. Is it a viable path, for UL prostheses control, to build a hierarchical algorithm, with multiple layers, each of them requiring an additional personalization step, without the assurance of a full accuracy? Such a complexity also builds black-box algorithms, incomprehensible for the user, which can reduce the trust s/he has in the prosthesis control and make the integration of the device into the body image difficult.

The accuracy issue of Motion Completion Control approaches

With MCC, the user has, in theory, only one task to be focus on: controlling her/his functional joints, whose motion is then completed by the prosthesis. Yet, the approximate synergy models can make prediction errors on prosthesis motion, which necessarily requires to let some control for the user to correct these possible errors. This correction first transforms the single task of MCC into a double task for the user, who has to both control her/his proper joints and beware of prosthesis motions. It then promotes compensatory motions, that the user tends to exhibit to rectify prediction errors. This accuracy issue is even more of concern when considering a versatile control scheme: the multiple synergy models required and the classification layer to select the appropriate one for each human motion ineluctantly increase the error probability of prosthetic motions. This lack of confidence in the device could here also be a source of frustration for the user, who would tend to favour his/her proper body motions at the expense of prosthesis mobility.

2.4 Necessity for a new control approach

The wide variety of control approaches for active UL prostheses can be classified into three main groups:

- ASC, which induced a double task for the user through the auxiliary signal generation, coming in addition to her/his body kinematics;
- ASC with automation of some prosthetic joints, which reduces the double task burden;
- MCC, which theoretically removes the double task by using the user natural motions as input of the prosthesis controller. The approximate models yet impose to let the user correcting the possible prediction errors, which nearly changes the single task into a double one.

None of these control schemes acquires a mass adhesion from the users [7, 13–15]. The one that predominates on the market is conventional myoelectric control, which has not much evolved for more than 60 years and requires a long learning phase, is cumbersome for the user, allows only sequential movements and becomes quickly limited with an increasing number of prosthetic DOF. But it is the most robust, and robustness is one of the first property desired by prosthesis' users [7, 13, 81]. Since the emergence of active UL prostheses, their control remains a major challenge. Why none of the existing approaches seems appropriate?

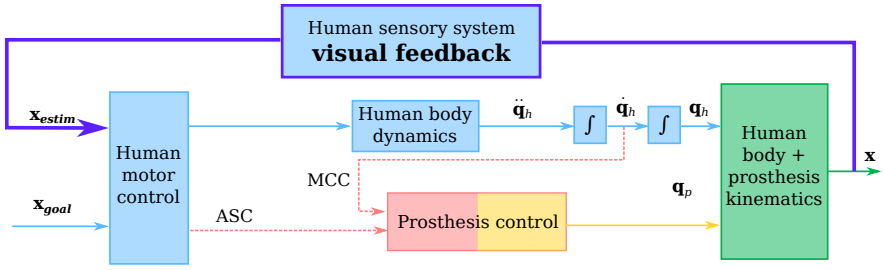

Figure 2.12: Simplified diagram of prosthesis control with existing approaches. The control loop of the system is closed by the user, who has to reverse-engineer the controller of the prosthesis to generate the signal corresponding to his/her motion intention

The problem of open-loop control

Besides the specific drawbacks of each previously described approach, a plausible reason is that, with all of these control schemes, the prosthesis control is open-loop. Once the output of the controller is computed, it is accomplished without any feedback. How the motion is performed and whether it corresponds to the real user's intention is not considered. As shown in Figure 2.12, **the control loop is only closed by the user**. To be satisfying, existing approaches must be absolutely accurate and allow no error. That is why most of current works are focusing on the search for the best control algorithms. In the meantime, before the – possible – advent of algorithms that are perfectly accurate in every situations of everyday life, no time-consuming, compact enough to be run in a microcontroller, and personalized (be it for pattern recognition, eye-tracking or joint synergies), the posssibility of a correction by the user is required.

To correct the prosthesis motion, there is no choice but to generate a new control signal, be it an auxiliary signal for ASC approaches or a body motion corresponding to the appropriate synergy for MCC. This requires understandable control scheme and algorithm, that can be *reverse-engineered* by the user, so that s/he knows what to do to correct the prosthesis motion. If the user is not able to predict the output of the controller, s/he will not be able to generate the proper signal. Black-box algorithms, such as those used in pattern recognition or joint synergies, do not seem suitable as long as they are not fully accurate.

Since generating a new control signal usually slows down the overall human-prosthesis motion, the user tends to correct the prosthesis position with his/her residual functional joints and neglect the device motion possibilities. This preference is at the origin of body compensations (further detailed in Chapter 3). A transhumeral amputee, for instance, will tend to adjust the reaching of an object on a table by bending his/her trunk forward rather than by switching between the different prosthetic DOF with co-contractions until controlling the elbow, or by performing a new stump motion to trigger the corresponding joint synergy. More precisely, prosthesis users exhibit compensations with ASC because they prefer to mobilize their residual functional joints rather than prosthetic joints with auxiliary signals; with MCC because they correct the inaccuracy of the synergy model predictions.

Another issue of existing control schemes is that the only way for the user to close the control loop is through visual feedback, since proprioception is unavailable and sensory feedback is in its early days (see Section 1.4.2). This increases the mental burden of the user, who has to manage both prosthesis control (sometimes unnatural) and correction, based on vision only. The demand for a reduced visual attention in UL prostheses control is indeed recursive [7]. Prosthesis control thus asks either for super algorithms or for means to reduce the cognitive charge of the user and discharge her/him from the correction of the prosthesis motion. The latter is the way I chose to explore in this PhD.

2.5 Chapter summary

In this chapter, I gave an overview of the existing control schemes available for UL prostheses, be it on the market or still under development in research laboratories, for reaching and grasping and for all amputation levels (except partial hand amputation which is a special case). A classification of these approaches, depending on the link they create between the user and the device, was proposed and it was explained how this link can influence the intuitiveness of the prosthesis control. Pros and cons of each were detailed, and it was concluded that none of them is fully satisfactory for amputated people (see Table 2.2 for a recap). While auxiliary signal approaches decorrelate prosthesis and human motions and create a double task for the user, joint synergies-based approach requires a complex algorithm structure, with multiple layers, which will never be default-free. The variability of human motor behavior and of daily lifetasks, the redundancy of human body and thus of motor strategies are indeed all factors which challenge the advent of an ideally suitable algorithm for synergy-based control.

Type of prosthesis control	Advantages	Limitations
ASC control with individual muscle contractions (conventional myoelectric control) – Section 2.1.1	• robustness • straightforward implementation	• heavy training • increased mental burden when more than one DOF to control (state machine with co-contractions) • sequential motion
ASC control with pattern recognition – Section 2.1.2	• no learning for the user • simultaneous multi-DOF motions	• algorithm learning • lack of robustness • limited number of motions
Partially automatic control – Section 2.2	• dimension of user's control space reduced • simultaneous multi-DOF motions	• controller input not convenient • individual prosthetic joint motions not allowed
MCC – Section 2.3	• no learning for the user • synchronous prosthesis and human motions	• task-dependency of joint synergies • limited number of motions

Table 2.2: Recap of main advantages and limitations of the existing UL prosthesis control schemes

All the presented schemes also share the same open-loop nature at the device level; the user is the only one in charge of the correction of the prosthesis motion, which increases her/his mental burden. My proposition is to tackle this open-loop issue: the following chapter describes how it is suggested to close the control loop at the prosthetic level, in order to minimize the cognitive charge of the user and improve the robustness of prosthetic control.

Chapter 3

Closing the control loop with body compensations

The main goal of closing the control loop at the device level is to avoid charging the user of the device configuration correction; this correction is directly performed by the prosthesis' controller. But this requires an error signal in order to compare the output with the user's command. This is the tricky aspect when applying this method to UL prostheses control: how to measure error? In this chapter, I probe this issue and outline the idea to employ human body compensations as error signal to close the prosthesis control loop. I then describe two experiments that confirm the feasibility of this idea.

3.1 Finding an appropriate error signal

Arm motions are mainly produced to reach and/or grasp a target; their predominant goal is a position and an orientation of the hand. A natural error signal would thus be the difference between the desired and the current hand positions and orientations. To access the defined hand location, a straightforward method is obviously to know the target of the user, but this is not possible in everyday life environment. Indeed, it is complex to know *a priori* the goal of a person among all the objects of her/his surroundings, and motion capture systems, that can give the coordinates of a target, are not usable in daily scenarios because of the cumbersomeness of their utilization. Another way to access the desired hand position and orientation would be to read in the user's brain the motor intent. Yet, as exposed in Section 2.1.3, neural signals decoding techniques are still far from such a capacity. A third option is a paradigm shift: instead directly measuring the user's goal, we measure whether the prosthesis is positionned or moves as s/he wants. For that, the user's reaction to the prosthesis motion (or non-motion) can be tracked.

3.1.1 The message of body compensations

As explained in Section 2.3.1, the human body is redundant. This redundancy leads the CNS to create joint synergies but it also makes possible to perform a same task in different ways. For example, we can either extend the elbow or flex the trunk to reach something on a table; or we can either flex the trunk or bend the knees to reach something on the floor. When the mobility of some joints is reduced, the CNS takes advantage of the body redundancy. If the wrist or the elbow are affected, the subject will tend to naturally use other joints, fully functional (like the hip, the shoulder, etc.), to compensate the arm mobility loss; this can be observed in post-stroke subjects for instance [167, 168]. This strategy is also visible for UL amputated subjects, even if the mobility may be considered as restored with an active prosthesis. Indeed, as exposed in Section 2.4, the inconvenience and slowness of prosthetic control are often bypassed by the user who rather performs the task with her/his residual functional joints [127]. This substitution of distal joint motions by proximal joint motions, thanks to body redundancy, is called body compensations. Their usage expresses a mismatch between the current prosthesis posture and the one desired by the user.
So far, these compensatory movemements have been regarded as motions to avoid because they cause musculoskeletal disorders [8, 72]; they have recently been integrated into procedures that assess prosthesis motion quality and control performance [126, 169]. The concept developed during

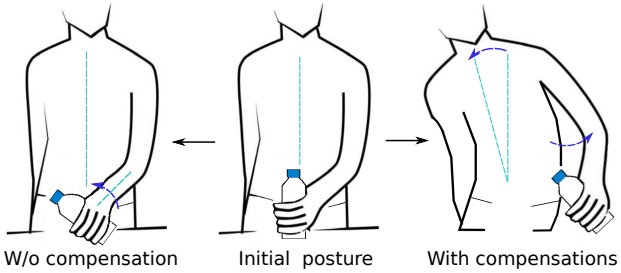

Figure 3.1: Illustration of typical body compensations for wrist pronosupination

my PhD proposes to go further: instead of studying body compensations once the prosthesis control scheme is built, only for evaluation, they could be employed in the control law. **Since body compensations express errors in the position of the prosthesis, they could define the error signal of the closed-loop controller**.
To do so, a first step is to identify these compensations: what are they? Which human functional joint compensate for which prosthetic joint? Are they similar between subjects? Many studies have investigated this topic for transradial amputees [71, 170–172]. They show that pronosupination is supplanted by trunk lateral bending or rotation (depending on the task), shoulder abduction/adduction and that elbow flexion is increased (see Figure 3.1). For transhumeral amputees, there are less data available [127]. I thus conducted an experiment to determine the compensatory movements associated to elbow mobility loss.

3.1.2 Characterization of induced body compensations

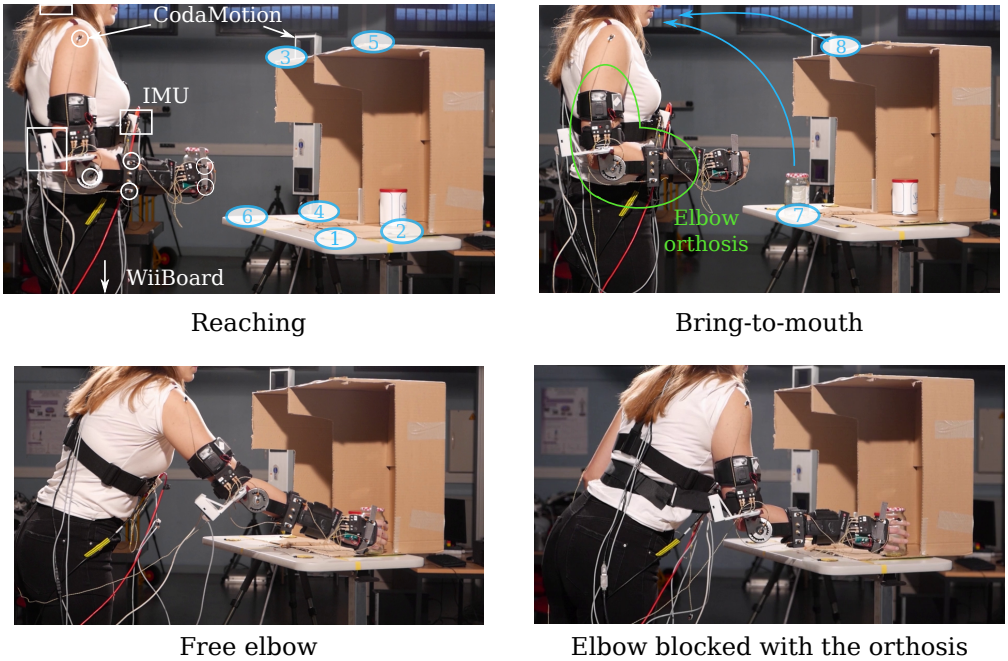

Figure 3.2: Experimental set-up to characterize body compensations in response to elbow mobility loss. Able-bodied subjects performed a reaching-and-return and a bring-to-mouth tasks, with an orthosis letting the elbow free of moving or locking it at 90 deg. The numbers identify the different movements (6 reaching targets and 2 heights for bring-to-mouth). CodaMotion®, IMU and Wii™Fit Balance Board were used for motion analysis.

This experiment aims at studying the compensations exhibited when the elbow mobility is reduced.

Materials and Methods

Ten able-bodied subjects were asked to perform 3D motions with their right arm, with their elbow either free of moving or blocked at 90 deg (angle between humerus and forearm) with an orthosis, as shown in Figure 3.2. The shoulder aperture mobility was also limited, with a strap, to mimick the socket of transhumeral amputees. The task was divided into two parts: (i) bringing an object to 6 locations and going back to the initial position; (ii) reaching an object on a table, at two different heights, bringing it close to the mouth, putting it back to the table and going back to the initial position. For the first part, there was no grasping, the object was already in the hand (see Figure 3.2). The whole task was repeated four times. Subjects were asked to be initially standing, with the arm along the trunk and the elbow flexed at 90 deg. For post-experiment analysis, three IMUs were placed, one at the back of the head, one on the sternum, the other on the shoulder, to measure head, trunk and shoulder angles; CodaMotion® motion capture system was used with markers on the hand, the forearm, the elbow, the shoulders and the sternum to measure body segment movements; and a Wii^{TM}Fit Balance Board measured subjects balance [173]. The Range of Motion (ROM) of the head Euler angles in the trunk frame, of the trunk angles and of the humerus aperture angle (see Figure 3.3), the acromion displacement and the weight repartition were analyzed. Statistical analysis was conducted on the metrics averaged over trials for each condition (natural and blocked elbow) and subject. Normality of the data was assessed with Lilliefors test [174]. Then, general linear models were used for normally distributed data and the nonparametric Friedman test was used for the others [175].

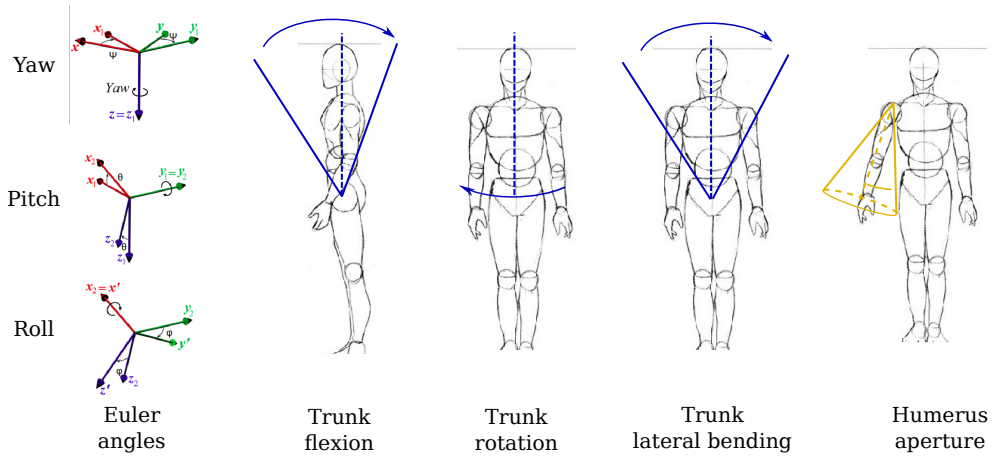

Figure 3.3: Definition of Euler angles, trunk angles and humerus aperture.

Results

Figure 3.4(a) shows the mean of trunk and humerus angular trajectories for one typical subject and two typical movements. As expected, humerus aperture decreases a bit when the elbow is blocked, since the shoulder mobility was also limited, to mimick socket constraint. We see that all trunk angles increase to compensate for elbow mobility loss and shoulder mobility reduction, whatever the task performed. This is confirmed Figure 3.4(b) for all subjects. Depending on the side, the distance and the height of the targets, one of the three trunk angles is particularly enhanced. A distant target enhances trunk flexion while a target on the contraleteral side (left side) enhances trunk rotation and lateral bending, for instance. To avoid considering too many measures but dealing with one compensatory metric, we can look at the acromion[1] displacement, which accounts for all three DOF of the trunk. It also indicates the possible scapular translations (retrac-

[1]Acromion is the lateral extension of the spine of the scapula, forming the highest point of the shoulder.

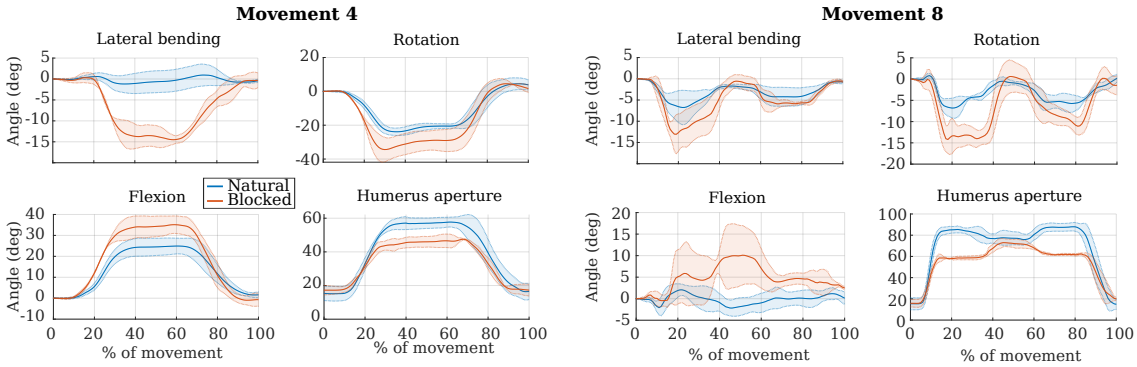

(a) Example of trunk and shoulder angular trajectories for one typical subject

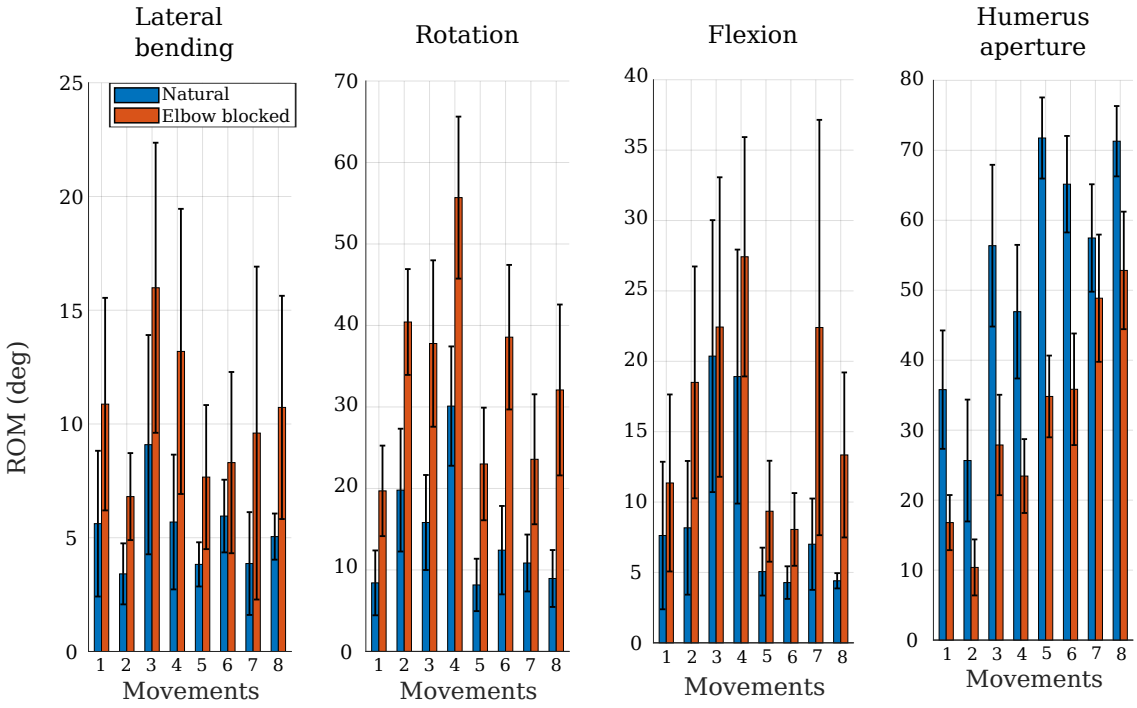

(b) Trunk and shoulder ROM

Figure 3.4: Trunk and shoulder motions, for natural and elbow-blocked motions. (a) Mean and confidence interval of angular trajectories of the trunk angles and humerus aperture (normalized in time), for one typical subject. Trajectories are presented for one reaching and one bring-to-mouth motion (see Figure 3.2 for the corresponding numbers). (b) ROM of trunk angles and humerus aperture, averaged over trials and subjects.

tion/protraction, elevation/depression), which was not limited in this experiment and was observed on the participants. Figure 3.5 shows a typical example of acromion displacement for one subject, and the maximum acromion displacement, averaged over all subjects for the 8 movements. It is clear that the acromion displacement significantly increases when the elbow mobility is lost. Head motions and weight repartition were also enhanced when the elbow was blocked, even if head angles ROM have a high variability between trials and subjects (see Figures C.1 and C.2 in Appendix C). While they both express a change in subjects' motor strategy, they are not considered here as body compensations since they are not a substitute to distal impaired joints (moving the head does not help to move the hand and weight repartition is only an image of upper body motions, reflecting trunk compensations).

Body compensations exhibited when the elbow flexion/extension is impaired are thus characterized by trunk and scapula motions. Interestingly, they can be gathered into **acromion displacement**.

Other parts of the body, like the head, also participate to modify motor strategies but are not identified as compensatory according to the definition used here. These observations are valid for a broad variety of tasks, be it reaching in 3D or bring-to-mouth. This experiment could have deserved to be complemented with amputated participants, but the main outcomes are similar to what was observed in [127] on three transhumeral amputees performing reaching tasks.

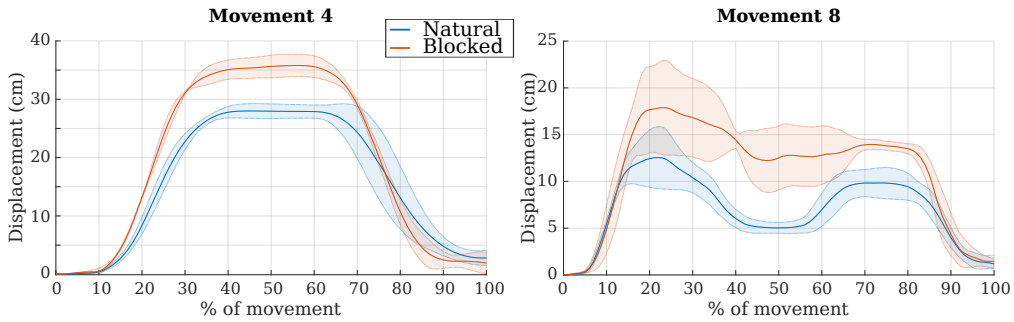

(a) Examples of acromion displacement for one typical subject

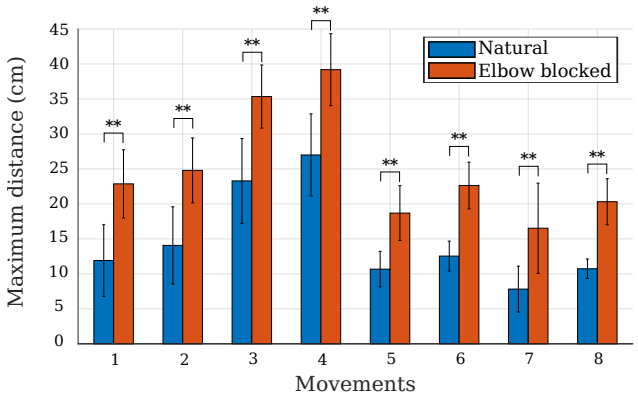

(b) Maximum acromion displacement

Figure 3.5: Acromion displacement, for natural and elbow-blocked motions. (a) Mean and confidence interval of acromion displacement (normalized in time), for the same typical subject and motions as in Figure 3.4. (b) Maximum acromion displacement, averaged over trials and subjects. ** indicates $p < 0.005$.

3.2 Proposed concept

Results from cited works on wrist, as well as those from the experiment described in Section 3.1.2 on elbow, point out that, when a distal joint mobility is reduced or missing, the CNS recruits the next more distal functional joint(s) that can perform the desired task. The wrist pronosupination is thus replaced by shoulder and trunk motions, while the elbow flexion/extension is replaced by trunk and scapula motions (shoulder motions cannot substitute elbow flexion). As explained in Section 3.1.1, these compensatory movements express an error in the device posture that may be used as error signal for the closed-loop controller we want to set-up. Before proceeding further, it must be noticed and kept in mind two points: (i) what is meant by closed-loop control at the prosthetic level is not a traditional position servoing of the prosthesis (which can be implemented additionally) but a servoing of the device on its user movements; (ii) no compensatory movement substitutes grasping; the proposed approach thus seems valid for all intermediate joints, responsible for positioning and orientating the end-effector, but not for finger configurations.
Now that compensatory motions are identified, the next step is to determine a prosthesis motion from their error signal.

Reducing body compensations with prosthesis reconfiguration

Since body compensations allow the prosthesis user to still perform the task in case of unefficient device motion or position, the idea proposed in this PhD thesis is to let the user in charge of the end-effector task, while reconfiguring the prosthesis kinematics with the aim of reducing the exhibited compensatory motions. Contrary to what is usually considered, the function of our prosthesis is not to perform a specific task in joint- or end-effector space but to **control and optimize its user's posture using internal (null-space) joint motions, while the latter is in charge of the task**. The prosthesis is servoed to its user's body compensations in order to reduce them. This assumes a human-robot coupling, in which the user reacts to the prosthesis motions.
The proposed prosthesis control works in three steps: measuring body motions and detecting compensations – defined as a deviation from an objective posture –; computing the prosthesis position error expressed by the detected compensatory motion; from this error, generating a velocity command for the prosthetic joints (see Figure 3.6). Following the velocity command, the device motion should make the user go back to the objective posture via human-robot coupling. This is embedded in a closed loop with relatively high frequency (e.g., 100Hz) to avoid the user exhibiting large compensations for the prosthesis to react.
The proposed prosthesis control is an integral control: the velocity of the device's joints is triggered by a change in user's posture. This is much more appropriate than a proportional control; the latter would rigidly link human joint positions and prosthetic joint positions and would force the user to keep a compensatory posture while achieving the task. All the benefits of the proposed concept would be removed. An integral control avoids this and allows the user to only initiate a compensatory motion and come back to a non-compensatory posture to obtain a proper prosthesis motion.

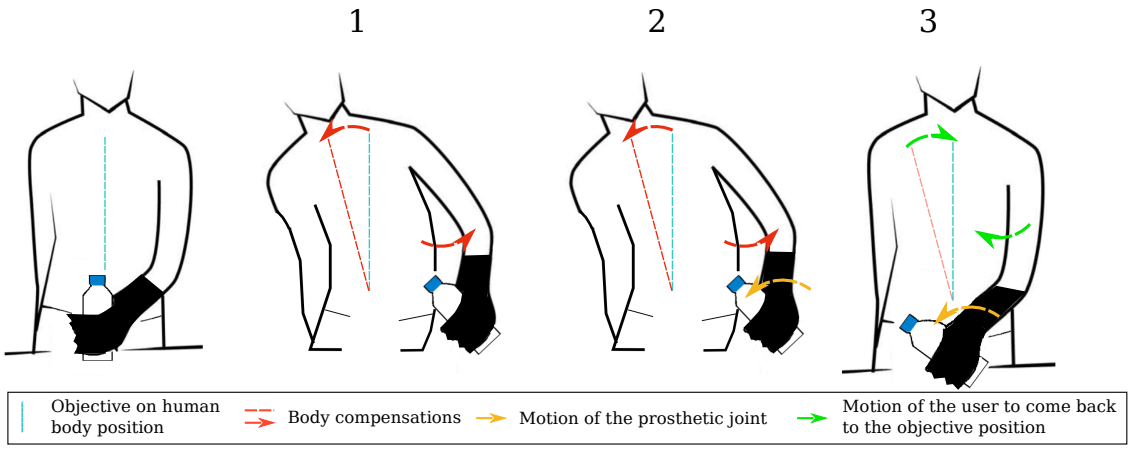

Figure 3.6: Illustration of the three steps of the proposed control scheme – closing the control loop at the prosthetic level with body compensations of the user – for a pouring task with a lower-arm prosthesis (in black). 1. Detecting compensations; 2. computing the corresponding prosthesis position error; 3. generating a velocity command from this error, which then allows the user to come back to the objective posture

A great benefit of this concept is that all intermediate prosthetic joints move **simultaneously**, while the user only takes care of the end-effector. The proposed control scheme indeed provides a human-robot coordination by distinguishing their objectives: **while the human's goal is to position the prosthetic hand, the device's goal is to position back the human body in a comfortable posture by reconfiguring the prosthesis kinematics**. Moreover, the user has

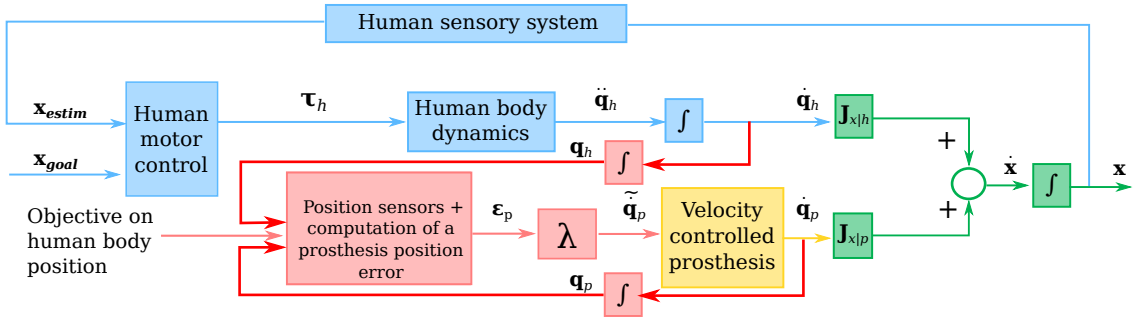

Figure 3.7: Proposed control scheme, named Compensations Cancellation Control. x, x_{goal} and x_{estim} are the real end-effector position, the desired one and the one estimated by the human sensory system, respectively. $\tilde{\dot{q}_p}, \dot{q_p}, q_p$ are the command prosthesis joint velocity, the prosthesis joint velocity and position respectively. τ_h is the torque of the human joints; $\ddot{q_h}, \dot{q_h}, q_h$ are the acceleration, velocity and position of the human joints, respectively. ϵ_p is the prosthesis position error and λ a scalar gain. Red and bold arrows indicate the differences with ASC and MCC

nothing to learn to control the device, since body compensations are **natural** CNS strategies. From now on, this closed-loop control based on body compensations will be refered to as Compensations Cancellation Control (CCC).

Figure 3.7 shows CCC diagram. When compared to Auxiliary Signal Control (ASC) and Motion Completion Control (MCC) control schemes (Figures 2.1 and 2.8 respectively), several differences appear. First, because the input of their controller is human motion, MCC and CCC get rid of the double task induced by the generation of the auxiliary signal in ASC. Then, while ASC and MCC approaches are open-loop for the device – the block diagram of the entire human-robot system is only closed by the human sensory feedback–, CCC indeed closes the control loop at the prosthesis level, which discharges the user from the potential correction of the device position. An estimate of the prosthesis position error is obtained with user's compensatory motions.

The **objective on human body position** – also named reference posture later on–, from which compensatory motions are deduced, can be defined as a non-compensatory and comfortable posture for the user. It is a body position s/he would be in to perform the task with a healthy limb; body compensations are thus deviations from this posture. It is obviously varying with time, and sometimes with the intented task. As a first step in this PhD, we will yet always consider situations where it can be viewed as constant. The generalization of the objective position to an everyday life use of CCC is a key limiting point of this approach. As it is not fixed, means to define a varying objective will have to be found. Via this objective, it must be possible to distinguish between functional and compensatory motions. Indeed, one joint is not either functional or compensatory, its role depends on the task and the context. A varying definition of the reference posture must take this into account. The way CCC is presented also allows to imagine other types of objectives than body posture, as soon as deviating from them indicates a prosthesis position error: a minimization of energetic cost, a minimization of some muscular groups activity or a stable balance for instance. All these remarks will be further discussed in Chapter 7.

3.3 Feasibility study on the wrist joint

Several questions are raised by the proposed concept: does the user react as expected in human-robot coupling? Namely, if a body position is detected as compensatory and a prosthesis movement is generated as a result, will the user naturally go back to the objective posture and cancel the compensation once the prosthesis is moving? Is the same implementation suitable for several

subjects? To answer these points, I first studied the feasibility to close the prosthesis control loop with body compensations for wrist pronosupination. The control law is detailed and is then applied to a prosthetic wrist control in two experiments, one with able-bodied subjects wearing an adapted device and the other with transradial amputees. An open-loop and direct control was also employed during these experiments to have a point of comparison to study control performance.

3.3.1 Control law

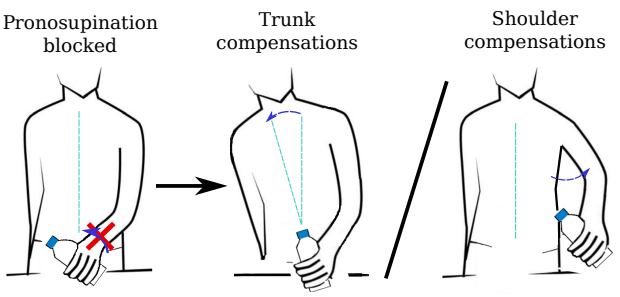

(a) Illustration of wrist pronosupination compensations, for a pouring task

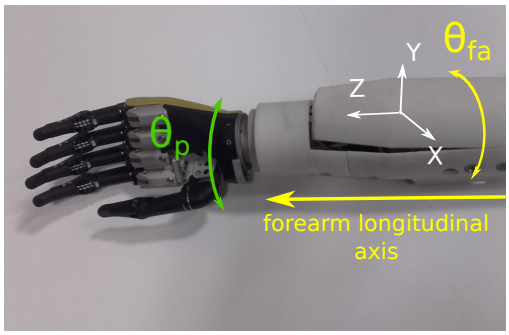

(b) Definition of forearm rotation (Z-Euler angle), θ_{fa}, and prosthetic wrist pronosupination, θ_p.

Figure 3.8: Measuring forearm rotation to detect wrist pronosupination compensations. (a) When the wrist pronosupination is blocked, it is compensated by trunk and/or shoulder motions. (b) To gather all compensatory motions in one measure, the forearm rotation around its longitudinal axis is considered

Studies on compensatory movements related to wrist pronosupination show that this DOF is generally compensated by trunk and shoulder motions [71, 170–172]. However, these compensations may differ depending on the subject's posture. Additionally, all trunk and upper arm motions are not compensations. To avoid approximate and rigid mappings between trunk, shoulder and prosthetic wrist motions and to limit the number of sensors, I propose to work at a more distal level and directly measure the rotation of the forearm around its longitudinal axis. If the forearm orientation is modified, it means that trunk and/or upper arm are moving to compensate and substitute wrist pronosupination (see Figure 3.8(a)). To define the error signal, a frame is attached to the prosthetic forearm, where Z axis is the forearm longitudinal axis, Y axis is perpendicular to Z axis in the forearm-arm plane, X axis is the cross-product of Y and Z (see Figure 3.8(b)). The Euler angle around Z axis of this frame, here called θ_{fa}, is then used to compute the error signal, defined as the difference between its current value and an objective value, θ_0 (as stated in the previous Section, this reference/objective posture defines the non-compensatory posture to go back to and can depend on the context):

$$\epsilon(t) = \theta_{fa}(t) - \theta_0 \tag{3.1}$$

When this error ϵ is not null, prosthetic wrist has to move to make the subject go back to the objective posture θ_0. To keep the hand orientation $\theta_{hand} = \theta_p + \theta_{fa}$ constant while θ_{fa} goes back to θ_0, the prosthetic wrist has to rotate. The pronosupination of the prosthesis supplants the user's compensations. ϵ is thus used as the input of the control law, which pilots the prosthetic wrist angular velocity, $\dot{\theta}_p$, as defined in the following equation:

$$\dot{\theta}_p(t) = \begin{cases} 0 \text{ if } |\epsilon(t)| < \epsilon_0 \\ \lambda(\epsilon(t) - \delta\epsilon_0) \text{ otherwise,} \end{cases} \tag{3.2}$$

where ϵ_0 is a deadzone threshold (set to avoid unwanted motions around the reference posture), $\delta = sign(\epsilon(t) - \epsilon_0)$, and λ is a scalar gain that tunes the rate of correction. Considering the law of Equation 3.2, it can be anticipated that the values of λ and ϵ_0 will influence the time response and the speed of the prosthesis, on which depend the reaction of the human user, and thus the human-robot system stability. Their role will be analyzed in details in Chapter 4. For the following experiment, ϵ_0 and λ were chosen empirically to ensure stability, and are set to 5 deg and 2 s^{-1} respectively.
This control law may seem close to the ones proposed in [176] and [150], which have also suggested to take compensations into account to control prosthetic wrist. Yet, in [176], the wrist rotation angle is merely proportionnal to a weighted combination of shoulder angles. Wrist is controlled in position, which limits the overall mobility of the user: for a large pronation or supination, large shoulder movement shall be produced by the user. Even if the aim of the controller is to minimize shoulder compensations, there is no error evaluation. In [150], Bennett et al. take only shoulder abduction/adduction as compensatory motion and do not consider trunk and other shoulder possibilities, which compensatory roles depend on the arm position. Moreover, none of these works present any human-robot coupling or closed-loop considerations.

3.3.2 Preliminary evaluation with able-bodied participants

This work has been published in Proceedings of the 2020 IEEE International Conference on Robotics and Automation (ICRA) [177].

With this first experiment, we aim at demonstrating that a human-robot coupling actually establishes when a CCC law is implemented to control a prosthetic joint. We tested that this coupling allows human subjects to perform a task without a reinforcement of body compensations and compared CCC performance with the one of an open-loop control.

Materials and Methods

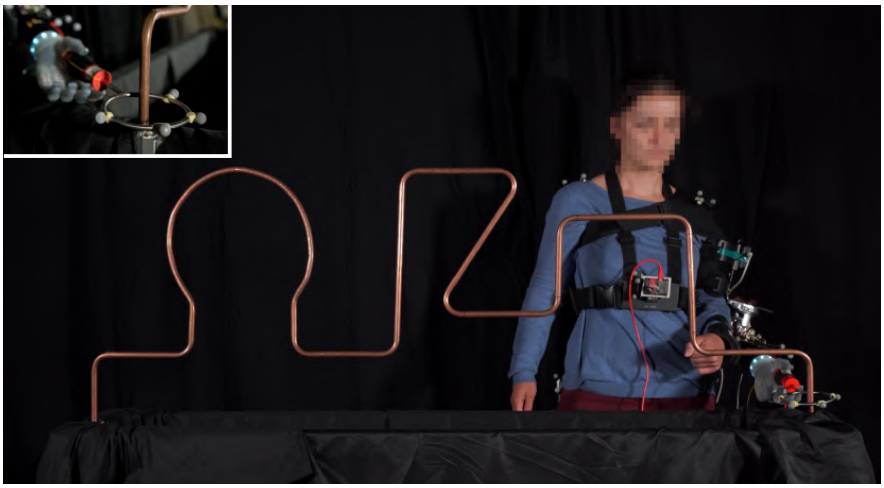

Figure 3.9: Cybathlon wire-loop task with the emulated prosthetic device. The upper left insert shows the handle hold by the prosthetic hand.

The first experiment performed to validate the proposed concept involved five healthy subjects (22 to 25 years old, one left-handed and four right-handed), wearing an emulated prosthesis on their left arm. They were asked to complete the wire-loop task of the Powered Arm Prosthetic Race of the Cybathlon©[178], particularly designed to challenge wrist pronosupination. The goal is to bring the handle through the wire-loop in a minimum time and without touching the wire (see Figure 3.9). The shape of the wire requires the participants to continuously adjust their hand orientation with pronosupination. To emulate UL prosthesis, the subjects wore a prosthetic prototype,

composed of a Touch Bionics hand (I-Limb^{TM}Ultra) and a motorized wrist rotator. The hand was pre-positioned holding the handle and kept grasped over it during the experiment (see Figure 3.9); the wrist angular velocity was controlled by a DC motor driver (Ion motor control, Ltd), itself controlled by a Raspberry Pi 3©. To measure body motions (mainly for post-experiment analyses), an OptiTrack (NaturalPoints Inc.) motion capture system and two IMU were used. Seven rigid bodies (or clusters), made of OptiTrack markers, were tracked: two on the hips, one on the torso, two on the shoulders, one on the device's forearm and one on the handle; the IMU were placed on the trunk and the upper-arm respectively (see Figure 3.10).
The prosthetic wrist was controlled with two different modes successively:

1. Open-Loop Control (OLC). A pair of push-buttons mounted on a handle was grasped by the free hand of the subjects (see Figure 3.10(a)). One push-button controlled the forward wrist rotation (pronation), the other the backward rotation (supination). When no push-button was pressed, the device stayed still. This command was used as a reference as it is an open-loop and direct control; the auxiliary signal here is the pressure on the buttons. It mimicks most of the myoelectric controllers currently available (on/off, proportional switch or even pattern recognition, see Section 2.1), while avoiding all the practical problems of EMG measurements. The joint angular velocity was fixed at 50 deg.s^{-1}, which is representative of values used for myoelectric control.

2. CCC. The forearm rotation, θ_{fa}, was computed in the initial forearm frame, from quaternions of the OptiTrack cluster placed on the device's forearm and sent in real time to the prosthesis. OptiTrack was convenient in lab environment and for post-experiment analyses but θ_{fa} could have also easily been obtained by gyroscope data from an IMU (see next Section). The objective θ_0 was supposed to be fixed and was set as the initial orientation of the forearm ($\theta_0 = 0\,\text{deg}$).

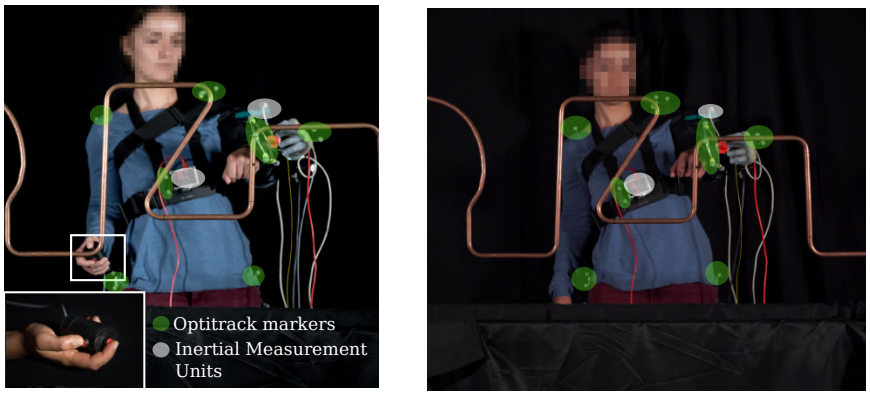

(a) OLC set-up (b) CCC set-up

Figure 3.10: Experimental set-up of the Cybathlon wire-loop task.

Before each recording session, subjects were allowed to train a few times on the wire-loop task. They trained between two and five times. A recording session consisted in five trials, and there were three recording sessions: one natural (N), with the own left forearm of the subjects, which provides a baseline from natural motions, one with OLC, one with CCC. Subjects always began with N while CCC/OLC order was randomized, to avoid measuring any effect of task learning. The initial position of the participants was imposed by the task: body parallel to the wire-loop plane and elbow flexed enough to reach the handle with the prosthetic hand. Post-experiment analyses were conducted with Matlab Mathworks ® scripts. This experiment was carried out in accordance with the recommendations of Université Paris Descartes ethic committee CERES, who approved

the protocol (NIRB: 20163000001072). All participants gave their written informed consent in accordance with the Declaration of Helsinki.

Results

Concept validation

Before any comparison with OLC, the supposed coupling induced by CCC must be analyzed. Figure 3.11 shows the shoulder abduction and the trunk lateral bending, that contribute to compensate for default of pronosupination, and the prosthetic wrist angular velocity, output of CCC. Red circles indicate the deadzone visible effect: perfect zero wrist velocity while the prosthesis error is less than the threshold ϵ_0. It is clear that there is a human-robot coupling: the user begins to compensate to achieve the task; once compensatory motions are detected, the prosthetic wrist rotates, which makes the user go back to the objective posture. It can be noticed that shoulder abduction is less coupled to the wrist angular velocity. Indeed, shoulder is also functional for this task (it is required to achieve it naturally), contrary to the trunk which is only compensatory. User-prosthesis coupling thus behaves as expected: the device corrects its user's posture, while the task stays accomplished. To complete the analysis and observe whether closing the control loop is indeed valuable, CCC is compared to OLC, on several criteria. The metrics characterize the good realization of the task but also the smoothness of the prosthetic motion, the easiness of the control and the amount of generated body compensations.

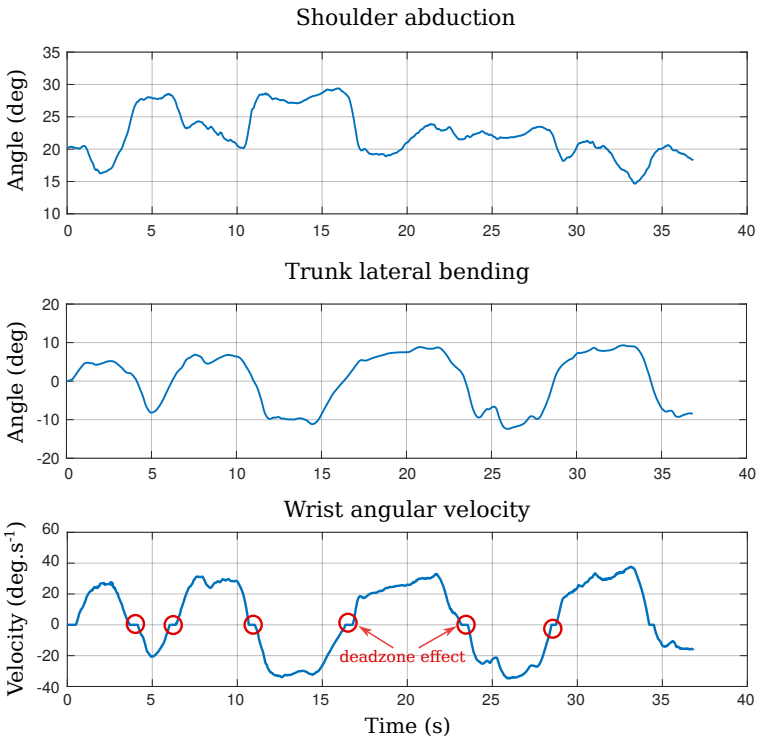

Figure 3.11: Human-prosthesis coupling induced by CCC, for one typical subject. Once the prosthetic wrist begins to rotate, the user reacts and stops compensating.

Task realization

The task performance is described with the time of the task and the number of touches (see Figure 3.12). Figure 3.12(a) shows the time for each trial of the two modes, with the mean difference between the two modes and the 95% Confidence Interval (CI). This representation was selected for the experiment because it allows for a more transparent statistical analysis than the p-value, especially for a small population [179]. If the 95% CI of the mean difference does not cross the zero dotted line, the two modes are statistically significantly different. The blue dashed lines are the minimum and maximum times obtained during natural achievement of the task by each subject.

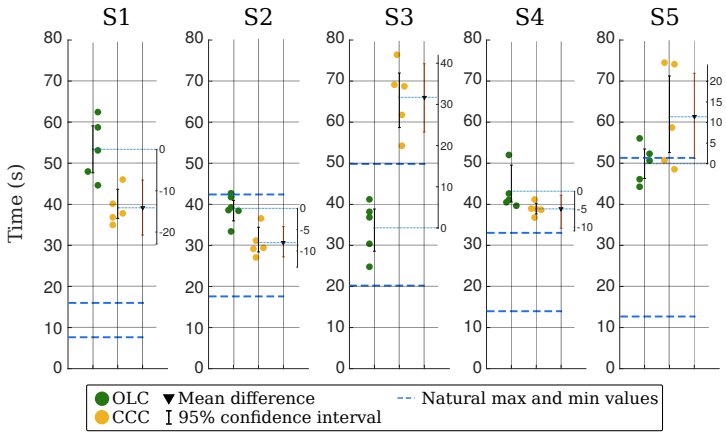

(a) Time of the task

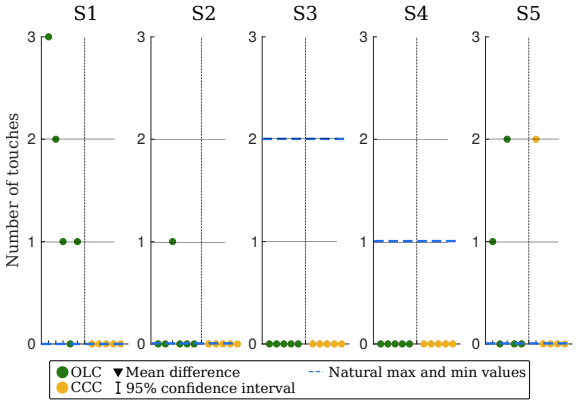

(b) Number of touches of the handle

Figure 3.12: Task realization performance metrics of the Cybathlon wire-loop task. (a) Time of the task: all trials of each of the five subjects, with the 95% confidence interval and the mean difference between the two control modes. (b) Number of times the handle touched the wire, for each trial. The blue dashed lines are (a) the maximum and minimum values of the time and (b) the maximum number of touches of the natural sessions.

It can be noticed that the natural times of the task are shorter for S1 because this subject was left-handed, but handedness did not affect any other results. We see here that for three out of five participants (S1, S2 and S4), the time is statistically significantly shorter with CCC than with OLC. For S5, the time with CCC is longer but without a real significant difference. S3 stands out from the others as CCC times are significantly longer than OLC ones. On Figure 3.12(b), we observe that the number of touches does not really distinguish OLC and CCC, except for S1. The latter touched the wire in four out of five trials with OLC and never with CCC, but this is partly due to the fact that this subject wanted to be fast more than being precise. Overall, it can also be noticed that CCC generates touches in only one trial out of the 25 (total of all trials for all subjects) whereas OLC does in 7 trials. Participants thus tended to be as good or better to realize the Cybathlon wire-loop task when controlling the wrist with CCC than with OLC.

Wrist motions

While healthy motions are naturally smooth [180], prosthetic motions are often jerky, due to the discrete nature of the command [181]. Since CCC allows for a continuous control of the movements, the smoothness of prosthetic motions with CCC may be improved, which would be a significant benefit. Figure 3.13 shows the wrist pronosupination angle and the wrist angular velocity of the

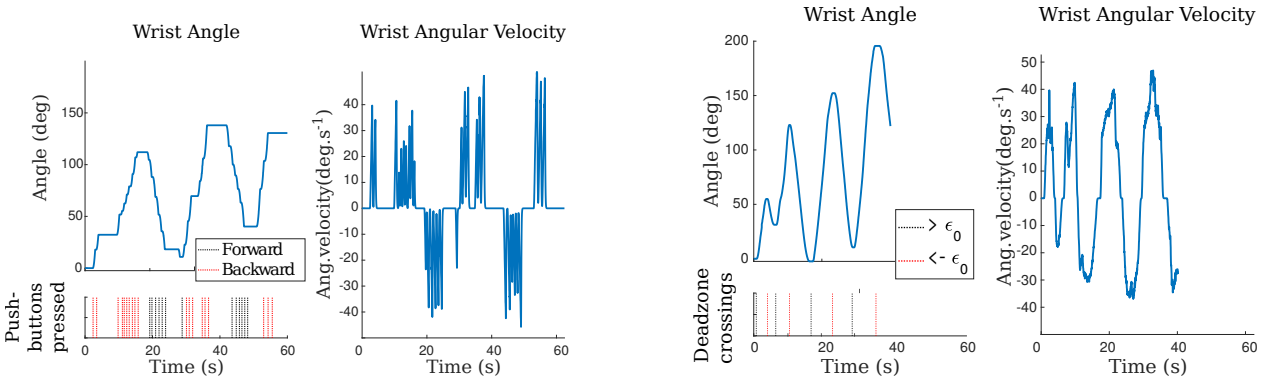

(a) OLC (b) CCC

Figure 3.13: Prosthetic wrist pronosupination angle and angular velocity for one trial of one typical subject with (a) OLC and (b) CCC. The red and black lines indicate when the push-buttons are pressed (for OLC) or when the subject's forearm angle went out of the deadzone (for CCC)

prosthesis for one typical subject, for OLC and CCC respectively. We see on Figure 3.13(a) that the OLC wrist angular velocity must be a series of pulses to obtain a motion as continuous as possible. It is clear that the wrist angular trajectory with OLC is jerky (it is a step function) while the one with CCC is smooth and continuous (see Figure 3.13(b)).
To quantitatively evaluate smoothness, we used the spectral arc length of the wrist angular velocity [182] (Figure 3.14(a), the more negative, the less smooth). The same statistical representation as above, with 95% confidence intervals and difference mean, is employed. There is no doubt that for the five participants, CCC wrist motions are significantly smoother than OLC wrist motions.
Yet, one can argue that the low smoothness of OLC is intrinsic to its binary nature. As often done in on/off prosthetic control, finer velocity profiles, e.g., trapezoidal, could have been implemented. However, this would not have created a fully continuous control, as enabled by CCC.

User's involvement
When the concept of CCC was exposed above, less user's involvement in the prosthetic control was claimed, due to the closure of the control loop at the prosthetic level. This reduction is first due to the removal of the double task of auxiliary signal generation. It can also be illustrated by comparing the low number of deadzone crossings with CCC to the high number of times the push-buttons were pressed with OLC (except for S3 who, here again, stands out from the other participants). Figure 3.14(b) shows these two metrics, with their mean and CI, for all trials of the five participants. It highlights the fact that the prosthesis user is more involved when using OLC than when using CCC. Indeed, with OLC, (i) s/he has to focus on individual wrist motions while CCC allows to focus only on the end-effector motion and (ii) s/he is her/himself the corrector that closes the control loop.

Body compensations
Using compensatory motions as input of the prosthesis controller with CCC may also promote them, which is not a desirable effect. It is essential to check if the action of the prosthesis can be correctly set to prevent any important and undesirable compensations or if the latter are favored with CCC. With the wire-loop task, identified compensations are shoulder abduction and trunk lateral bending (see Figure 3.3 page 31 for angles definition); they are thus the two motions to analyze in details.
Figure 3.15 shows the mean and confidence interval of the two angular trajectories, normalized in time, for each participant. Blue dashed lines represent the maximum and minimum values of each subject's natural angular trajectories. We first note that the timing of the angular variations are similar between the two modes of control. The shoulder abduction angle (up panel) is similar

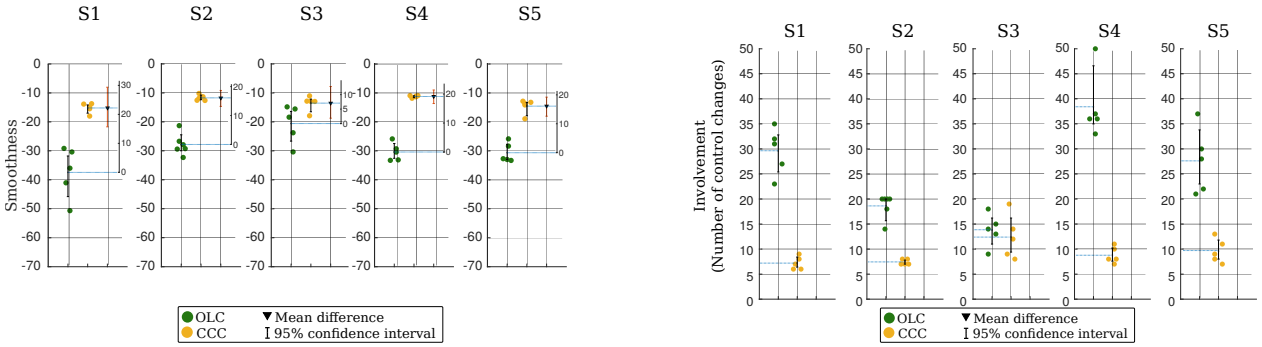

(a) Smoothness of the prosthesis motion

(b) User's involvement in the prosthesis control

Figure 3.14: Smoothness and user's involvement induced by OLC and CCC. (a) Motion smoothness measured by the spectral arc length of wrist angular velocity. The more negative, the less smooth. (b) Involvement of the subjects measured by the number of times the push-buttons are pressed (OLC) and the number of deadzone crossings (CCC).

between OLC and CCC, except for S3, for which the abduction is higher with OLC.
Contrary to shoulder abduction, trunk lateral bending is a bit heightened with CCC, especially for left-side bending (negative values). This can be explained by the fact that we chose the reference as the initial position of the subject, with the arm along the body. The amplitude of shoulder adduction was thus very limited. The latter was so difficult to perform that it was nearly not exhibited (mean shoulder adduction never goes under 6 deg, see Figure 3.15); to induce wrist pronation, the subjects used only left lateral bending (see Figure 3.16). If the arm was not along the body but a bit abducted at the reference position, wrist pronation could have been compensated by shoulder adduction. This observation points out the issue of the objective definition, which can affect the exhibited compensatory motions. It must thus be carefully defined to optimize the use of CCC.

This first experiment confirms that the human-robot coupling induced by CCC indeed allows the device to correct user's posture. Moreover, CCC performance – in terms of task realization, mo-

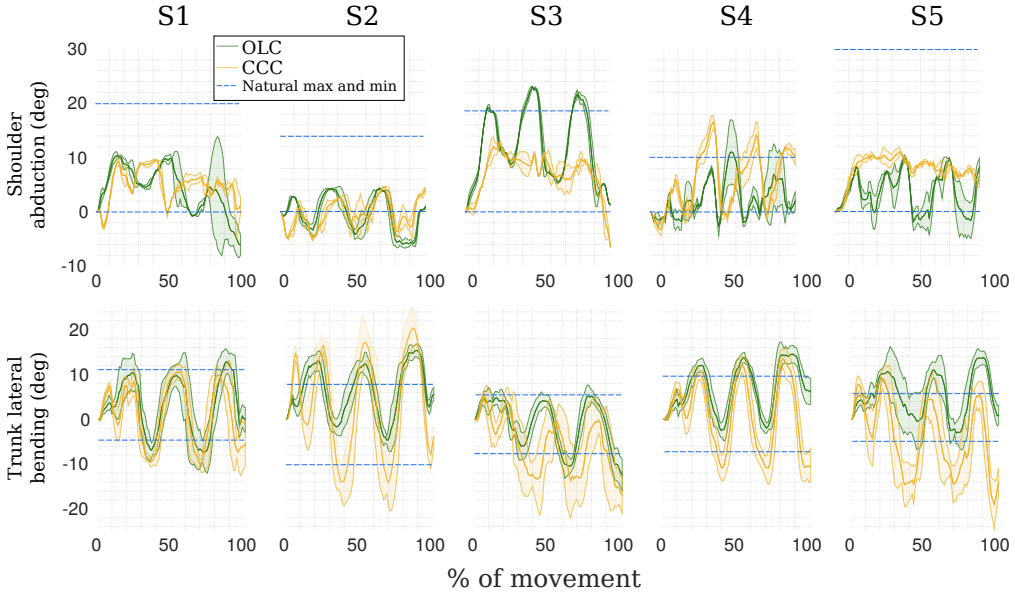

Figure 3.15: Mean and confidence interval of shoulder abduction and trunk lateral bending angular trajectories (normalized in time), for each subject. Blue dashed lines are the maximum and minimum values of the subject's natural joint trajectories.

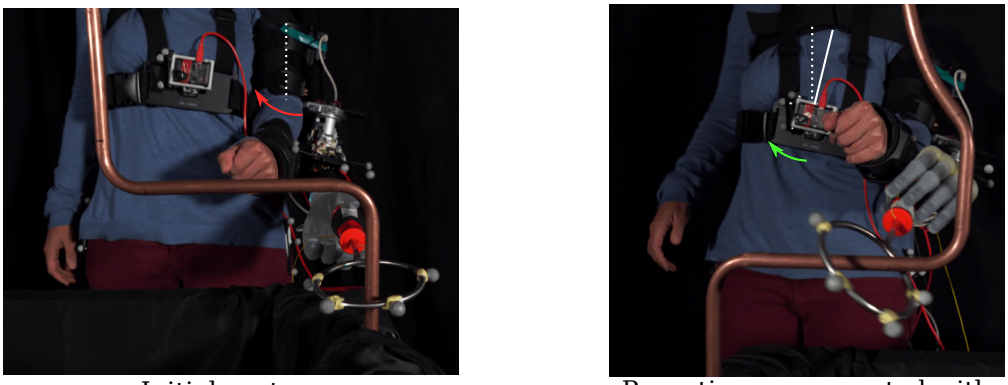

Figure 3.16: Illustration of participants behavior that can explain higher trunk lateral bending with CCC

tion smoothness, user's involvement and body compensations–, compared to a standard open-loop control, is promising.

3.3.3 Preliminary evaluation with amputated participants

This work has been published in Proceedings of the 5th International Symposium on Wearable Robotics (WeRob) [183].

The last encouraging results call for a test with amputated subjects and a comparison with true myoelectric control. A second experiment was thus performed, in collaboration with the Institut Régional de Réhabilitation (IRR) UGECAM Nord-Est of Nancy, with two transradial amputees, who were both regular prosthesis users, used to proportional myoelectric control for 2 DOF (hand and wrist), for several years.

Materials and Methods

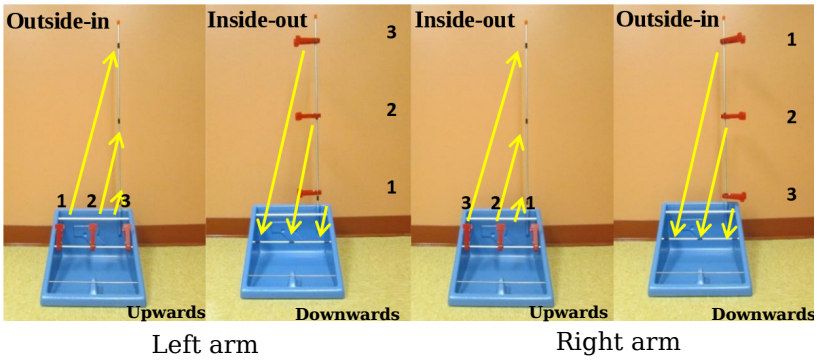

(a) Order of the pins to move

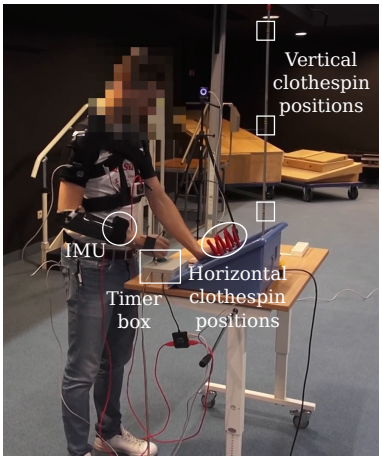

(b) Set-up

Figure 3.17: Refined Rolyan Clothespin test. (a) Pins order and (b) set-up with transradial amputees, controlling wrist pronosupination either with proportional myoelectric control or with CCC

The task proposed was the Refined Rolyan Clothespin test [184, 185], a standard upper limb functional test. It consists in bringing three clothespins, initially located on an horizontal bar, to a

vertical bar and vice-versa. The order of pins to move is predefined to facilitate inter-subjects analysis (see Figure 3.17(a)). Both grasping and wrist pronosupination are required to properly achieve this task. The Rolyan was successively performed with the usual myoelectric control of each participant and with CCC. For CCC, the participants' wrist rotator was replaced with one from the laboratory, including an encoder, and controlled with an external Raspberry Pi 3©. As CCC cannot be implemented for the hand (see Section 3.2), the usual myoelectric control of each participant was conserved for the grasping function. For this experiment, θ_{fa} was obtained with an IMU located on the prosthetic forearm (instead of an OptiTrack marker as previously), that sent quaternions in real time to the Raspberry Pi 3©. The OptiTrack motion capture system was used for post-experiment analysis of body motions (see Figure 3.17(b)), which was conducted with Matlab Mathworks ® scripts.
The Rolyan was performed 5 times with each control mode and without any specific training session. For CCC, a brief explanation was given to the participants: they were told that the prosthetic wrist would move depending on their body compensations. The reference posture was defined as the initial one: standing, with the arm along the body, with no constraint on the elbow position. In light of the previous observation on the significance of the objective definition, the subjects were asked to begin with the arm slightly abducted. Before each trial and between upwards and downwards motions, they had to press a push-button as a timer, with their prosthetic hand. This experiment was carried out in accordance with the recommendations of Université Paris Descartes ethic committee CERES, who approved the protocol (NIRB: 20163000001072). All participants gave their written informed consent in accordance with the Declaration of Helsinki.

Results
As above, prosthetic control performance is assessed on the task achievement and on wrist and compensatory motions.

Task performance

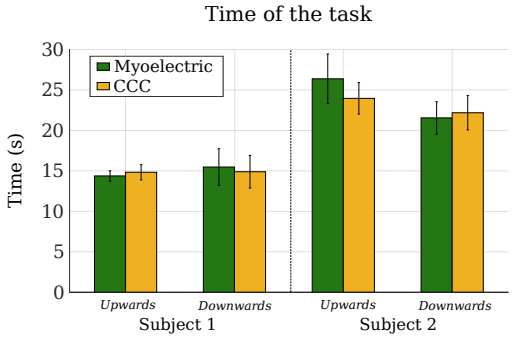

Figure 3.18: Time of the task of the two transradial amputated participants, for the Refined Rolyan Clothespin test.

The Refined Rolyan Clothespin test is assessed with the time of the task, which was measured distincly for upwards and downwards motions. Figure 3.18 shows the mean of the time over trials, for the two control modes and both subjects. The total time for Subject 1 (around 30s) is comparable to the time obtained with transradial users in [185]; the one of Subject 2 is a bit higher. For both participants, the time is clearly similar between the direction of the motion (upwards or downwards) and the control modes. It can also be noticed that the standard deviation is small for both control modes, which indicates that there is no noticeable learning phase. This is particularly noteworthy for CCC, which was totally unknown from the participants. CCC is thus as good as myoelectric control to complete the task although it was completely new for the participants.

Wrist motions

Figure 3.19 shows the mean and CI of the wrist pronosupination angular trajectory, normalized in time, for the two control modes and both subjects. The timing of the variations is very similar between myoelectric and CCC. For Subject 2, the amplitudes are also very close; for Subject 1, the amplitude with CCC is a bit smaller than the one with myoelectric control. Actually, it seems that the wrist is over-used with myoelectric since a rotation of 90 deg (obtained with CCC) is widely sufficient to perform the Rolyan task correctly. CCC would allow a finer control of the prosthetic joint. Motion smoothness is not significant here because the spectral arc length is only meaningful for discrete movements (like reaching or circle-drawing) [186], which clothespin rearrangement is not. Even if smoothness of a rythmic movement can be computed by segmenting it into discrete sub-movements, this procedure is not really relevant here. Indeed, the segmentation is far from being obvious because subjects made many sub-movements during clothespin positionning.

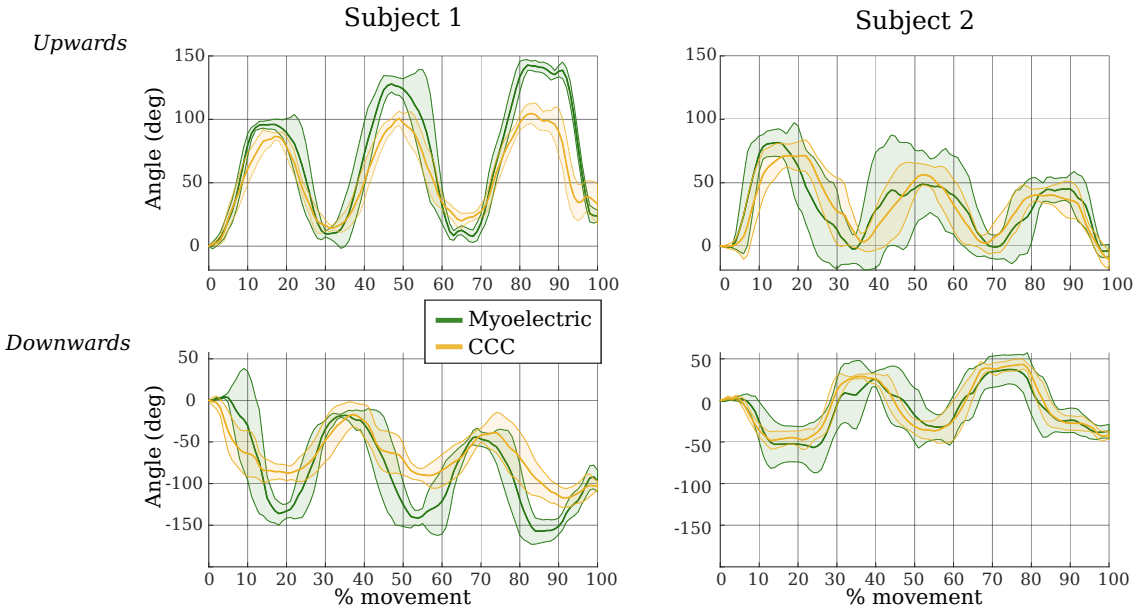

Figure 3.19: Mean and confidence interval of prosthetic wrist pronosupination trajectory (normalized in time), for myoelectric control and CCC, for the two transradial amputated participants.

Body compensations

With the Refined Rolyan clothespin test, subjects have much more freedom to move, compared to the Cybathlon wire-loop task; there is no imposed trajectory. It is thus more delicate to know whether, among the three trunk angles, one is especially responsible for pronosupination compensations, as was done for the wire-loop task. Shoulder abduction and all three trunk angles are thus analyzed to confirm that, for this task and with amputated people, CCC does not enhance compensatory motions. As there is no natural reference here, they are only compared to the ones exhibited with myoelectric control. We first analyze the maximum ROM of shoulder abduction and the three trunk angles (flexion, rotation and lateral bending) with myoelectric control and CCC respectively (see Figure 3.20). The maximum is computed over all trials and motion directions (upwards or downwards). For each participant, this maximum value is similar between myoelectric and CCC, showing that the latter does not enhance compensatory motions compared to myoelectric. For both control modes, the ROM stays in acceptable ranges [187]. However, even similar between control modes, joint motion strategies differ between the two subjects: Subject 2 solicited his shoulder and trunk much more than Subject 1 (+ 20 deg for the shoulder and + 10 deg for the trunk angles). Collecting data with more participants would allow us to have an overview of these strategies.
To have a compact metric to compare control modes at a glance, the difference between myoelectric

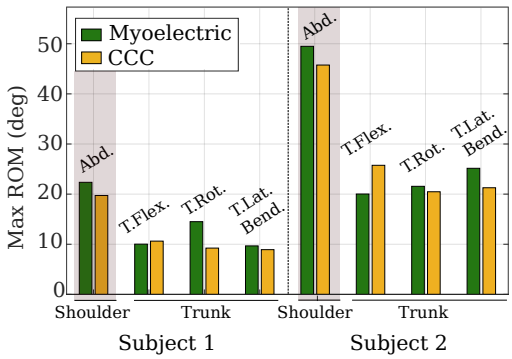

Figure 3.20: Body compensations: maximum ROM over trials and direction of motion of shoulder abduction (Abd.), trunk flexion (T.Flex.), rotation (T.Rot.) and lateral bending (T.Lat.Bend.).

and CCC maximum ROM, over all trials, is computed:

$$\delta = max_{trials}(ROM_{myo}) - max_{trials}(ROM_{CCC}) \tag{3.3}$$

It was decided to keep apart the two direction of motions here, to allow a more detailed analysis. Figure 3.21 shows δ for shoulder abduction and trunk angles. As visible on Figure 3.20, the difference of compensations between myoelectric and CCC is small (maximum 10 deg), with slightly more compensations with myoelectric, except for Subject 2 trunk flexion for upwards motions and Subject 2 shoulder abduction and trunk lateral tilt for downwards motions. This means that Subject 2 tended to solicit more his shoulder and trunk with CCC than with myoelectric for downwards motions. These compensations were yet not higher than compensations with myoelectric for upwards motions, since the overall maximum ROM is obtained with myoelectric, as illustrated on Figure 3.20. CCC thus does not heighten body compensations compared to myoelectric control when used with a real UL prosthesis.

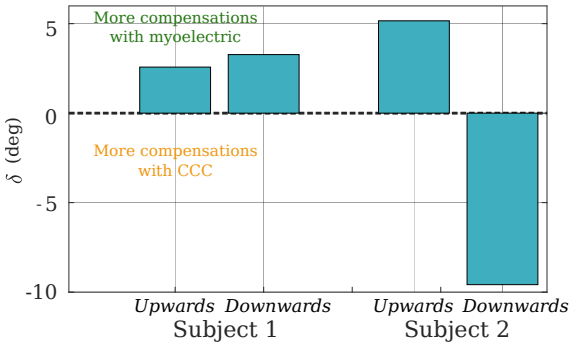

(a) δ for shoulder abduction/adduction

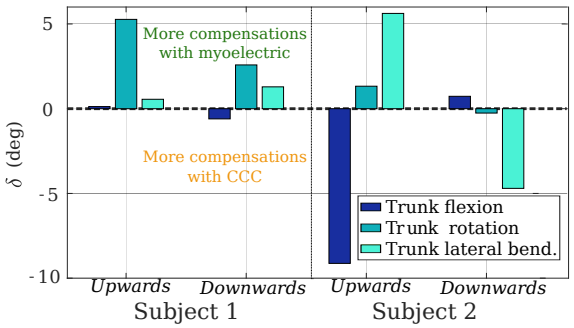

(b) δ for trunk angles

Figure 3.21: Body compensations: δ is the difference between the maximum ROM with myoelectric and the maximum ROM with CCC. (a) Shoulder abduction. (b) Trunk angles. Positive δ means that the ROM with myoelectric control is higher (more compensations).

Validation of the concept of Compensations Cancellation Control

This evaluation with amputated participants confirm and extend the results of Section 3.3.2. The concept of CCC – closing the prosthesis control loop with body compensations – is efficient in real life: the induced human-robot coupling allows the prosthesis to correct its user's posture while s/he is performing a task, and the body compensations are not enhanced even if they are input of the controller. CCC for wrist pronosupination was successfully

tested on two very different tasks (constraint path-tracking with the Cybathlon wire-loop, and free reaching and positionning with the Refined Rolyan Clothespin test), which shows the versatility of this control scheme. Indeed, as the prosthesis function is not to perform a specific task in space but to correct its user's posture, the range of possible motions is much larger. CCC implemented for wrist pronosupination is also valid for many subjects, able-bodied and amputated, without any individualization or algorithm training, which is a great benefit. The two transradial amputees also reported that CCC reduces the cognitive load, compared to myoelectric control, when controlling the prosthesis.

3.4 Chapter summary

Albeit negative on the long term, body compensations are often exhibited by prosthesis users as they allow them to perform a task or correct prosthesis position or motions in an easier and faster way than with prosthetic control. We thus identify them as accessible error messages, which indicate that the UL prosthesis position is not the one desired by the user. Instead of trying to reduce them with decorrelated control schemes, I proposed to use them to close the control loop at the prosthesis level. Once some compensations for wrist pronosupination and elbow flexion were identified, the proposed concept was described: while the user takes care of the end-effector task, the prosthesis regulates the human posture to avoid significant compensatory motions. A first feasibility study for wrist pronosupination control was conducted, both with able-bodied and transradial amputated participants. In spite of the simple formulation of the control law, the results were very promising and showed that the coupling created by CCC allows to achieve different tasks with the prosthesis, without increasing body compensations.

Chapter 4

Compensations Cancellation Control: general formulation

The previous chapter described how it is proposed to employ body compensations of the user to close the prosthesis control loop. CCC has then been implemented to control prosthetic wrist pronosupination. Two evaluations, conducted with able-bodied and amputated participants, confirm the potential of this concept and call for further exploration of compensations usage for a prosthetic closed-loop controller. How then to extend CCC to multiple joints control? In this chapter, a theoretical framework for a unified control of all intermediate prosthetic joints is proposed.

4.1 Model and control law

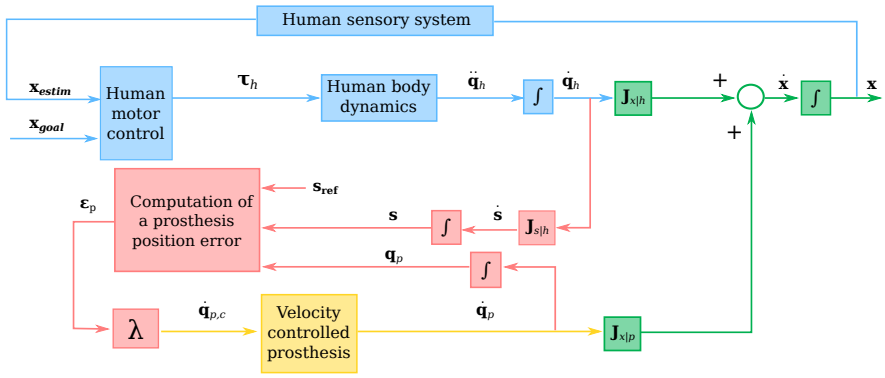

Figure 4.1: Block diagram of CCC. x, x_{goal} and x_{estim} are the real end-effector position, the desired one and the one estimated by the human sensory system, respectively. $\dot{q}_{p,c}, \dot{q_p}, q_p$ are the command prosthesis joint velocity, the prosthesis joint velocity and position respectively. τ_h is the torque of the human joints; $\ddot{q_h}, \dot{q_h}, q_h$ are the acceleration, velocity and position of the human joints, respectively. ϵ_p is the prosthesis position error and λ a scalar gain. s_{ref}, s and $\dot{s}$ are the reference sensor signal, the current sensor signal and its velocity respectively. $\mathbf{J}_{x|h}$ and $\mathbf{J}_{x|p}$ are the jacobian matrices mapping the human and the prosthesis joint movements into end-effector movements

As explained in Section 3.2, CCC relies on the hypothesis that the user correctly positions the hand, while the prosthesis is in charge of her/his posture. We could nearly consider that **it is the prosthesis that controls the user** and not the opposite: prosthetic joint motions aim at maintaining the user at the objective posture. The solution exposed in the previous Chapter, that maps the prosthesis pronosupination to the body compensations, is very specific for the wrist joint. To generalize CCC for the control of any intermediate prosthetic joint and find an appropriate mapping between prosthesis motions and body compensations, the human and prosthesis kinematics are modeled as multi-joints and linear (see Figure 4.1).

The human kinematic chain and the prosthesis one are serial (similar to Equation 2.1):

$$\dot{\mathbf{x}} = \mathbf{J}\dot{\mathbf{q}} = \begin{pmatrix} \mathbf{J}_{x|h} & \mathbf{J}_{x|p} \end{pmatrix} \begin{pmatrix} \dot{\mathbf{q}}_h \\ \dot{\mathbf{q}}_p \end{pmatrix} = \mathbf{J}_{x|h}\dot{\mathbf{q}}_h + \mathbf{J}_{x|p}\dot{\mathbf{q}}_p \tag{4.1}$$

where $\mathbf{q}_h$ and $\mathbf{q}_p$ are the vectors of human and prosthesis joint positions respectively, $\mathbf{J}_{x|h}$ and $\mathbf{J}_{x|p}$ the jacobian matrices mapping the human and the prosthesis joint movements into end-effector movements, and $\dot{\mathbf{x}}$ is a parametrization of the user's end-effector (subscript e) position/orientation with respect to a fixed frame (subscript 0). In other words, $\dot{\mathbf{x}}$ is a parametrization of the twist $\mathcal{V}_{e/0} = \begin{pmatrix} v_{e/0} & \omega_{e/0} \end{pmatrix}$ expressed at an arbitrary point E of the end-effector:

$$\dot{\mathbf{x}} = \mathbf{J}_{par_x}\mathcal{V}_{e/0} \tag{4.2}$$

$\mathbf{J}_{par_x}$ denoting the parametrization matrix.
Starting from here, I will now detail the three steps of the control: (i) human posture measurement and analysis, (ii) prosthesis error computation, (iii) generation of a prosthesis motion.

Human posture measurement and analysis
The human posture is measured by a set of sensors, attached to the human body and not on the prosthesis (the motion of the prosthesis have no direct effects on the measures). Any change of posture induces a change in the sensor signals $\mathbf{s}$, modelled as:

$$\dot{\mathbf{s}} = \mathbf{J}_{s|h}\dot{\mathbf{q}}_h \tag{4.3}$$

The posture analysis allows to detect compensatory movements, which are defined as deviations from the objective posture. This objective may vary with the context. As human posture is accessed via sensor signals, the reference is also defined in term of sensors $\mathbf{s_{ref}}$; compensations are detected each time the error signal $\boldsymbol{\epsilon}_s$,

$$\boldsymbol{\epsilon}_s = \mathbf{s_{ref}} - \mathbf{s} \tag{4.4}$$

is not zero. In other words, the objective of installing a set of sensors on the prosthesis wearer is to be able of measuring a signal associated with a nominal value corresponding to a non-compensated posture. We will see in the applications how this assumption can be verified in practice.

Prosthesis error computation
As said above, the set of sensors is voluntary positioned in such a way that $\dot{\mathbf{s}}$ is not directly affected by $\dot{\mathbf{q}}_p$; it may therefore seem impossible to reduce $\boldsymbol{\epsilon}_s$ to zero by controlling the prosthesis movement. However, a coupling is operated by the subject who wears the prosthesis: if the prosthesis moves, s/he has to move in reaction in order to keep the hand at a desired $\mathbf{x}$. A movement $\dot{\mathbf{q}}_p$ of the prosthesis joints will thus generate a change of posture from the user and then a non null $\dot{\mathbf{s}}$:

$$\dot{\mathbf{s}} = \mathbf{M}\dot{\mathbf{q}}_p \tag{4.5}$$

where $\mathbf{M}$ accounts for the measured human movement generated in order to maintain $\dot{\mathbf{x}} = 0$, governed by

$$\mathbf{J}_{x|h}\dot{\mathbf{q}}_h + \mathbf{J}_{x|p}\dot{\mathbf{q}}_p = 0 \tag{4.6}$$

Obviously, the method for computing $\mathbf{M}$ strongly depends on the nature of the signal $\mathbf{s}$. We give hereafter two examples.

- Direct measurement: the wearer joint configuration is directly accessed: $\mathbf{s} = \mathbf{q}_h$. Such an option can be implemented from real time body posture tracking coupled with a skeleton reconstruction, see e.g. [188] or [189]. In this case, $\mathbf{M}$ can be computed from Equation 4.6. If $\mathbf{J}_{x|h}$ is full rank,

$$\dot{\mathbf{q}}_h = \underbrace{-\mathbf{J}_{x|h}^{-1}\mathbf{J}_{x|p}}_{\mathbf{M}}\dot{\mathbf{q}}_p \tag{4.7}$$

If the human kinematics is redundant with $n_h > 6$ DOF, a general solution is

$$\dot{\mathbf{q}}_h = -\mathbf{J}^+_{x|h}\mathbf{J}_{x|p}\dot{\mathbf{q}}_p + (I - \mathbf{J}_{x|h}\mathbf{J}^+_{x|h})\zeta \tag{4.8}$$

with ζ an arbitrary human joint velocity vector and $\mathbf{J}^+_{x|h}$ the pseudo-inverse of $\mathbf{J}_{x|h}$. A possible option is to assume that the internal human reconfiguration velocity is low, $(I-\mathbf{J}_{x|h}\mathbf{J}^+_{x|h})\zeta \approx 0$ and therefore

$$\dot{\mathbf{q}}_h \approx \underbrace{-\mathbf{J}^+_{x|h}\mathbf{J}_{x|p}}_{\mathbf{M}}\dot{\mathbf{q}}_p \tag{4.9}$$

Finally note that if the human kinematics has $n_h < 6$ DOF, then the parametrization $\mathbf{x}$ has to be chosen in such a way that $\mathbf{J}_{x|h}$ is square and of full rank, to be able to compute $\mathbf{M}$ from Equation 4.7.
In case the wearer posture cannot be directly accessed, it might be possible to model the relationship between the change of sensor signal and the change of human posture as given in Equation 4.3. In this case, $\mathbf{M} = -\mathbf{J}_{s|h}\mathbf{J}^+_{x|h}\mathbf{J}_{x|p}$.

- Measurement of stump position/orientation: a second example is when $\mathbf{s}$ comes from a sensor that measures the position and orientation of the prosthesis base body (i.e. the human stump, subscript t). In this case, $\mathbf{s}$ is a parametrization of body t position and orientation and, similarly to Equation 4.2, one has

$$\dot{\mathbf{s}} = \mathbf{J}_{par_s}\mathcal{V}_{t/0} \tag{4.10}$$

with $\mathbf{J}_{par_s}$ the parametrization matrix.
We write Equation 4.6 as

$$\mathcal{V}_{e/0} = \mathcal{V}_{e/t} + \mathcal{V}_{t/0} = 0 \tag{4.11}$$

to get

$$\dot{\mathbf{s}} = -\mathbf{J}_{par_s}\mathcal{V}_{e/t} = \mathbf{J}_{par_s}\mathcal{V}_{t/e} \tag{4.12}$$

Considering now the prosthesis *backwards*, i.e. with the hand as the base body and the stump as its end-effector, one can straightforwardly obtain its natural jacobian matrix defined by

$$\mathcal{V}_{e/t} = \mathbf{J}_N(\mathbf{q}_p)\dot{\mathbf{q}}_p \tag{4.13}$$

We finally obtain

$$\dot{\mathbf{s}} = \underbrace{\mathbf{J}_{par_s}\mathbf{J}_N(\mathbf{q}_p)}_{\mathbf{M}}\dot{\mathbf{q}}_p \tag{4.14}$$

Note that the model of $\mathbf{M}$ depends only on the prosthesis kinematics and the parametrization of the sensor signal.

Generation of a prosthesis motion
The last step consists in generating a joint velocity command from the prosthesis error $\boldsymbol{\epsilon}_p$ as followed:

$$\dot{\mathbf{q}}_{p,c} = \lambda Z_{q_0}(\boldsymbol{\epsilon}_p) = \lambda Z_{q_0}\left(\mathbf{M}^+\boldsymbol{\epsilon}_s\right) \tag{4.15}$$

with λ a scalar gain and Z_{q_0} a deadzone function centered around 0 with a width of $2q_0$. As observed in Section 3.2, generating a velocity command is much more appropriate than generating a position command since it avoids a rigid link between prosthesis and human joint positions. To make CCC operational, three functions or parameters have to be determined: $\mathbf{M}$, the mapping between the sensor error signal and the prosthesis error; the gain λ, which can impact the stability of the human-robot system, and the width of the deadzone q_0. A great choice of sensors is also available; practical issues (such as cost, number of sensors, wearability) will obviously matter.

4.2 Simulation examples

The CCC formulation described above is very general. Before implementing and adapting it to a real human-and-prosthesis system, let us consider some simulation examples in simple situations: we will consider robotic systems, with a well-defined kinematics, composed of a distal part controlled with CCC from the motions of a proximal part. The coupling between robotic parts and the stability of the entire system will be carefully analyzed. The bandwidth of the proximal part is taken as 2Hz, the one observed for human subjects [190].

4.2.1 Linear 2P

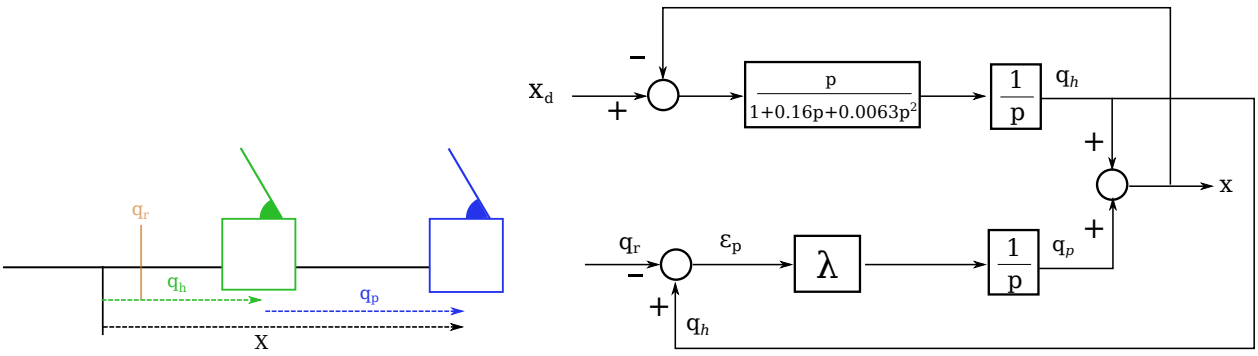

(a) Illustration of the 2-DOF system.

(b) Block diagram of the system, as implemented in Simulink, Matlab Mathworks ®.

Figure 4.2: Linear 2P example: (a) illustration of the system and (b) block diagram.

The first example is a 2-DOF linear system, redundant, composed of two slide links in series (see Figure 4.2(a)). It has to perform a 1D translation task, with its two DOF q_h, the proximal part, and q_p, the distal part (q_h and q_p notations are conserved to match the ones of the previous Section). Noting x the coordinate, the kinematics of the system is:

$$x = q_h + q_p \tag{4.16}$$

The aim of the task is to bring x, the end-effector, to a desired position, x_d. The controller of q_h is chosen as a second order with a cut-off frequency at 2Hz (transfer function $\frac{p}{1+0.16p+0.0063p^2}$); q_p is controlled with CCC from q_h. The "compensations" of the first joint is any position different from the reference q_r. In this ideal example, q_h is not measured with a sensor but is directly and precisely accessed ($s = q_h$). We thus have $J_{x|h} = J_{x|p} = J_{s|h} = 1$, $M = -1$ and $\epsilon_p = q_h - q_r$.
This system was implemented in Simulink, Matlab Mathworks ®, following the block diagram of Figure 4.2(b) with a fixed time step of 0.0001. x_d was set to 1, q_h and q_p are initially set to 0. On Figure 4.3, an example of x, q_h and q_p evolution is shown, with λ set to 1 and two different reference q_r. The coupling between q_h and q_p is obvious: the task is firstly achieved with q_h, which goes back to q_r once supplanted by q_p. x_d is reached after a small overshoot, due to the response time of q_h controller. Note that the behaviour of the system is similar whatever the value of q_r.
It could be now of interest to study the influence of λ on the system stability. Intuitively, it can be anticipated that if λ is too high, q_p will move so quickly that q_h controller will not manage to stabilize at q_r; if λ is too low, CCC is not beneficial because the task will be mainly achieved with compensations. The response of the system is thus computed with $q_r = 0$ and λ varying between 0 and 14s^{-1}. Results are displayed Figure 4.4. When $\lambda = 0\text{s}^{-1}$, there is no coupling, the task is only performed by q_h. The more λ increases, the higher is the overshoot, until the system becomes completely unstable, which happens for $\lambda \geqslant 12\text{s}^{-1}$. When $\lambda = 12\text{s}^{-1}$, the system permanently oscillates around q_r; for higher values, it diverges. This confirms that **the value of the gain must be carefully determined for CCC to properly work**; in particular, a high gain destabilizes the coupling.

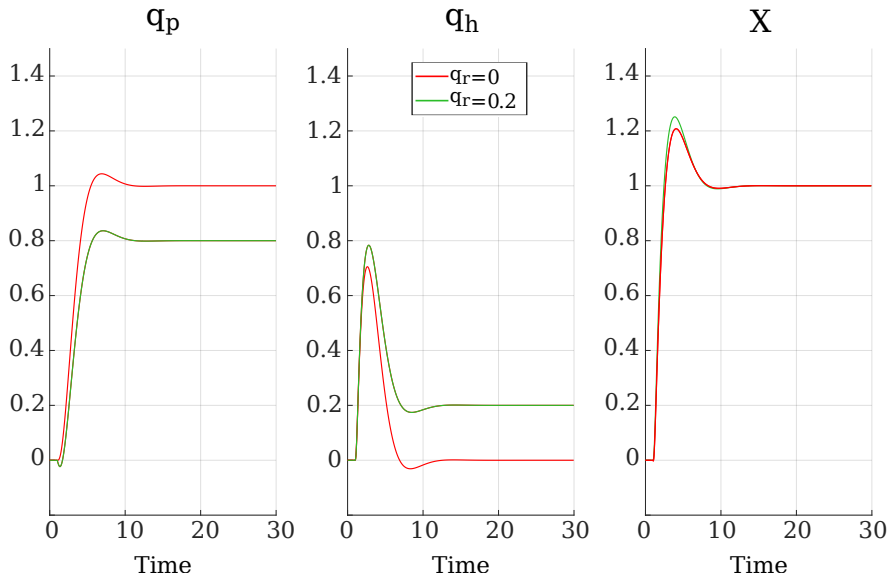

Figure 4.3: Example of responses of the linear 2P system, with $\lambda = 1$, $x_d = 1$ and $q_r = \{0; 0.2\}$

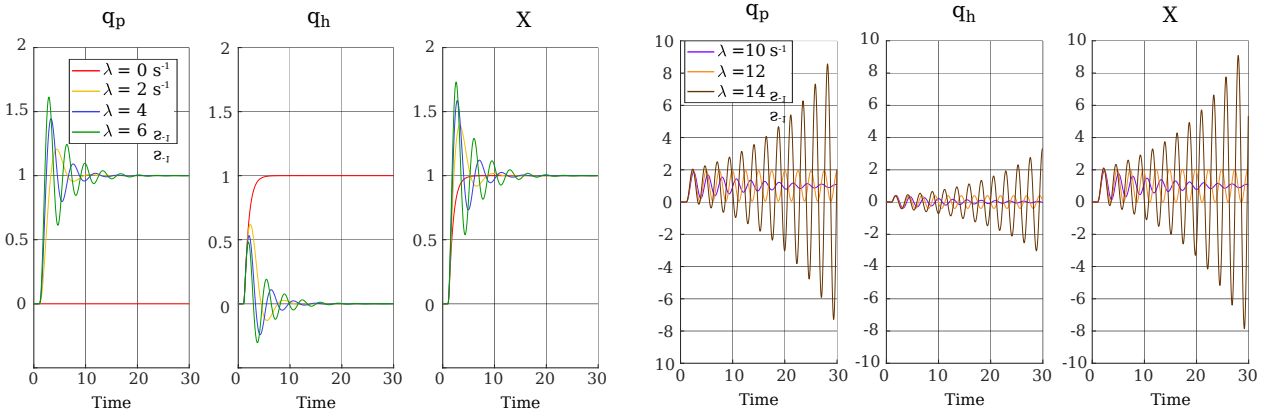

(a) Response with $\lambda = \{0; 2; 4; 6\}$

(b) Response with $\lambda = \{10; 12; 14\}$

Figure 4.4: Stability study of the linear 2P system, depending on the value of the gain λ. $q_r = 0$ and $x_d = 1$.

4.2.2 Planar 3R

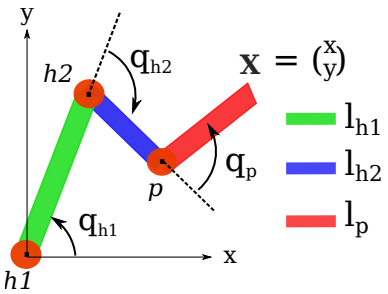

(a) Sketch of the planar 3R system, with angles and lengths definitions.

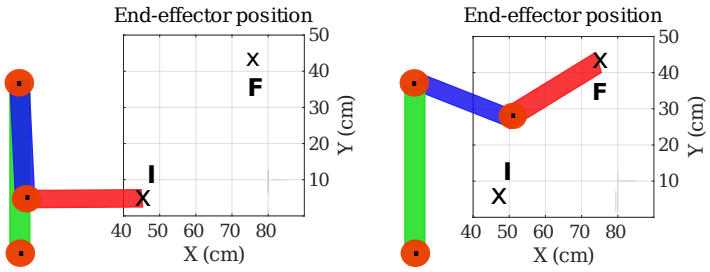

(b) Illustration of the reaching task, with the planar 3R system.

Figure 4.5: Model of a reaching task with a planar 3R system. (a) Definition of the parameters. (b) Illustration of the reaching task, without any compensations. I: initial position. F: final position.

The second example is a planar 3R; q_{h1}, q_{h2} are the proximal part and q_p is the distal part (see Figure 4.5(a)). The task is a reaching task in 2D. CCC is implemented to control q_p.
With $\mathbf{x} = \begin{pmatrix} x \\ y \end{pmatrix}$ the current position of the end-effector, l_{h1}, l_{h2} and l_p the lengths of the three segments (as indicated Figure 4.5(a)), we have:

$$\mathbf{x} = \begin{pmatrix} l_{h1}\cos(q_{h1}) + l_{h2}\cos(q_{h1}+q_{h2}) + l_p\cos(q_{h1}+q_{h2}+q_p) \\ l_{h1}\sin(q_{h1}) + l_{h2}\sin(q_{h1}+q_{h2}) + l_p\sin(q_{h1}+q_{h2}+q_p) \end{pmatrix} \tag{4.17}$$

and

$$\begin{aligned} \dot{\mathbf{x}} &= \begin{pmatrix} -l_{h1}\sin_{h1} - l_{h2}\sin_{h1h2} - l_p\sin_{h1h2p} & -l_{h2}\sin_{h1h2} - l_p\sin_{h1h2p} \\ l_{h1}\cos_{h1} + l_{h2}\cos_{h1h2} + l_p\cos_{h1h2p} & l_{h2}\cos_{h1h2} + l_p\cos_{h1h2p} \end{pmatrix} \begin{pmatrix} \dot{q}_{h_1} \\ \dot{q}_{h_2} \end{pmatrix} + \begin{pmatrix} -l_p\sin_{1h2p} \\ l_p\cos_{h1h2p} \end{pmatrix} \dot{q}_p \\ &= \mathbf{J}_{x|h} \begin{pmatrix} \dot{q}_{h_1} \\ \dot{q}_{h_2} \end{pmatrix} + \mathbf{J}_{x|p}\dot{q}_p \end{aligned} \tag{4.18}$$

with $\sin_{h1} = \sin(q_{h1})$, $\sin_{h1h2} = \sin(q_{h1}+q_{h2})$, $\sin_{h1h2p} = \sin(q_{h1}+q_{h2}+q_p)$, and similarly for cosine function.
In this example, we consider joint *h2* as functional to perform the task, whereas joint *h1* is a compensatory joint. In other words, *h1* is redundant with *h2* and *p*, and shall not be used to perform the task with an optimal control. Correcting compensatory motions thus means moving *h1* back to its objective value, noted q_r.
The error signal is now chosen to give an example of a non-direct access to the exhaustive posture: we take the displacement of the upper extremity of segment l_{h1}. The error is thus

$$\epsilon_s = s_{ref} - s = 2l_{h1}\sin(\frac{q_r - q_{h1}}{2}) \tag{4.19}$$

In the case considered here, the kinematics of the system is perfectly known, we can precisely assess $\mathbf{M}$.
Following the approach presented in Section 4.1, we write

$$\dot{s} = \mathbf{J}_{s|h}\dot{\mathbf{q}}_h = \begin{pmatrix} -l_{h1}\cos(\frac{q_r - q_{h1}}{2}) & 0 \end{pmatrix} \begin{pmatrix} \dot{q}_{h1} \\ \dot{q}_{h2} \end{pmatrix} \tag{4.20}$$

As the *h1-h2* chain is not redundant, $\mathbf{J}_{x|h}$ is square and: $\mathbf{M} = -\mathbf{J}_{s|h}\mathbf{J}_{x|h}^{-1}\mathbf{J}_{x|p}$ where

$$\mathbf{J}_{x|h}^{-1} = \frac{1}{det(\mathbf{J}_{x|h})} \times \begin{pmatrix} l_{h2}\cos_{h1h2} + l_p\cos_{h1h2p} & l_{h2}\sin_{h1h2} + l_p\sin_{h1h2p} \\ -l_{h1}\cos_{h1} - l_{h2}\cos_{h1h2} - l_p\cos_{h1h2p} & -l_{h1}\sin_{h1} - l_{h2}\sin_{h1h2} - l_p\sin_{h1h2p} \end{pmatrix} \tag{4.21}$$

$$\mathbf{J}_{x|p} = \begin{pmatrix} -l_p\sin_{h1h2p} \\ l_p\cos_{h1h2p} \end{pmatrix} \tag{4.22}$$

and finally,

$$\dot{q}_{p,c} = \lambda Z_{q_0}\left(\mathbf{M}^{-1}\epsilon_s\right) = \lambda Z_{q_0}\left(-\left(\mathbf{J}_{s|h}\mathbf{J}_{x|h}^{-1}\mathbf{J}_{x|p}\right)^{-1}\epsilon_s\right) \tag{4.23}$$

with $\mathbf{J}_{s|h}$, $\mathbf{J}_{x|h}^{-1}$ and $\mathbf{J}_{x|p}$ given by Equations 4.20, 4.21 and 4.22 respectively. In this case, the deadzone threshold q_0 is set to 0.
To test this formulation, this example is implemented in Matlab, Mathworks ®. q_p is controlled with CCC, following the formulation established from Equations 4.20 to 4.23, with $q_r = 0$. q_{h1} and q_{h2} are controlled with standard inverse kinematics, as a non-redundant 2D system, according to

$$\dot{\mathbf{q}}_h = \begin{pmatrix} \dot{q_{h1}} \\ \dot{q_{h2}} \end{pmatrix} = \mathbf{J}_{x|h}^{-1}\mathbf{v} \tag{4.24}$$

where $\mathbf{v} = k(\mathbf{x}_d - \mathbf{x})$, with k a gain set to 2 and $\mathbf{x}_d$ the position of the target to reach.
This CCC formulation is also compared to another scheme where the whole system is controlled with standard inverse kinematics for a redundant system, with a postural condition on the more proximal DOF, q_{h1}, according to

$$\dot{\mathbf{q}} = \begin{pmatrix} \dot{q_{h1}} \\ \dot{q_{h2}} \\ \dot{q_p} \end{pmatrix} = \mathbf{J}^{+}\mathbf{v} + (I_3 - \mathbf{J}^{+}\mathbf{J}) \begin{pmatrix} -\gamma q_{h1} \\ 0 \\ 0 \end{pmatrix} \tag{4.25}$$

with $\mathbf{J}$ the jacobian of the entire system, $\mathbf{v} = k(\mathbf{x}_d - \mathbf{x})$, I_3 the 3x3 identity matrix and $\gamma = 5$. This control scheme is to illustrate the achievement of the task with a redundant system, where the motion of *h1* is penalized (compensatory motion).
For the simulation, the values of the length parameters are $l_{h1} = 44$, $l_{h2} = 37$, $l_p = 48$, the initial values of the angles are $q_{h1} = \frac{\pi}{2}$, $q_{h2} = \pi$, $q_p = \frac{\pi}{2}$ and q_r is set to $\frac{\pi}{2}$. The target to reach is $\mathbf{x}_d = \begin{pmatrix} 75 \\ 44 \end{pmatrix}$, which is attainable with a negligible q_{h1} (see Figure 4.5(b)). The time step is 0.01 and the simulation loop is stopped when the joint velocities fall under a given threshold (set to 0.02 rad.s^{-1}).

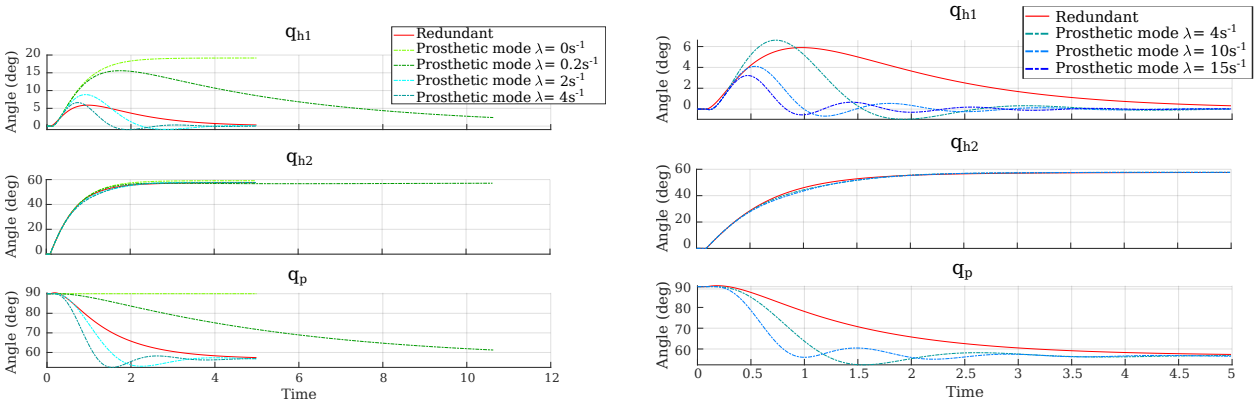

(a) Evolution of the planar 3R system with redundant model and CCC with $\lambda = \{0; 0.2; 2; 4\}$

(b) Evolution of the planar 3R system with redundant model and CCC with $\lambda = \{4; 10; 15\}$

Figure 4.6: Results of CCC applied to planar 3R system. (a) with $\lambda = \{0; 0.2; 2; 4\}$; (b) with $\lambda = \{4; 10; 15\}$

Figure 4.6 shows the trajectories of q_{h1}, q_{h2} and q_p obtained with the redundant model and with q_p controlled with CCC, with varying gain λ. First thing to notice is that q_{h2} is very similar, between CCC and the redundant model, whatever the value of λ. q_{h1} and q_p are coupled in such a way that the **kinematics of the remaining part of the system stays unchanged**. Translating to human application, this is a great advantage since it means that no new motion strategies would need to be learnt. Second, we see that, when $\lambda = 0\text{s}^{-1}$, the whole task is performed with q_{h1}; then, the higher λ, the lower q_{h1} since it is replaced by q_p. Yet, here again, the value of λ has a great influence on the system stability: for $\lambda \leq 4\text{s}^{-1}$, the system is stable; for $\lambda > 4\text{s}^{-1}$, it starts oscillating around q_r. It confirms the necessity to study more in depth the system stability with λ to identify the possible range of the gain. A last element to observe is the time required to stabilize q_{h1} and q_p. With a low value of λ (0.2s^{-1} in this case), the angular velocities meet the stop criteria after an increased delay compared to the one obtained with the other values of λ. The global task (reaching the target) is achieved in a similar timing but *h1* and *p* keep moving until stabilization of the robot. A too low value for λ indeed requires the robot to wait for q_p to reach the position that allows a non-compensatory posture for *h1*. There is indeed a trade-off to find between stability and

velocity. On Figure 4.6, it seems that the best value for λ is around $2s^{-1}$, since it allows a response of the system very close to the redundant model with postural condition on *h1*.

These two examples illustrate the coupling created by CCC between proximal and distal joints, as well as the role of λ on the response of the non-"prosthetic" (proximal) joints and on the stability of the considered robotic systems. A theoretical stability study has thus been conducted to get general conditions for an appropriate choice of λ.

4.3 Stability study

This theoretical study was performed by Alexis Poignant, who did an internship in the lab, under the supervision of Guillaume Morel, Nathanaël Jarrassé and myself.

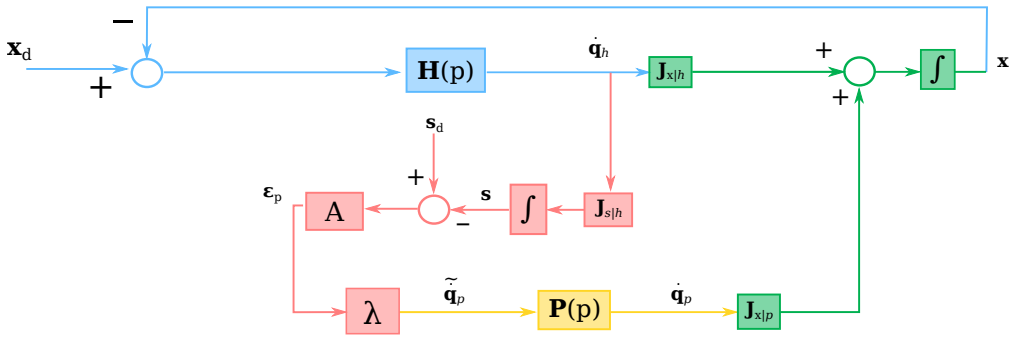

Figure 4.7: Block diagram of the dual robot system, with the distal part controlled with CCC. $\mathbf{H}(p)$ is the closed-loop transfer function of the proximal part, $\mathbf{P}(p)$ is the transfer function of the distal part, $\mathbf{A} = \mathbf{M}^+$, $\mathbf{J}_{x|h}$, $\mathbf{J}_{x|p}$, $\mathbf{J}_{s|h}$ and λ are defined in the equations developped Section 4.1

The general control scheme of CCC (see Figure 3.7) cannot be analyzed with standard tools of automation, because of the highly non-linear human system and the unknown transfer function of the human-robot coupling. It is thus proposed to consider, as in previous examples, a robotic system composed of a proximal robot coupled to a distal one; we have two linear systems, following the scheme of Figure 4.7.
We note $\mathbf{H}(p)$ the closed-loop transfer function of the proximal part (playing the role of human subject), $\mathbf{P}(p)$ the transfer function of the distal part (playing the role of the prosthesis) and $\mathbf{A} = \mathbf{M}^+$ the mapping matrix between $\boldsymbol{\epsilon}_p$ and $\boldsymbol{\epsilon}_s$. λ, $\mathbf{J}_{x|h}$, $\mathbf{J}_{x|p}$ and $\mathbf{J}_{s|h}$ are the gain of CCC and the different jacobian matrices respectively, as defined in Section 4.1. In the first instance, we take $\mathbf{P}(p) = 1$, assuming that the response time of the distal part is very short compared to the response time of the proximal part (in the human-prosthesis case considered forward, $\mathbf{P}$ indeed represents the prosthesis motors, controlled in speed with a closed-loop, whose response time is usually very short compared to human one).
As the block diagram has two inputs, the desired end-effector position/orientation $\mathbf{X}_d$, and the objective posture defined at sensors level $\mathbf{s}_d$, the superposition theorem is used: $\frac{X}{X_d}$ is first studied and then $\frac{X}{s_d}$.
Considering that $\mathbf{s}_d$ is zero, the open-loop transfer function of the entire system is

$$\left[\frac{X}{X_d}\right]_{OL} = \frac{\mathbf{H}(p)}{p}(\mathbf{J}_{x|h} - \mathbf{J}_{x|p}\mathbf{A}\mathbf{J}_{s|h}\frac{\lambda}{p}) \tag{4.26}$$

As a first step, we consider a single-input single-output case, for which there is no redundancy; Equation 4.8 has only one solution. It follows

$$\mathbf{A} = \mathbf{M}^{-1} = -\left(\mathbf{J}_{s|h}\mathbf{J}_{x|h}^{-1}\mathbf{J}_{x|p}\right)^{-1} \tag{4.27}$$

$$\text{and} \quad \mathbf{J}_{x|h} = -\mathbf{J}_{x|p}\mathbf{A}\mathbf{J}_{s|h} \tag{4.28}$$

Then, the open-loop transfer function becomes

$$\begin{aligned}\left[\frac{X}{X_d}\right]_{OL} =& \frac{\mathbf{H}(p)}{p}\mathbf{J}_{x|h}\left(1+\frac{\lambda}{p}\right) \\ =& \left[\frac{X}{X_d}\right]_{HOL}\frac{p+\lambda}{p} = \left[\frac{X}{X_d}\right]_{HOL}F(p,\lambda)\end{aligned} \tag{4.29}$$

with $\left[\frac{X}{X_d}\right]_{HOL} = \frac{\mathbf{H}(p)}{p}\mathbf{J}_{x|h}$ the open-loop transfer function of the proximal part (in blue on Figure 4.7), and $F(p,\lambda) = \frac{p+\lambda}{p}$.
For the following, MG_h, $M\phi_h$ and ω_c identify the gain margin, the phase margin and the cut-off pulse of $\left[\frac{X}{X_d}\right]_{HOL}$ respectively. The proximal part of the robotic system is given the observed bandwidth of human subjects, with a cut-off frequency, $f_c = \frac{\omega_c}{2\pi}$ that ranges from 2 to 5 Hz [190] and thus a cut-off pulse ω_c that ranges from 12.6 to 31.4 rad.s^{-1}.

Gain margin
Assuming that the dephasing induced by F is not too high, the total gain margin of $\left[\frac{X}{X_d}\right]_{OL}$ is

$$MG = MG_h + |F(\omega_c,\lambda)|_{dB} \tag{4.30}$$

As $|F(p,\lambda)| = 0dB$ for $p \gg \lambda$, a sufficient condition to respect the gain margin is

Stability condition

$$\omega_c \gg \lambda \tag{4.31}$$

Phase margin
Assuming that the cut-off pulse of the entire system is close from the one of the proximal part alone, we have

$$M\phi = M\phi_h - Arg\left(F(\omega_c,\lambda)\right) \tag{4.32}$$

with a dephasing induced by F of 90 deg when $p \ll \lambda$ and 0 deg when $p \gg \lambda$. To avoid a deterioration of the phase margin, it is thus necessary to have $\omega_c \gg \lambda$. From $\lambda = \frac{\omega_c}{10}$, a degradation of the behaviour could be observed.

If we now consider that $\mathbf{X}_d = 0$, the open-loop transfer function is

$$\begin{aligned}\left[\frac{X}{\mathbf{s}_d}\right]_{OL} &= \frac{\lambda}{p}\mathbf{J}_{x|p}\mathbf{A}\mathbf{J}_{s|h}\frac{\frac{\mathbf{H}(p)}{p}}{1+\frac{\mathbf{H}(p)}{p}\mathbf{J}_{x|h}} \\ &= \frac{\lambda}{p}\frac{\frac{\mathbf{H}(p)}{p}\mathbf{J}_{x|h}}{1+\frac{\mathbf{H}(p)}{p}\mathbf{J}_{x|h}} \\ &= \frac{\lambda}{p}\left[\frac{X}{X_d}\right]_{HCL}\end{aligned} \tag{4.33}$$

where $\left[\frac{X}{X_d}\right]_{HCL}$ is the closed-loop transfer function of the proximal part. The gain and phase margins of $\left[\frac{X}{X_d}\right]_{HCL}$ are similar to the ones of the open-loop transfer function. From the stability in $\left[\frac{X}{X_d}\right]$, we have $\lambda \ll \omega_c$ so the module is 0dB for $\omega = \lambda$ and the phase margin is -90deg. The gain margin is high since we have an integrator. The condition found above, $\omega_c \gg \lambda$, is thus also valid to ensure the stability of this loop.

This condition can be confronted to the results of the examples proposed in the previous Section. In the first one (1D translation), the cut-off frequency of the system is $f_c = 2$Hz, which corresponds to $\omega_c \approx 12.6\text{rad.s}^{-1}$. We indeed observed that the system begins to oscillate from $\lambda = 4\text{s}^{-1}$ and becomes unstable around $\lambda = 12\text{s}^{-1}$. The second example (planar 3R) is a first-order system, so it does not exactly correspond to the theoretical analysis detailed above, but oscillations of the system is also observed from $\lambda = 4\text{s}^{-1}$. These results are thus consistent with the theory, which predicts that the system response is deteriorated when λ is not small enough compared to the cut-off pulse. However, if λ is too small, the distal part will move slowly and enhance compensations, as seen in the two examples; a trade-off is thus necessary between stability of the entire system and response of the distal ("prosthetic") part.
The analysis performed above relies on many simplifications. The condition on λ yet stays valid for more complicated cases, such as a multivariate system, imperfect motors command ($\mathbf{P}(p) \neq 1$), or the addition of a deadzone. The justifications are detailed in Appendix E.

4.4 Chapter summary

Following the proof of concept of Chapter 3, a more theoretical framework was presented, which generalizes CCC to the control of several prosthetic joints simultaneously. Two simulation examples were described to apply the general formulation to simple situations. They confirmed the beneficial role of the coupling induced by CCC, but only when the parameters are correctly tuned. The stability of the considered systems indeed relied on the good choice of the gain of the integrator λ. To establish a criterion that guarantees stability, an analysis was performed on a simplified scheme; this criterion was consistent with the simulation outcomes.

Chapter 5

Validation of Compensations Cancellation Control on one prosthetic joint

Part of the work presented in this Chapter has been published in IEEE Transactions on Medical Robotics and Bionics (Early Access) [191].

A general formulation of CCC and the condition for stability with a simplified robotic system have been theoretically established in Chapter 4. The results obtained shall now be tested experimentally, with a human-prosthesis system. This validation is all the more important that many assumptions that may be correct for a robot are not for a human. A validation experiment on one joint, the elbow, is presented in this chapter: the influence of the parameters on the human-robot system stability is first analyzed, then followed by the evaluation of prosthetic elbow control with CCC on different tasks and on a large population. We aim at answer three main questions:

- is the tuning of the controller actually valid for every subject (as suggested by the theoretical study) or will a personalization be required?
- how natural is the prosthesis manipulation for a naive subject, or more precisely, is a naive subject able to use a prosthesis equipped with CCC without any explanation on the concept?
- is CCC valid to perform different tasks, as long as the objective posture stays the same?

A more complete validation, on two joints, will be the topic of Chapter 6.

5.1 Material and methods

The validation experiment described in this chapter is composed of three steps: parameters tuning with one subject, in order to study their overall influence on a human-prosthesis system behavior; a functional test on three different tasks with able-bodied subjects wearing an emulated prosthesis and a functional test on one task with a congenital arm amputee. The control law implemented in the prosthetic elbow case is first introduced, followed by the experimental set-up common to the three validation steps.

5.1.1 Control law

Applying the general formulation of CCC implies to define the matrix $\mathbf{M}$, i.e. to map prosthesis motions to sensor signals, which capture the change in user posture. In the specific case of elbow joint, we can bypass the modelling stage and directly access the prosthesis position error, ϵ_p, without the need to determine $\mathbf{M}$. Indeed, with geometrical considerations, we can get the elbow angle required to keep the prosthetic hand where the user placed it, without any body compensations. The error between this value and the current elbow angle can then be computed and used as input of the prosthesis controller.

It has been observed, in Section 3.1.2, that **a loss of elbow mobility is compensated by trunk**

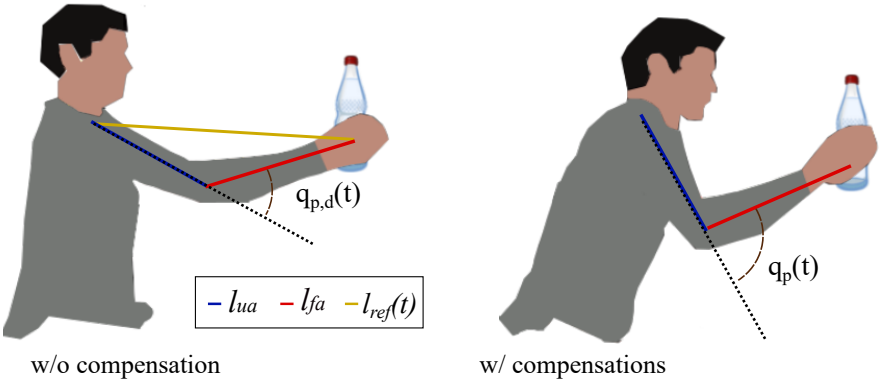

Figure 5.1: Anatomical parameters definition for the elbow CCC law

and scapula motions, which can be gathered into acromion motions. Body compensations are thus identified through the latter. Let us note $\mathbf{x}_{A_{ref}}$ the reference position of the acromion, which corresponds to a non-compensatory posture; $\mathbf{x}_{EE}(t)$ the current position of the end-effector (i.e. the hand), and $q_{p,d} \in \mathbb{R}$ the desired position of the elbow angle, corresponding to the hand at $\mathbf{x}_{EE}(t)$ and the acromion at $\mathbf{x}_{A_{ref}}$ (task achieved in a non-compensatory posture). We first estimate $l_{ref}(t)$, the distance between the acromion position in the reference posture and the current end-effector position

$$l_{ref}(t) = ||\mathbf{x}_{EE}(t) - \mathbf{x}_{A_{ref}}|| \tag{5.1}$$

where $||.||$ is the euclidian norm. Given this distance $l_{ref}(t)$, and knowing l_{ua} and l_{fa} the lengths of the subject's upper-arm and forearm (see Figure 5.1), standard inverse kinematics, in the upper-arm plane, yields:

$$q_{p,d}(t) = \pi - acos\left(\frac{l_{fa}^2 + l_{ua}^2 - l_{ref}(t)^2}{2 l_{ua} l_{fa}}\right) \tag{5.2}$$

Note that this computation requires to measure the user's limb lengths and to integrate them into the controller parameters. The prosthesis position error is thus

$$\epsilon_p(t) = q_{p,d}(t) - q_p(t) \tag{5.3}$$

with $q_p(t)$ the current prosthetic elbow angle, and the velocity of the prosthetic joint is controlled according to Equation 4.15:

$$\dot{q}_p(t) = \lambda Z_{q_0}(\epsilon_p(t)) = \lambda Z_{q_0}(q_{p,d}(t) - q_p(t)) \tag{5.4}$$

In this 1DOF case, $Z_{q_0}()$ is defined by:

$$\forall \epsilon \in \mathbb{R}, Z_{q_0}(\epsilon) = \begin{cases} 0 \text{ if } |\epsilon| \leqslant q_0 \\ \epsilon - sign(\epsilon) q_0 \text{ otherwise} \end{cases}$$

This formulation is equivalent to the one described Section 4.1, for small displacements, where ϵ_p is expressed as a function of $\boldsymbol{\epsilon}_s$, an error of posture measured by the sensors. Here, $\boldsymbol{\epsilon}_s$ could be defined as the acromion displacement to take into account both trunk and scapula compensations. We can write

$$l_{ref}(t) = ||\mathbf{x}_{EE}(t) - \mathbf{x}_{A_{ref}}|| = ||\mathbf{x}_{EE}(t) - \mathbf{x}_A(t) + \mathbf{x}_A(t) - \mathbf{x}_{A_{ref}}|| \tag{5.5}$$

where $\mathbf{x}_A(t)$ is the current position of the acromion.

With $\mathbf{x}_{EE}(t) = \begin{pmatrix} e_1 \\ e_2 \end{pmatrix}$, $\mathbf{x}_A(t) = \begin{pmatrix} a_1 \\ a_2 \end{pmatrix}$ and $\overrightarrow{\boldsymbol{x}_{A_{ref}}\boldsymbol{x}_A(t)} = -\boldsymbol{\epsilon}_s = -\begin{pmatrix} \epsilon_{s,1} \\ \epsilon_{s,2} \end{pmatrix}$, $\epsilon_{s,1} \ll 1$, $\epsilon_{s,2} \ll 1$,

Equation 5.5 is equivalent to

$$\begin{aligned} l_{ref}(t)^2 &= (e_1 - a_1 - \epsilon_{s,1})^2 + (e_2 - a_2 - \epsilon_{s,2})^2 \\ &\approx (e_1 - a_1)^2 + (e_2 - a_2)^2 - 2\left(\epsilon_{s,1}(e_1 - a_1) + \epsilon_{s,2}(e_2 - a_2)\right) \\ &\approx (l(t))^2 - 2\left(\epsilon_{s,1}(e_1 - a_1) + \epsilon_{s,2}(e_2 - a_2)\right) \end{aligned} \tag{5.6}$$

with $l(t) = ||\mathbf{x}_{EE}(t) - \mathbf{x}_A(t)||$.
Hence,

$$\begin{aligned} q_{p,d}(t) &\approx \pi - acos\left(\frac{l_{fa}^2 + l_{ua}^2 - l(t)^2}{2l_{ua}l_{fa}} + \frac{\epsilon_{s,1}(e_1 - a_1) + \epsilon_{s,2}(e_2 - a_2)}{l_{ua}l_{fa}}\right) \\ &\approx \pi - acos\left(\frac{l_{fa}^2 + l_{ua}^2 - l(t)^2}{2l_{ua}l_{fa}}\right) + \frac{\epsilon_{s,1}(e_1 - a_1) + \epsilon_{s,2}(e_2 - a_2)}{l_{ua}l_{fa}\sqrt{1 - \left(\frac{l_{fa}^2 + l_{ua}^2 - l(t)^2}{2l_{ua}l_{fa}}\right)^2}} \\ &\approx q_p(t) + \frac{\epsilon_{s,1}(e_1 - a_1) + \epsilon_{s,2}(e_2 - a_2)}{l_{ua}l_{fa}\sqrt{1 - \left[\cos(q_p(t))\right]^2}} \\ &\approx q_p(t) + \mathbf{A}\boldsymbol{\epsilon}_s \end{aligned} \tag{5.7}$$

and

$$\epsilon_p = \mathbf{A}\boldsymbol{\epsilon}_s \tag{5.8}$$

with

$$\mathbf{A} = \mathbf{M}^{-1} = \frac{1}{l_{ua}l_{fa}|\sin(q_p(t))|}\begin{pmatrix} e_1 - a_1 & 0 \\ 0 & e_2 - a_2 \end{pmatrix} \tag{5.9}$$

With this CCC formulation applied to the elbow joint, acromion (and thus trunk and scapula) motions are mapped into one prosthetic DOF motion. Note that the latter does not depend on individual compensatory motions but on the user's whole body posture. For instance, if the arm is in the sagittal plane, a flexion of the trunk or a scapula protraction will lead to an elbow extension (to straighten up the user), while a trunk lateral rotation will not lead to any elbow motion; neither elbow flexion nor elbow extension will allow to correct the user's posture in this case. However, if the arm is in the frontal plane, a trunk flexion will not lead to any elbow motion while a trunk lateral rotation will lead to elbow flexion or extension, depending on the rotation side.

5.1.2 Experimental set-up

The three stages of the validation study (parameters tuning, evaluation with able-bodied and amputated participants) have some common elements in their protocol, which are described in this Section. The specific details will be described later on, in the corresponding Sections. All three steps were carried out in accordance with the recommendations of Université Paris Descartes ethic committee CERES, which approved the protocols (NIRB: 20163000001072). The participants gave their informed consent, in accordance with the Declaration of Helsinki.
The first two experiments were performed with able-bodied participants, aged 20-24, without any previous experience on prosthetic devices. A prosthesis prototype was adapted to imitate the wearing of a prosthesis. The prototype is a 1-DOF robotic joint (actuated by a 9W Faulhaber 2232U006S, fitted with 1:1000 gear ratio reducer) controlled by a Raspberry Pi 3©, through a DC motor driver running a low level velocity control loop. The maximum angular velocity is limited to 50 deg.s^{-1} because of the actuation capacities. The device was fixed on an orthosis, attached to the participants' arm (see Figure 5.2(a)). The elbow is not backdriveable so that elbow motions of the subjects were fully controlled by the prosthesis movements, as for a prosthetic elbow. The third experiment was performed with a congenital amputee, wearing his own prosthesis which has a motorized elbow (see Figure 5.2(b))

(a) Emulated elbow prosthesis prototype for able-bodied subjects

(b) Prosthesis of the amputated subject

Figure 5.2: Prosthesis prototypes (a) mounted on an able-bodied subject's arm, in such a way that his elbow motions are totally governed by the prosthesis; (b) for the amputated subject, for which only the elbow joint was actuated

During the experiments, subjects were sitting and were asked either to follow a moving target in their sagittal plane, or to reach fixed targets in 3D space. In order to observe whether they were compensating, acromion and end-effector positions were recorded with the motion capture system OptiTrack NaturalPoint Inc. These positions were transmitted in real time to the prosthesis during the experiment to implement the proposed controller. The movements of the body segments were also recorded for post-experiment analysis, with clusters placed on the end-effector, forearm, elbow, upper-arm, right and left acromions and trunk. Two IMU were also placed one on the sternum and one on the upper-arm, to measure the humerus aperture angle in trunk frame. Post-experiment analysis was conducted with Matlab Mathworks ® scripts.
At the beginning of the experiment, the reference acromion position – corresponding to the initial one – was measured while the subjects were sitting with a vertical torso and the upper arm along their body. **No instruction nor any explanation on how CCC works were given to any subject**. They were only told that they had to focus on the achievement of the task (positioning the tip of the prosthesis) and that the prosthetic device would "move to try helping them". The targets to reach and trajectories to follow for the different experiments were materialized with a WAM® Arm (Barrett Technology).

5.2 Parameters tuning for human-in-the-loop stability

Section 4.3 shows that the choice of the gain λ is crucial for coupling dynamics and that a condition to ensure the overall system stability is $\lambda \ll \omega_c$, with ω_c the cut-off pulse of the proximal part of the system. It is now essential to test this stability condition with a human-prosthesis system, by determining λ experimentally. The proximal part of the system is now the human user (with a cut-off frequency f_c between 2 and 5 Hz) and the distal part is the prosthesis. The influence of the deadzone must also be validated in real situation, with user in the loop.

5.2.1 Specific protocol

One able-bodied subject participated in the experiment. The participant had to follow a target moving along a 20 cm straight line, carried by the WAM® Arm. When arrived at one extremity of the line, the WAM® paused for 2 seconds before leaving again in the opposite direction (see Figure

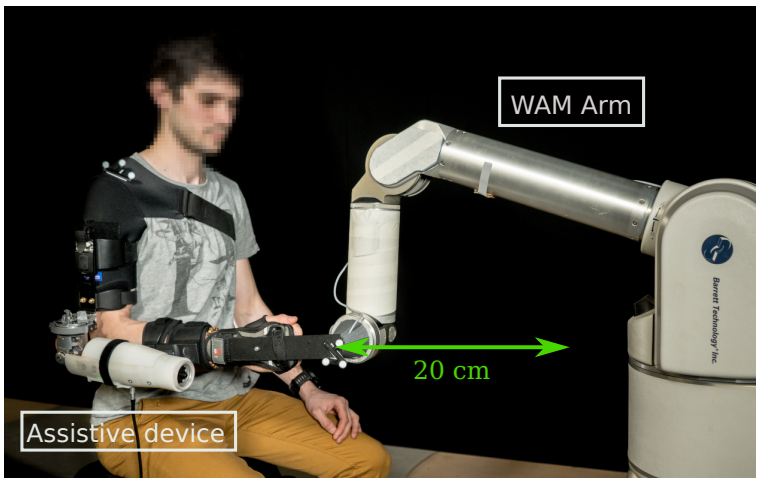

Figure 5.3: Set-up of the tuning study. The participant had to follow a target moving along a 20 cm straight line, carried by the WAM® Arm

5.3). The prosthesis motions were controlled with CCC, with $\lambda \in \{0.4; 2; 10\}\,[s^{-1}]$. For each value of λ, the task was repeated five times. First, we studied the influence of the gain with no deadzone (q_0 was set to 0 deg). Then, in a second time, we set q_0 to 5 and 15 deg to evaluate its impact on compensatory motions reduction. Here again, five trials were performed for each value of q_0.

5.2.2 Results

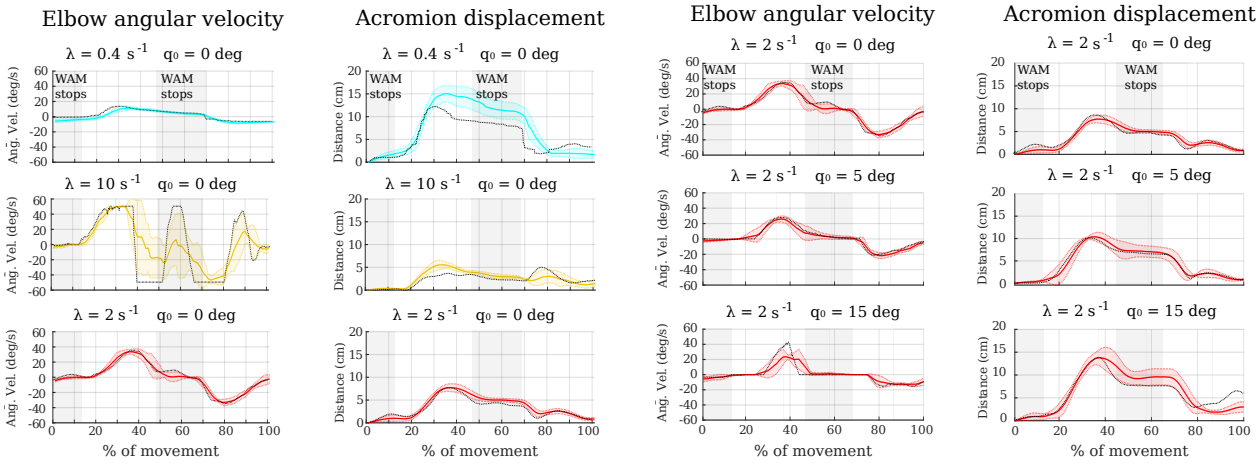

(a) Gain impact on the stability of the system

(b) Impact of the deadzone threshold on compensatory motions reduction

Figure 5.4: Mean and confidence interval of elbow angular velocity profile and of acromion displacement (body compensations) during a back and forth of the moving target, with (a) different λ and (b) different q_0. Black dashed lines are examples of one trial for the corresponding λ and q_0. Grey areas are when the target stops before leaving again

Human acromion displacement and elbow velocity are observed in order to evaluate their coupled dynamic evolution. Figure 5.4(a) shows the mean and confidence interval of the robotic elbow angular velocity and the acromion displacement (marker of compensations) over the five trials, for the different values of λ and $q_0 = 0\,\text{deg}$ (no deadzone). When $\lambda = 0.4\text{s}^{-1}$ (first row, cyan), the velocity command magnitude is very small, leading to a slow movement of the elbow. As the prosthesis is not reactive enough, the subject largely mobilizes compensatory movements to perform the task; mean acromion displacement goes up to 15cm. When $\lambda = 10\text{s}^{-1}$ (second row, yellow), the

magnitude of the compensatory acromion displacement is drastically reduced (5 cm, at most, for the mean plot). However, the prosthesis velocity command is jerky and quickly reaches high values, as illustrated with the black line plot corresponding to an example trial. Notice that the mean plot smooths this oscillatory behavior as the time-reproducibility between trial is low: the velocity commutes at different times between trials, leading to large variability. All in one, the movement of the prosthesis is not mastered, as it oscillates even when the WAM arm is still (gray areas). With $\lambda = 2\text{s}^{-1}$ (last row, red), the profile is much gradual and smoother, the confidence interval is small and the subject can monitor the prosthesis motion. Yet, the subject does not mobilize large compensations, as the maximal acromion displacement, for the mean plot, is limited to about 7.5 cm. These results thus confirm the outcomes of the theoretical study. Note that $\lambda = 2\text{s}^{-1}$ was also the gain used in the wrist pronosupination control law in Chapter 3. It corresponds to a frequency $f = \frac{\lambda}{2\pi} \approx 0.32\text{Hz}$, one order of magnitude smaller than f_c, the frequency of the human hand position controller [190]. As viewed by the human controller, the prosthesis position can thus be considered as a slowly varying – or quasi-static – disturbance. **Following these results, λ is now set to 2s^{-1} to have a good trade-off between command stability and prosthesis response time.**

On Figure 5.4(a), we see that, with $q_0 = 0$ deg, the prosthetic device never stops in practice. Indeed, the subject is never totally still with a perfectly null acromion displacement. This can be seen in Figure 5.4(a), where the velocity commands hardly stay at zero when the WAM does not move. A perfectly null deadzone necessarily leads to a permanent (even slow) oscillation of the prosthesis, which is not desirable. A non-null deadzone has thus to be added so that the device can stop without requiring the subject to be exactly at the reference position. Yet, a too high threshold will increase the zero-velocity zone around the reference posture, which may lead to higher acromion displacement for a same prosthesis motion. Two values of q_0 were tested: 5 and 15 deg. Figure 5.4(b) shows that, compared to $q_0 = 0$ deg (first row), $q_0 = 5$ deg (middle row) only increases the acromion displacement by 3 cm (≈40%) while slightly decreasing the elbow joint velocity, and without altering the motion dynamics. With $q_0 = 15$ deg (last row), the maximum elbow angular velocity is similar to the one with $q_0 = 5$ deg (≈ 25 deg.s^{-1}) but with higher acromion displacement (+5 cm, ≈50%, compared to $q_0 = 5$ deg and +8 cm, ≈100%, compared to $q_0 = 0$ deg). The motion dynamics is also affected since the temporal evolution of the elbow angular velocity is less smooth. **A deadzone threshold of 5 deg is thus selected.** To further support this choice, it can be noticed that a gap of 5 deg is never considered as uncomfortable in posture assessments (see [187, 192] for instance).

Impact of parameters tuning

This first step of validation highlights the impact of the two parameters of CCC, λ and q_0, on human-in-the-loop stability and body compensations reduction. To ensure both, we propose to set λ to 2s^{-1} and q_0 to 5 deg. This tuning, performed with one subject only, is applied for all participants of the following validation steps, in order to verify that it is not individual-dependent.

5.3 Evaluation of CCC for elbow joint control

Once the gain and the deadzone threshold are chosen to ensure an appropriate human-robot coupling, functional tests of CCC, for elbow joint control, can be performed. Two evaluations were conducted: one with able-bodied participants and one with a congenital amputee participant. **Besides the validation of the individual-independent tuning of the parameters, this evaluation experiment aims at studying how natural CCC is as well as its potential versatility.** By natural, we mean that a naive subject can master the prosthesis control without any

specific knowledge on the control scheme; by versatility, we mean that different tasks (trajectories and/or dynamics) can be performed with CCC without any modification. Indeed, it was criticized in Section 2.3 that model-based control approaches, especially MCC with joints synergies, were task-dependent (until now, they have only been developed for fast reaching tasks [145, 146, 151–154]). To give the user the ability to perform different tasks, a classification layer that chooses the model to load would be required, increasing algorithm complexity and errors eventuality (see Section 2.3.2). Since CCC does not rely on a task but on human posture, one can think that a same implementation can allow the user to achieve several tasks, with different trajectories or different dynamics. The only condition to fulfill is that the objective posture remains the same.

5.3.1 Specific protocol

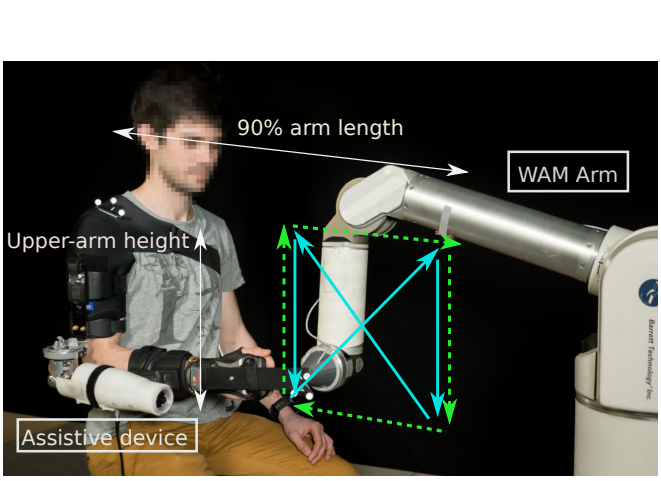

(a) Path tracking task

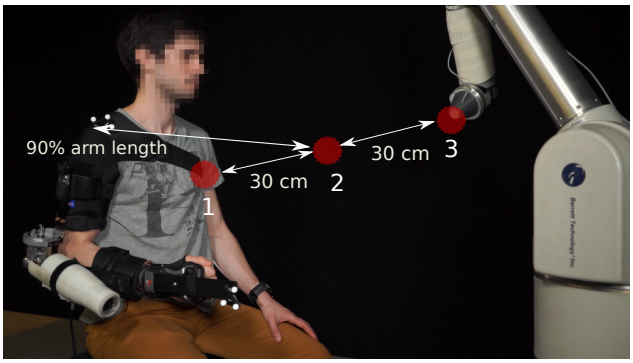

(b) Reaching task

Figure 5.5: Tasks for the evaluation of CCC. (a) Path tracking task for able-bodied participants (left) and congenital amputated participant (right). Dimensions of the rectangle are adjusted to the subjects' morphology. Green and blue lines distinguished the two trajectories, rectangle and diagonal. (b) Reaching task for able-bodied participants. The target positions are defined according to the subjects' morphology

Tasks

Ten able-bodied subjects, aged 20-24, and one congenital arm amputee subject participated to the evaluation experiments. They all performed a path tracking task: they had to follow a material target carried by the WAM® Arm, that slowly moved along a rectangular trajectory in their sagittal plane (see Figure 5.5(a)). The moving target paused briefly at each corner. The dimensions of the rectangle were adapted to the subjects' morphology; for the amputated participant, the dimensions

were smaller to be adjusted to the reduced accessible space due to the socket (see Figure 5.5(a), on the right).
To study the potential versatility of CCC, able-bodied participants were asked to perform another path tracking task as well as a reaching task. This allows to **examine versatility through two aspects: trajectory of the end-effector and dynamics of the task**. The second path tracking trajectory was still in the participants' sagittal plane and passed through the diagonals of the first trajectory rectangle (see blue arrows on Figure 5.5(a) on the left). The moving target also paused briefly at each corner. The reaching task was in 3D and consisted in attaining three fixed targets (without any path or time constraint), whose positions were defined according to subjects' morphology. All targets are at shoulder height, with target 2 in the middle and target 1 and 3 at 30cm from target 2 (see Figure 5.5(b)). The path tracking tasks were deliberately made slow to ensure a progressive reconfiguration of the subjects' posture during the task, while reaching is a faster movement that calls for a different motor control strategy. Path tracking seems to suit better to CCC framework but we assume that the latter also allows to correctly perform reaching. For all three tasks, the initial position was the upper-arm along the trunk and the elbow flexed at 90 deg.

Prosthesis control
Able-bodied participants successively controlled the prosthetic elbow with three modes:

1. natural (mode N), without wearing the device. This was used as a reference;
2. with the elbow joint Locked at 90 deg (mode L), preventing from any movement of the elbow. This mode was chosen to evaluate the magnitude of compensations when the elbow is inoperative. This mode was not used during the diagonal path tracking task;
3. CCC, with the law described in Section 5.1.1. q_0 was set to 5 deg and λ to 2s^{-1}.

A full session included five trials for rectangular path tracking and reaching, and two trials for diagonal path tracking ($(5 \times 2 \text{ tasks}) \times 3 \text{ modes} + 2 \times 1 \text{ task} \times 2 \text{ modes} = 34$ trials in total). For CCC, subjects could also train ten times on the rectangular path tracking task; the data are not considered in the presented results. There was no training on the diagonal path tracking and the reaching tasks, in order to test CCC use on totally new tasks.
The congenital amputee participant successively controlled the elbow joint of his prosthesis with two modes:

1. myoelectric control (MYO): a conventionnal myoelectric control with two electrodes (one on the biceps and the other on the triceps) was used to control the elbow flexion/extension. MYO controls the angular velocity with a trapezoidal profile. The participant was not used to myoelectric control because he began to wear a prosthesis shortly before the experiment. He had tested this mode only twice, in a different context, few days before the experiment;
2. CCC, with the law described in Section 5.1.1. q_0 was set to 5 deg and λ to $2s^{-1}$.

The prosthetic wrist and hand were locked during the whole experiment. The rectangular path tracking task was repeated five times with each control mode and there was no specific training with CCC. Tables 5.1 and 5.2 sum up the tasks and the prosthesis control schemes for able-bodied and amputated participants.

5.3.2 Evaluation with able-bodied subjects

Before any inter-modes comparison, it is worthy to validate CCC behavior on the different tasks. To analyze human-robot coupling and joint trajectories, let us first consider one example participant. On Figure 5.6, the end-effector trajectories for both path tracking tasks are presented. Two significant points can be noticed: the tasks are correctly performed (the end-effector of the subject follows the moving target quite well) and the control is mastered (the confidence interval is

	Tasks		
	Rectangular path tracking	Diagonal path tracking	Reaching
Able-bodied participants	x	x	x
Amputated participant	x		

Table 5.1: Tasks performed by the participants of the evaluation experiments

	Prosthesis control			
	Natural	Blocked	Myoelectric	CCC
Able-bodied participants	x	x		x
Amputated participant			x	x

Table 5.2: Control modes used by the participants to control the prosthesis

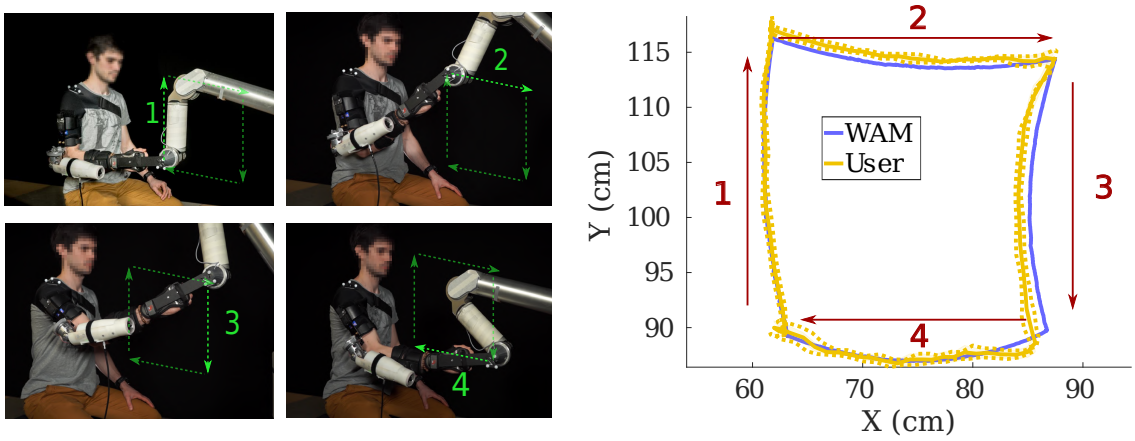

(a) Rectangular trajectory

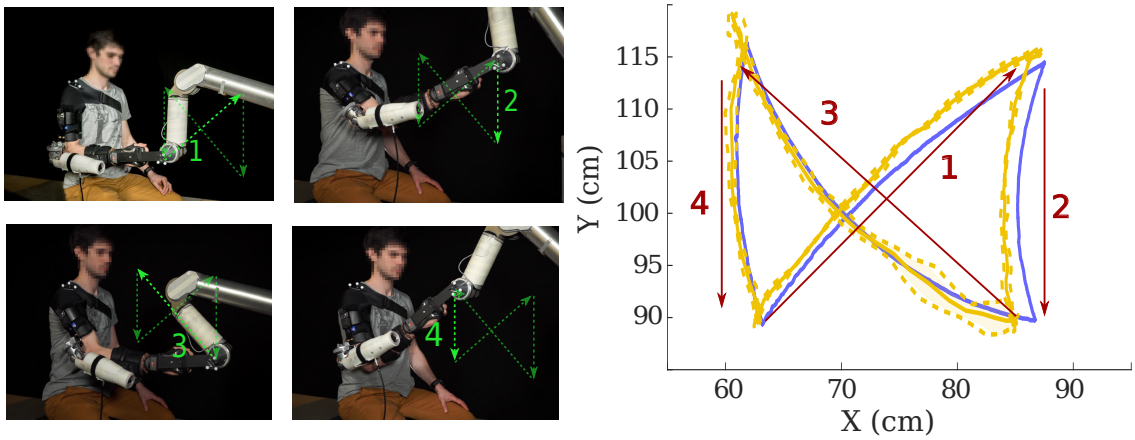

(b) Diagonal trajectory

Figure 5.6: Mean and confidence interval of the end-effector and WAM trajectories, for one representative subject, when prosthetic elbow is controlled with CCC. (a) Rectangular and (b) diagonal trajectories. Numbers indicate movement phases

very small). Regarding motion characteristics, Figure 5.7 shows the mean trajectories of humerus aperture, elbow flexion angle and acromion displacement for the three tasks; CCC is in yellow. The expected human-robot coupling is clearly visible, whatever the trajectories or the tasks: the subject begins to perform each task with compensatory motions (acromion displacement increases), the prosthetic elbow is activated, which reduces body compensations without stopping the achievement of the task. **In this example, the response of the user-prosthesis system with CCC is thus faithful to the theoretical prediction.**

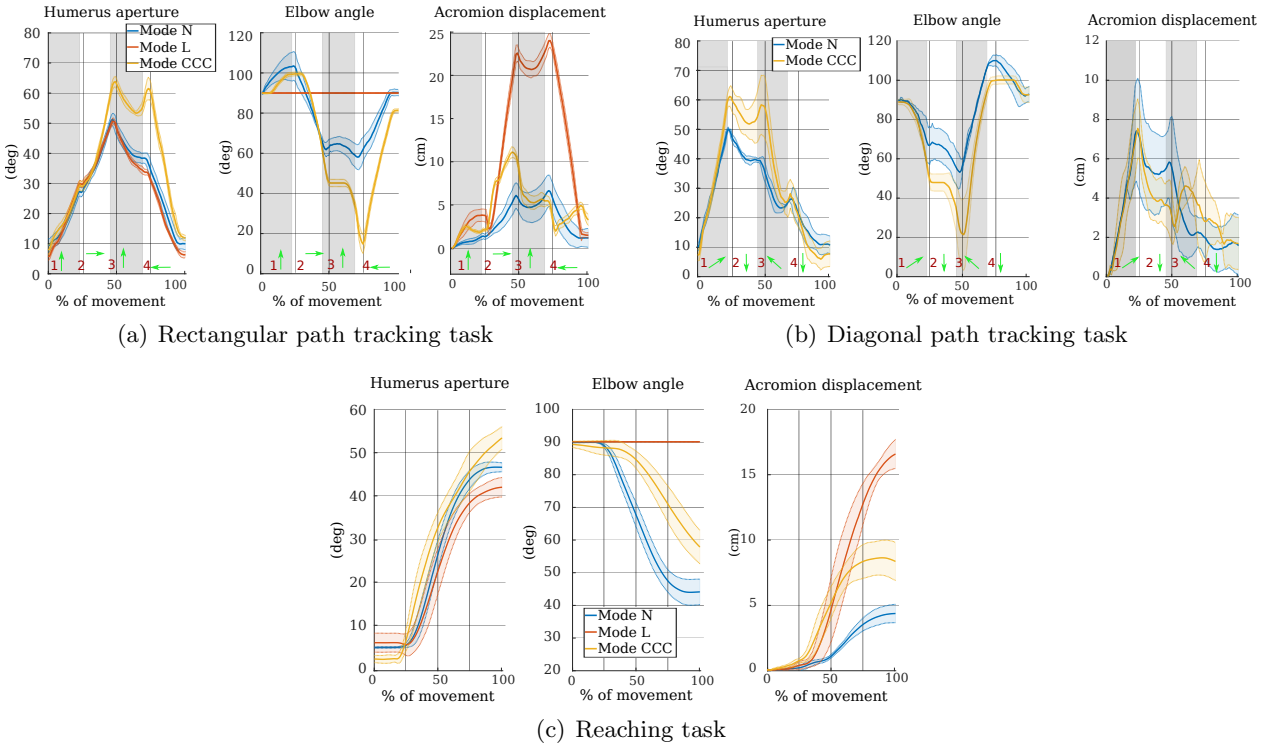

(a) Rectangular path tracking task

(b) Diagonal path tracking task

(c) Reaching task

Figure 5.7: Mean over trials and confidence interval of shoulder and elbow angles and acromion displacement, for one subject, for the three control modes. (a) and (b) are the path tracking tasks. Grey areas and numbers indicate the motion phases (see Figure 5.5(a)). (c) is the reaching task of the target 1

When comparing CCC with modes N and L, we can first observe that the acromion displacement induced by CCC is much lower than the one with mode L and very close to the natural one, whatever the task achieved (Figure 5.7). As for shoulder motions, the trajectory is similar between the three modes. This means that the shoulder joint is not compensatory but fully functional and that its motion is little affected by CCC. This human behavior is similar to the simulated planar 3R example in Section 4.2. Concerning the elbow joint, we can observe that the angular trajectory with CCC is also close to the natural one, with continuous variations allowed by the closed-loop. Yet, a more accurate analysis of the path tracking tasks shows that humerus aperture and elbow flexion are increased when the subject arrived at the furthest bottom corner of the trajectory (third and beginning of fourth phases for the rectangular trajectory, second and beginning of third phases for the diagonal one). We indeed noticed that some subjects (including the example one) tended to lean towards prosthetic side around this location to have a better vision of tracking error; this induced an acromion displacement which led to an important elbow extension. This points out the fact that trunk motions are not always compensatory but can also be functional (e.g., to position the head); our approach does not yet separate these two situations. As shoulder and elbow motions are connected to achieve the task, an over-extension of the elbow may be corrected by a higher shoulder angle to place the end-effector in a desired position. Once our approach will distinguish

functional and compensatory roles of trunk and scapula, shoulder and elbow motions with CCC shall be close to natural ones during the entire task. This was actually already observed for the participants who did not need to lean towards the prosthetic side to improve their vision of tracking error.

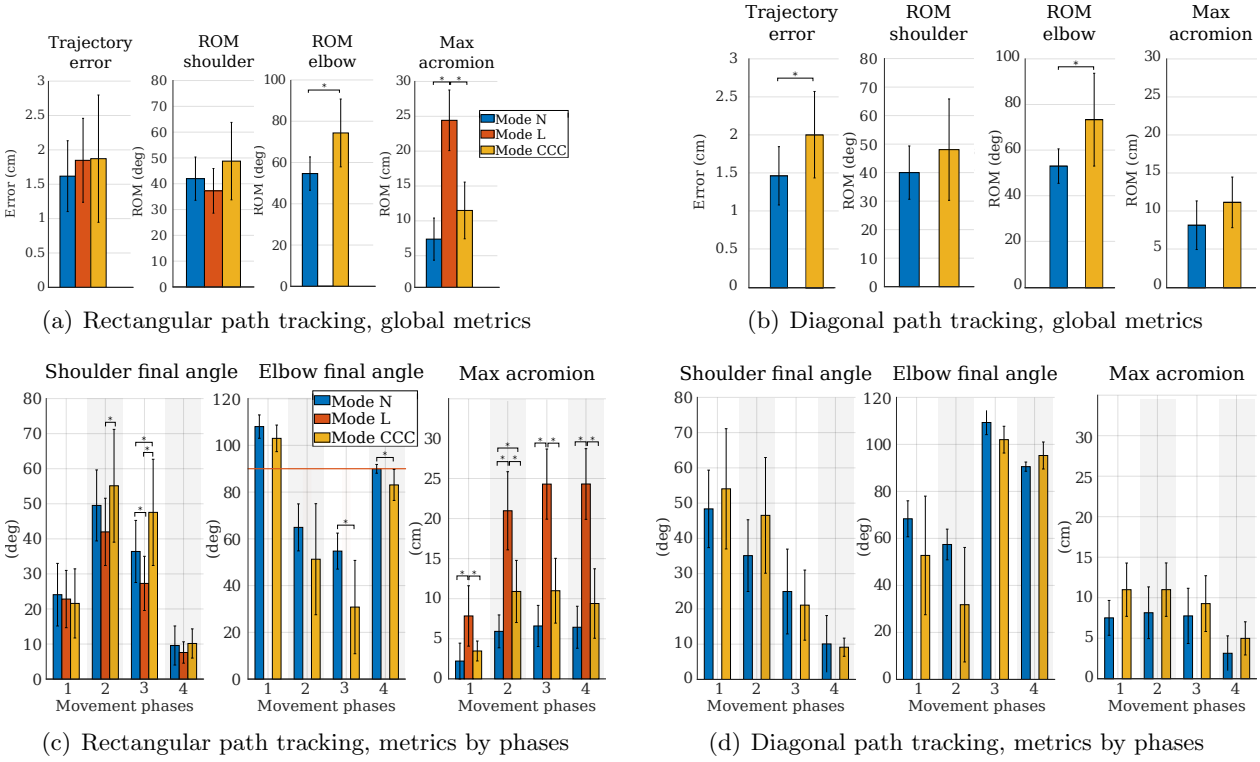

(a) Rectangular path tracking, global metrics

(b) Diagonal path tracking, global metrics

(c) Rectangular path tracking, metrics by phases

(d) Diagonal path tracking, metrics by phases

Figure 5.8: Task performance, joint motions and body compensations metrics, for the two path tracking trajectories. Metrics are averaged over trials and subjects. (a) and (b) show metrics for the overall task; (c) and (d) show metrics for each movement phase. * indicates $p < 0.05$

Figures 5.8 and 5.9 complement the example, displaying the mean over trials and subjects of different metrics that respectively characterize the task performance, the prosthetic and human joint motions as well as the body compensations (see Appendix D for the individual results of each subject). Task performance is characterized by the trajectory error (mean distance between the WAM and the subject's end-effectors) for the path tracking tasks and by the time of the task for reaching (final position error was not relevant here since the targets were always reached). Joint motions are characterized by the ROM of the shoulder angle (humerus aperture) and the ROM of the elbow flexion angle; body compensations are measured with the maximum acromion displacement. For path tracking tasks, joint motions and body compensations are also assessed with task-phases dependent metrics: the final shoulder angle, the final elbow flexion angle and the maximum displacement of the acromion, computed for each of the four phases (see Figures 5.8(c) and 5.8(d)). Indeed, as the four corners of the trajectories are at different depths and heights from the subject, joint motion strategies may vary with movement phases, as already observed on Figure 5.7. While we can compare the prosthetic control modes at a glance with global metrics, we may miss some variations in joint motion strategies. Both global and more accurate metrics are thus necessary.

Statistical analysis was conducted on the metrics averaged over trials for each mode and subject. Normality of the data was assessed with Lilliefors test [174]. Then, general linear models were used for normally distributed data and the nonparametric Friedman test was used for the others [175]. Tests were performed with Statistica©, Statsoft. Statistics were not performed for diagonal path tracking, as there were only two trials per mode.

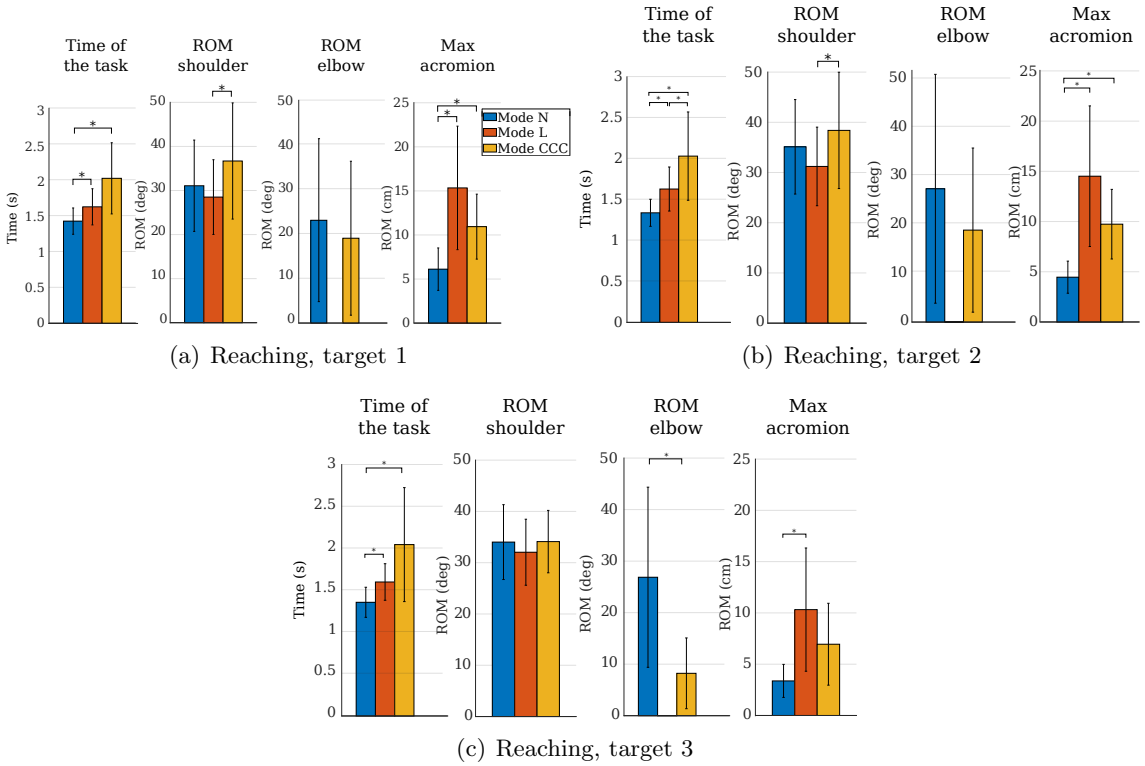

(a) Reaching, target 1

(b) Reaching, target 2

(c) Reaching, target 3

Figure 5.9: Task performance, joint motions and body compensations metrics, for the reaching task. Metrics are averaged over trials and subjects. * indicates $p < 0.05$

Task performance

The tasks are correctly achieved with all three control modes, even with the elbow locked, owing to human body redundancy. There is no statistical significant difference between the trajectory errors for path tracking tasks, and the targets were always reached. Yet, it can be noticed that the time of the reaching task is significantly higher with modes L and CCC than with natural motions ($p < 0.05$) while there is no significant difference between both (see Figure 5.9). The slower motion with L may be due to the large use of trunk motions that compensate for the locked elbow; the slower motion with CCC is both a limitation of the prosthesis and a limitation of the command. Indeed, on the one hand, the angular velocity of the prosthesis is limited to 50 deg.s^{-1}, while natural elbow angular velocity went up to 100 deg.s^{-1}. On the other hand, when CCC-controlled elbow motion is triggered, the reaching movement, which is very fast, is nearly finished. The activation delay can be reduced by tuning the deadzone threshold q_0 but the main part could not be shortened because of the integrator in the command, essential to create a smooth angular velocity. **CCC thus allows to achieve multiple tasks, even if it is less appropriate for reaching than path tracking because of the fast dynamics required.** For a more extensive validation, it would be relevant to study to which extent prosthesis users accept a longer reaching time.

Body compensations

For path tracking, the compensations exhibited with mode L are significantly larger than for the other modes ($p < 0.05$), be it for the global motion or for the different phases; with CCC, they are comparable to natural values (no significant difference with mode N, see Figure 5.8).
For reaching, the acromion displacement is significantly increased with CCC compared to mode N: as the response time of the prosthesis was too slow compared to the natural speed of reaching, participants tended to perform the task with body compensations instead of waiting for the prosthesis to move. Compared to mode L, compensatory motions are, in average, smaller with CCC but

this difference is not statistically significant across the ten subjects (see Figure 5.9). **CCC thus reduced body compensations, up to natural body motions for path tracking, a bit less for reaching.**

Prosthetic and human joints motions
For path tracking, the observations made on Figure 5.7 are confirmed. The shoulder angle with CCC is globally close to the natural one (see Figure 5.8(a) and Figure 5.8(b)) but a phase-dependent analysis with Figures 5.8(c) and 5.8(d) shows a higher angle when attaining the furthest bottom target (end of phase 3 for the rectangular trajectory and end of phase 2 for the diagonal one). The over-extension of the elbow is directly visible with the global ROM ($p < 0.05$ between CCC and mode N) while the final angle at each phase allows to refine the analysis: elbow motions induced by CCC are close to the natural ones except around the identified corner. For the corresponding movement phases, there is an important variability of shoulder and elbow metrics across subjects, since they did not all lean over the prosthetic side at the same extent.
Concerning reaching (see Figure 5.9), the shoulder angle is similar between CCC and mode N. Elbow ROM is also similar between CCC and mode N for the first two targets; it is significantly lower with CCC for the third one. Note that standard deviations are high, for both N and CCC, illustrating that reaching motion strategies can vary a lot between subjects.

This first validation experiment, with ten able-bodied participants, confirms the results of Chapter 4 and adds also new elements. **CCC is not limited to one task**: it works for different trajectories and different dynamics, maybe with some modifications to tackle the triggering issue observed with the reaching task. **It is also natural**, in the sense that subjects quickly mastered prosthesis control without any knowledge on the controller behavior and with very short training.

5.3.3 Evaluation with an amputated subject

CCC theoretical properties have been validated with ten able-bodied subjects. However, it is necessary to perform such a validation with final end users, since the reaction of an amputated person might differ (because of distinct motion strategies or the wear of a real prosthesis, among other possible reasons).
A second validation experiment was thus conducted with a congenital arm amputee, who realized the rectangular path tracking task. CCC was here compared to a conventional on/off myoelectric control, with biceps and triceps contractions controlling flexion and extension of the elbow joint. Figure 5.10(a) shows the trajectories of humerus aperture, elbow and acromion, averaged over the 5 trials. It can be observed that shoulder motions are indeed a bit different from the ones of able-bodied subjects. The coupling between acromion and elbow motions is still efficient to control the prosthetic joint.
When analyzing the same metrics as for able-bodied participants (see Figure 5.10(b)), we see that the trajectory error is similar between the two control modes, with a very small standard deviation. The prosthesis user adapted and managed to perform the task whatever the control mode, but the comfort and easiness of the motion can change. The joint metrics actually differentiate the two modes. Concerning the shoulder joint, it is not solicited at the same movement phases with MYO and CCC; this solicitation may depend on the elbow motion. The maximum displacement of the acromion is much higher with myoelectric control than with CCC, while the ROM of the elbow is smaller. With the first mode, the participant underused the prosthetic elbow and prefered to use body compensations to move his hand; this is also visible Figure 5.10(a). As stated at the end of Section 2.1, **when the prosthesis user is not familiar with myoelectric control, s/he does not intuitively use it because of the cognitive burden induced by the parallel loop.** S/he rather uses body motions, to bring the hand to a desired position. Comparatively, **CCC reduces compensations and allows for an increased use of elbow joint, while the user focuses only on the task.** A fifth metric is analyzed to compare myoelectric control and

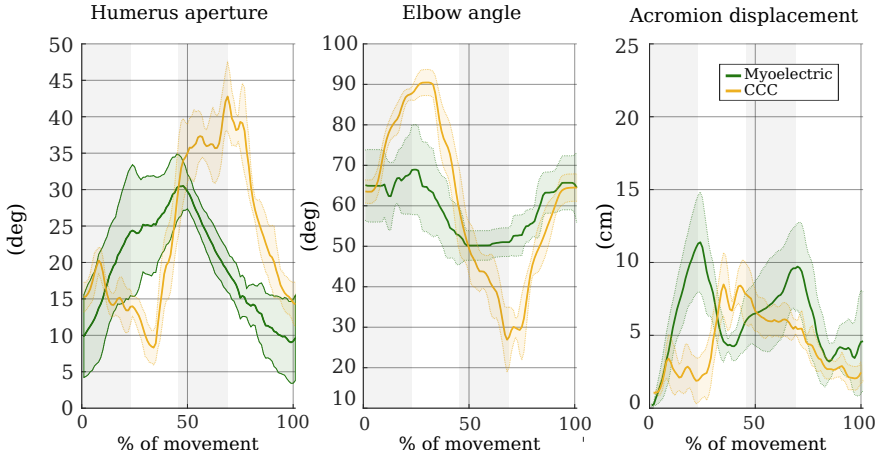

(a) Mean and confidence interval of shoulder and elbow angles and acromion displacement

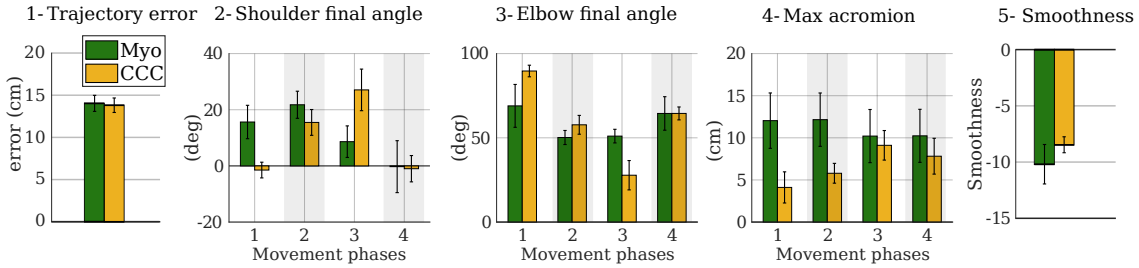

(b) Task performance, body compensations and prosthetic joint motions metrics

Figure 5.10: Comparison of conventional on/off myoelectric control and CCC for the rectangular path tracking task, performed by one congenital amputee. (a) Joint trajectories and (b) performance metrics

CCC: the smoothness of the elbow angular velocity, measured by the spectral arc length [182]. The smoothness is the sum of the spectral arc lengths computed for each of the four sub-movements which composed the rectangular trajectory. Figure 5.10(b) -5 shows that motions performed with CCC are smoother than the ones performed with the on/off myoelectric control. While the closed-loop character of CCC induces continuous and smooth joint motions, on/off myoelectric is much more sequential. CCC could have also been compared to proportional myoelectric control, which allows more continuous motions than on/off, but this scheme is rarely implemented for prosthetic elbow.

A conclusive evaluation

This experiment, evaluating CCC implementation for one joint, with both able-bodied and amputated participants, confirms that the user reacts as expected to the human-prosthesis coupling induced by the closure of the control loop at the device level. The subject can stay focused on the task while the prosthesis takes care of his/her posture, which allows a natural control; CCC was indeed mastered by all participants, without any information on the prosthesis motion law. This validation also shows that CCC is suitable for various tasks: it is very well adapted for path tracking tasks, whatever the trajectories; it also allows –maybe with some adjustments– to perform reaching, despite its faster dynamics. This is a valuable benefit in comparison with pattern recognition-based ASC and MCC. Even if body compensations are input of the controller, compensatory motions are reduced with CCC compared to a fully-locked elbow joint but also compared to conventional myoelectric control. They are

not completely inexistent either according to the general paradox in control theory: the error signal shall be minimized; yet, if it was always null, the controller would not be of any help. The evaluation with able-bodied participants still shows that trunk and scapula motions are very close to natural ones for slow and continuous motions (like path tracking).
Another noteworthy advantage of CCC now becomes perceptible: the individual-independence of the parameters. This is highlighted by the fact that the exact same law, with the same two parameters λ and q_0, has been used for every participants, able-bodied and amputated, and for the three tasks of the experiment. Even if a finer tuning around the values found in Section 5.2 could be performed, it seems that there is no critical need to train any algorithm or to personalize a set of parameters.

5.4 Chapter summary

The general formulation of CCC, presented in Section 4.1, has been implemented in this chapter for the control of an elbow prosthetic joint. A human-in-the-loop experimental validation has been realized with able-bodied subjects wearing an emulated prosthesis and an amputated subject wearing his own prosthesis. The stability condition on the gain λ found for a coupled robotic system in Section 4.3 has been tested on a human-prosthesis system, and the deadzone threshold impact on compensations reduction has been analyzed with one able-bodied subject. An evaluation study has then been conducted both on able-bodied and amputated subjects, to study the individual-dependence of the parameters, the natural character (ease of discovery without any knowledge on the control scheme) and the versatility of CCC. It has been confirmed that the same set of parameters suits to all participants, that the latter managed to use CCC without any explanation and for tasks with different trajectories and dynamics.

Chapter 6

A simultaneous control of two prosthetic joints: experimental validation

In the previous Chapter, CCC has been validated for the control of one prosthetic joint, the elbow. Its general formulation, developed in Section 4.1, is yet not limited to one DOF and can be adapted to as many DOF as the device has.
The experiment presented in this Chapter aims at validating the use of CCC with two DOF, extending CCC study to more amputated participants [1] and assessing the cognitive load it induces.

6.1 Materials and Methods

Following CCC validation on wrist and elbow joints distincly, it is now relevant to test its use to control two prosthetic joints on a same device. As UL prostheses for transhumeral amputees are mainly composed of hand, wrist pronosupination and elbow flexion, we decided to apply CCC to control the last two DOF (we remind that CCC concept is not valid for grasping control, since this motion cannot be compensated by any other proximal joint). The experiment performed for that purpose focuses on the feasibility, on the potential reduction of the induced cognitive load, compared to a traditional open-loop Auxiliary Signal Control (ASC), and on the participation of final end users in the validation.

6.1.1 Control law

As in Chapter 5, the general formulation of CCC must be adapted to the case considered here: a prosthesis with two DOF, elbow flexion/extension and wrist pronosupination. We decided not to merely combine the 1-DOF control laws of Section 3.3 (wrist) and Chapter 5 (elbow), in order to get a single unified formulation for both joints.
To implement the control law, we consider the case where the sensor signal $\mathbf{s}$ is the position and/or the orientation of the stump, which was tracked through acromion. As prosthetic joints (wrist and elbow) are revolute, we decided to work with orientation only. It allows to work in 2D and thus have a square natural prosthetic jacobian matrix $\mathbf{J}_N$, as explained below.

Prosthetic arm model and simplification of the jacobian expression
Figure 6.1 shows the 2-DOF prosthetic arm model considered in this Chapter. θ_1 is wrist pronosupination ($\theta_1 > 0$ is pronation) and θ_2 is elbow flexion/extension ($\theta_2 > 0$ is flexion). The different frames are defined as followed:

- frame 0 (attached to the palm): $\mathbf{z}_0$ is the forearm axis, $\mathbf{y}_0$ is perpendicular to the plane of the hand, pointing left and $\mathbf{x}_0$ is the cross-product of $\mathbf{y}_0$ and $\mathbf{z}_0$;
- frame 1 (attached to the forearm): $\mathbf{y}_1 = \mathbf{z}_0$, axis of rotation of the wrist pronosupination, $\mathbf{z}_1 = -\mathbf{y}_0$ and $\mathbf{x}_1 = \mathbf{x}_0$ when there is no wrist rotation ($\theta_1 = 0\,\text{deg}$). The rotation matrix

[1] Due to Covid-19 restraints, several scheduled experiments have been canceled. As it is, results from only one subject are presented here but we hope to be able to add extra results prior to the defense.

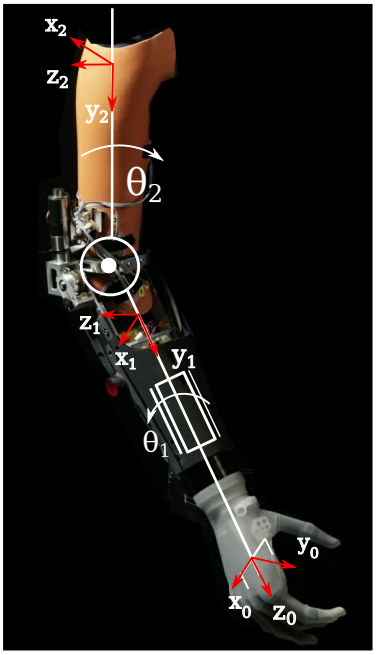

Figure 6.1: 2-DOF prosthesis model

from frame 0 to frame 1 is:

$$\mathfrak{R}_{0\to1} = \begin{pmatrix} \cos(\theta_1) & \sin(\theta_1) & 0 \\ 0 & 0 & 1 \\ \sin(\theta_1) & -\cos(\theta_1) & 0 \end{pmatrix} \tag{6.1}$$

- frame 2 (attached to the upper arm): $\mathbf{z}_2 = \mathbf{z}_1$, axis of rotation of the elbow, $\mathbf{y}_2$ is the upper-arm axis ($\mathbf{y}_2 = \mathbf{y}_1$ when $\theta_2 = 0\,\text{deg}$) and $\mathbf{x}_2$ is the cross-product of $\mathbf{y}_2$ and $\mathbf{z}_2$ ($\mathbf{x}_2 = \mathbf{x}_1$ when $\theta_2 = 0\,\text{deg}$). The rotation matrix from frame 1 to frame 2 is:

$$\mathfrak{R}_{1\to2} = \begin{pmatrix} \cos(\theta_2) & -\sin(\theta_2) & 0 \\ \sin(\theta_2) & \cos(\theta_2) & 0 \\ 0 & 0 & 1 \end{pmatrix} \tag{6.2}$$

As only the orientation part is considered, the natural prosthetic jacobian matrix is:

$$\mathbf{J}_N = \begin{pmatrix} \mathbf{z}_0 & \mathbf{z}_1 \end{pmatrix} \in \mathbb{R}^{3\times2} \tag{6.3}$$

with $\mathbf{z}_0$ and $\mathbf{z}_1$ expressed in frame 0. Assuming that the sensor signal is a direct measure of the stump orientation ($\mathbf{J}_{par_s} = I_3$), the prosthesis error $\boldsymbol{\epsilon}_p$ is then given by:

$$\boldsymbol{\epsilon}_p = \mathbf{M}^{+}\boldsymbol{\epsilon}_s = \begin{pmatrix} \mathbf{z}_0 & \mathbf{z}_1 \end{pmatrix}^{+} \boldsymbol{\epsilon}_s \tag{6.4}$$

with $\boldsymbol{\epsilon}_s$, the sensor error signal, in $\mathbb{R}^3$.
An equivalent and simpler solution can be considered by projecting $\boldsymbol{\epsilon}_s$ in the 2D-base defined by the jacobian vectors: ($\mathbf{z}_0$, $\mathbf{z}_1$). In this case, the projected error signal $\boldsymbol{\epsilon}_s^{'}$ is in $\mathbb{R}^2$ and $\mathbf{J}_N = I_2$ the identity matrix, in $\mathbb{R}^{2\times2}$. The pseudo-inverse of $\mathbf{J}_N$ becomes the inverse, namely the identity matrix.
The velocity commands of the prosthetic joints were the ones described Equation 4.15:

$$\dot{\mathbf{q}}_{p,c} = \lambda Z_{q_0}\left(\boldsymbol{\epsilon}_p\right) = \lambda Z_{q_0}\left(\boldsymbol{\epsilon}_s^{'}\right)$$

6.1.2 Experimental set-up

One congenital amputee participated to this experiment, that was performed in accordance with the recommendations of Université Paris Descartes ethic committee CERES, which approved the protocol (NIRB: 20163000001072). The participant gave his informed consent, in accordance with the Declaration of Helsinki. This participant does not daily wear a prosthesis but has already tested myoelectric control; he trained for the Cybathlon, during which he used an array of six electrodes to control his three prosthetic DOF (hand, wrist and elbow) with different muscles pairs. Here, we reproduced the generic two electrodes (biceps and triceps) set-up used in arm amputees. He had also tested CCC for elbow joint control before the present experiment and knew the general principle of CCC.

Task

CCC was tested for the control of wrist pronosupination and elbow flexion/extension on the Refined Rolyan Clothespin test [184, 185], as described in Section 3.3.3. The protocol was slightly modified to adjust to the restrained reachable space of transhumeral amputated people: instead of moving three clothespins from horizontal to vertical bars (and vice-versa), the participant was asked to move only two (see Figure 6.2).

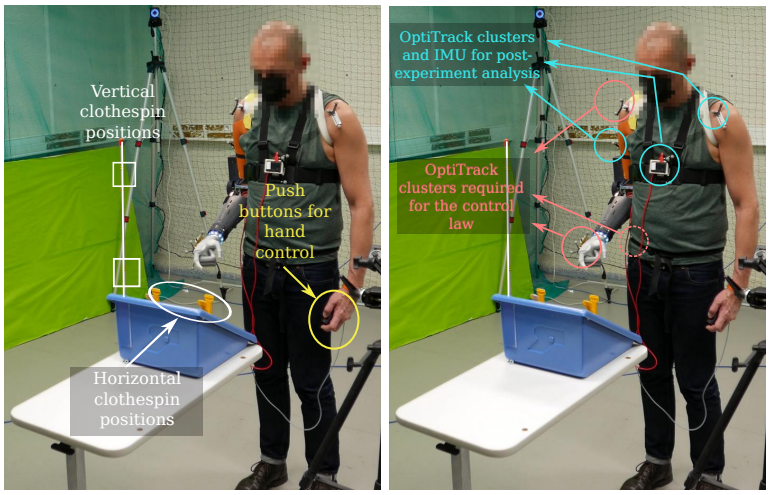

(a) Adapted Refined Rolyan Clothespin test, with remote hand control

(b) Sensors for control and post-experiment analysis

Figure 6.2: Experimental set-up of the Refined Rolyan Clothespin test adapted to transhumeral amputated people. See also Figure 3.17 for a better visibility of pin locations

Prosthesis control

The prosthetic intermediate joints (wrist and elbow) were successively controlled by a conventional on/off myoelectric control, using the contraction of the biceps and triceps as inputs (MYO, see Section 2.1), and by CCC. MYO was implemented with a trapezoidal velocity profile for each joint; co-contraction was required to switch from the wrist control to the elbow one and vice-versa. As explained just below, the hand was not included in the myoelectric sequence, contrary to what it would be in a real life scenario. CCC law was the one described in the previous Section. To homogenize wrist and elbow velocity during the task, λ was different for the two joints: it was set to 4s^{-1} for the wrist and to 2s^{-1} for the elbow, which still fulfills the stability condition given in Section 4.3. The deadzone threshold vector $\mathbf{q}_0$ was $\begin{pmatrix}5\\5\end{pmatrix}$ deg.

The control of the prosthetic hand was chosen to be the same for the two control modes. Like

most of UL prostheses functional assessments, the Refined Rolyan Clothespin test involves hand grasping. Yet, as the evaluation of this function is out of purpose here, it was decided to set it apart, with a simplified control: the fingers of the polydigital hand (Quantum from Touch Bionics Ossur) were preliminarily positioned in pinch and the closing/opening of the hand was controlled with two push-buttons hold in the contralateral hand of the participant. Functional assessment thus focused on wrist and elbow mobility only and was not biased by the difficulty of myoelectric grasping. This was particularly helpful for MYO, for which the usual 3-DOF control is complex (see Section 2.1): adding a third DOF in the myoelectric sequence indeed increases the number of co-contractions and thus muscle fatigue and mental burden.
The Refined Rolyan Clothespin test was performed six times with both modes; MYO and CCC were alternated to avoid any effect of task learning with one of the two modes.

Cognitive load

The cognitive load was evaluated with both objective and subjective means. The objective measure was a double task, performed in parallel to the Rolyan test: participant was asked to perform serial 3 or 7 subtraction [193]. The serial 3 (resp. 7) subtraction consists in substracting from a random number by 3 (resp. 7); the outcome is the number of errors produced and the number of subtractions performed. Serial 3 subtraction was performed in parallel of the Rolyan during the fourth and fifth trials of each control mode; serial 7 subtraction during the last trial. Subjective measure was the Raw-TLX score [194, 195], in which the participant rates six categories (mental, physical and temporal demands, frustration, effort and performance, see Appendix F) after completing the task; the final score is the sum of the six sub-ratings. Each control mode is given a score and the smaller the score, the less demanding the control mode. Table 6.1 provides an overview of the entire set-up.

		Trial 1		Trial 2		Trial 3		Trial 4		Trial 5		Trial 6		After
Main Task (Rolyan)	CCC	x		x		x		x		x		x		
	MYO		x		x		x		x		x		x	
Double task	Serial 3 subtraction							x	x	x	x			
	Serial 7 subtraction											x	x	
Raw-TLX														x

Table 6.1: Summary of the experimental set-up

Implementation of CCC

The sensor error signal projected into ($\mathbf{z}_0$,$\mathbf{z}_1$) base, $\boldsymbol{\epsilon}_s^{'}$, was defined as the rotation of the hip-acromion vector around $\mathbf{z}_0$ and $\mathbf{z}_1$, obtained as follows.
Two OptiTrack clusters were placed, one on the hip, the other on the acromion, to extract the spatial coordinates of the hip-acromion vector. Denoting $\overrightarrow{H_0A_0}$ and $\overrightarrow{HA}$ the (normalized) initial and current hip-acromion vector respectively, in the global laboratory frame, we have the successive computation steps:

$$t = acos(\overrightarrow{H_0A_0}.\overrightarrow{HA}) \tag{6.5}$$

$$u = \mathfrak{R}_{\text{lab}\to i}\frac{\overrightarrow{H_0A_0} \times \overrightarrow{HA}}{||\overrightarrow{H_0A_0} \times \overrightarrow{HA}||} \tag{6.6}$$

$$q^i = \begin{pmatrix} q_1^i & q_2^i & q_3^i & q_4^i \end{pmatrix} = \begin{pmatrix} \cos(\frac{t}{2}) & \sin(\frac{t}{2})u_{x_i} & \sin(\frac{t}{2})u_{y_i} & \sin(\frac{t}{2})u_{z_i} \end{pmatrix}, i \in \{0;1\} \tag{6.7}$$

$$R^i = \begin{pmatrix} 1-2((q_3^i)^2+(q_4^i)^2) & 2(q_2^iq_3^i - q_1^iq_4^i) & 2(q_2^iq_4^i + q_1^iq_3^i) \\ 2(q_2^iq_3^i + q_1^iq_4^i) & 1-2((q_2^i)^2+(q_4^i)^2) & 2(q_3^iq_4^i - q_1^iq_2^i) \\ 2(q_2^iq_4^i - q_1^iq_3^i) & 2(q_3^iq_4^i + q_1^iq_2^i) & 1-2((q_2^i)^2+(q_3^i)^2) \end{pmatrix}, i \in \{0;1\} \tag{6.8}$$

$$\boldsymbol{\epsilon}_s^{'} = \begin{pmatrix} atan2(R^0(1,2), R^0(1,1)) \\ atan2(R^1(1,2), R^1(1,1)) \end{pmatrix} \tag{6.9}$$

where t is the angle between the initial and the current hip-acromion vector, $u = \begin{pmatrix} u_{x_i} & u_{y_i} & u_{z_i} \end{pmatrix}^T$ the rotation vector expressed in frame $i \in \{0; 1\}$, q^i and R^i the corresponding quaternion and rotation matrix. $\mathfrak{R}_{\text{lab}\to i}$ is the rotation matrix from the global laboratory frame to frame i of the prosthetic arm.
$\mathfrak{R}_{\text{lab}\to 0}$ was obtained from the quaternion of an OptiTrack cluster located on the prosthetic hand and $\mathfrak{R}_{\text{lab}\to 1} = \mathfrak{R}_{0\to 1}\mathfrak{R}_{\text{lab}\to 0}$ (with $\mathfrak{R}_{0\to 1}$ defined in Equation 6.1) was computed at each time step with θ_1 given by the prosthetic wrist encoder. OptiTrack data (hip and acromion coordinates and hand quaternion) were sent in real time to the prosthesis and processed by a Rasperry Pi 3©. The OptiTrack system as well as an IMU on the trunk were also used to measure motions of body segments for post-experiment analysis (see Figure 6.2(b)), that were performed with Matlab Mathworks ® scripts.
$\boldsymbol{\epsilon}_s'$ as defined above is a parametrization of the acromion orientation for which it is an approximation to consider that $\mathbf{J}_N$ is the identity matrix. It was adopted for practical reasons of implementation but it would have been more exact to consider the rotation of a rigid body attached to the acromion. It has been checked on Matlab that the prosthesis command was not significantly different with one or the other.

6.2 Results and discussion

The same assessment framework as in previous chapters is considered: task achievement, prosthetic joint motions and body compensations are analyzed. The double task outcome and the Raw-TLX score completed the overview with cognitive load evaluation. No statistical study was conducted as results come from one subject only.
As in Section 3.3.3, upwards and downwards motions are disassociated for each metric. One downwards trial with CCC and one with MYO were removed, as prosthetic wrist motions were totally different from the other trials, due to unintended upper pin slippage within the fingers of the prosthetic hand.

6.2.1 Task performance

The task performance is assessed with the duration of the task. Figure 6.3 shows the mean and standard deviation of this metric over all trials (6 for upwards motions and 5 for downwards motions), for the two control modes. The average time is higher than the ones reported in [185] but comparable to those of S2 in Section 3.3.3. It is clear that **there is no difference between CCC and MYO, both control modes allow completing the task with similar performance**. This metric does not allow to discriminate CCC and MYO here and nothing can be concluded on control modes efficiency without analyzing prosthetic joint motions and body compensations.

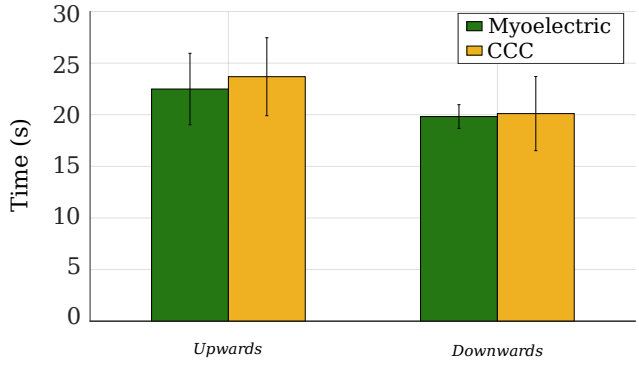

Figure 6.3: Time of the task for the Refined Rolyan Clothespin test adapted for transhumeral amputees, averaged over all trials performed by the participant

6.2.2 Prosthetic joint

In this experiment, both prosthetic wrist and elbow were active; many points can be raised on the strategy developed by the participant with CCC and MYO, be it for individual joint motions or for simultaneous prosthetic joint or prosthetic-and-human joint activation.

Individual motions

Wrist pronosupination

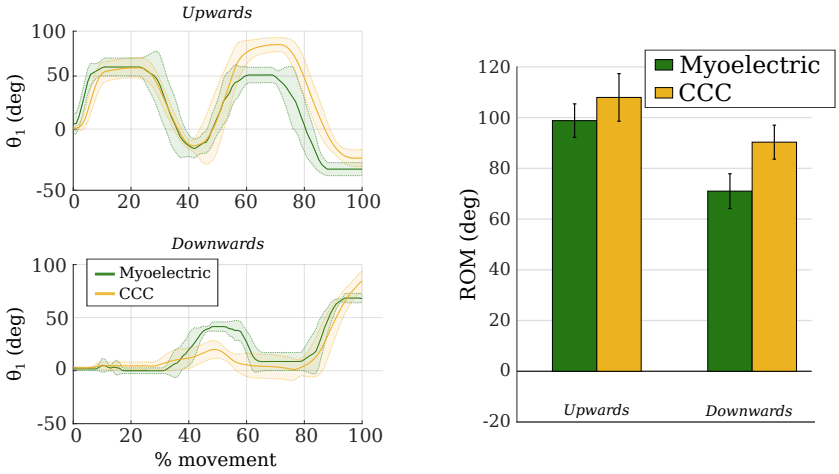

(a) Mean and confidence interval of wrist angular trajectory

(b) ROM of wrist pronosupination

Figure 6.4: Prosthetic wrist motions, with CCC and MYO. (a) Angular trajectory, normalized in time and averaged over trials. (b) Mean over trials and standard deviation of wrist ROM

Figure 6.4 shows metrics for wrist pronosupination: the angular trajectory (Figure 6.4(a)), normalized in time and averaged over all trials, with the corresponding confidence interval (CI) and the ROM (Figure 6.4(b)). On Figure 6.4(a), wrist rotations corresponding to clothespin reorientations from the horizontal to the vertical bar (and vice-versa) are easily identifiable. We can notice that the timing of motion variations is similar between CCC and MYO: **the wrist strategy to perform the Rolyan Clothespin test is not altered with one control mode compared to the other**. Moreover, the CI is small (maximum 30 deg while the ROM is more than 100 deg for upwards motions and maximum 23 deg while the ROM is more than 70 deg for downwards motions), meaning that the wrist angular trajectory has a good repeatability between trials. The mean trajectory yet shows some differences in amplitude between control modes. For upwards motions, pronation (negative values) is higher for the second clothespin with CCC, which leads to a higher global ROM (see Figure 6.4(b)). For downwards motions, pronation is higher with MYO for the first clothespin and with CCC for the second one, giving a global ROM higher with CCC. This still did not affect the realization of the task; it could be a consequence of the way the subject took the clothespin in the hand (which is not invariant).

Elbow flexion/extension

While prosthetic wrist motions do not really discriminate CCC and MYO, motions of the prosthetic elbow make the difference. Indeed, with MYO, the participant used the elbow joint during the first trial only; then, he kept the elbow still (see Figure 6.5(a)). This confirms that the participant tended to minimize the global effort made for MYO and avoid co-contractions whenever possible. Even when used, the elbow joint with MYO has a minimalist motion. With CCC, it was activated at each trial since no additional effort was required. Moreover, the angular trajectory is repeatable between trials (the CI is less than 20 deg). Figure 6.5(b) supports this observation. Elbow is thus

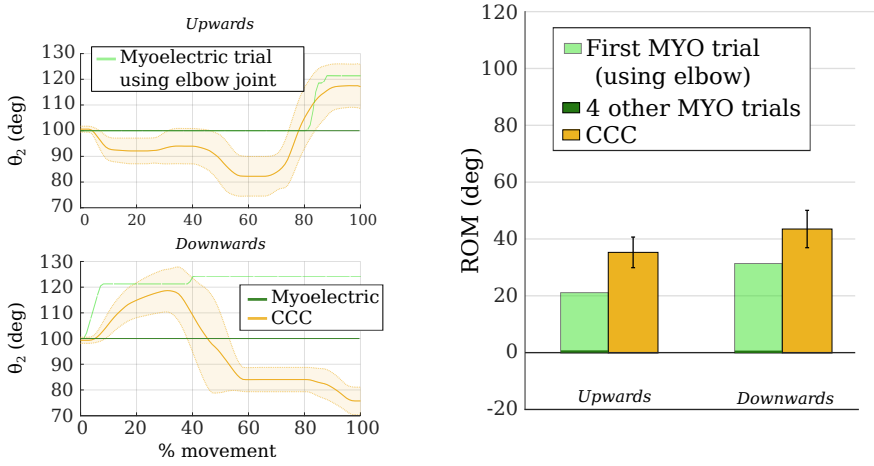

(a) Mean and confidence interval of elbow angular trajectory

(b) ROM of elbow flexion/extension

Figure 6.5: Prosthetic elbow motions, with CCC and MYO. (a) Angular trajectory, normalized in time and averaged over trials. For MYO, the first trial –in light green– was not included to compute the mean, as it was the only time the participant used the prosthetic elbow. (b) Mean over trials and standard deviation of ROM. For MYO, the first trial –in light green– is separated from the others.

less solicited with MYO, to minimize muscular fatigue. **The absence of voluntary switching between prosthetic joints with CCC allows the use of multiple prosthetic joints while the user tends to only move the most helpful with MYO.**

Simultaneous activation

A possible significant advantage of CCC is the simultaneous activation of several prosthetic DOF within a same control law, when the sequential pattern of prosthesis movements with conventional myoelectric control is often criticized [7, 15]. It thus seems relevant to analyze whether wrist and elbow were activated together with CCC for this task. Figure 6.6(a) shows the time during which both wrist and elbow were activated (joints were considered as active when their angular velocity was higher than 3 deg.s^{-1}), expressed in percentage of the total time of the task, and averaged over trials. While it is zero for MYO, due to the intrinsic sequential nature of this control, it goes up to 24% and 13% for CCC, for upwards and downwards motions resp. This value has no specific significance since it depends on the task but it confirms that **CCC eliminates the sequential pattern of intermediate prosthetic joint motions and allows coordination**.
It is also of interest to look at a similar simultaneity metric for prosthetic hand and wrist motions. CCC does not directly allow for hand motions – since the latter cannot be compensated by any other joints – but it discharges myoelectric control which is now dedicated to the hand. For the experiment considered here, we recall that a pair of push-buttons supplanted myoelectric control of the hand, to avoid being biased by myoelectric grasping for the task assessment. The prosthetic hand is thus considered as activated when one push-button is pressed (wrist activation is still when the angular velocity is higher than 3 deg.s^{-1}). Figure 6.6(b) shows that the time of simultaneous hand-wrist activation is not null for CCC (9 and 8 % of task time for upwards and downwards motions resp.); it is nearly zero with MYO. We observed that the simultaneous activation occured when releasing clothespins; the participant anticipated and began to open the hand before the wrist stopped. Even if simultaneous hand-wrist activation was possible with both MYO and CCC due to remote hand control with push-buttons, the participant only made use of it with the second. Myoelectric control actually requires the user to focus on the individual joint s/he is moving whereas

CCC is built to allow prosthesis user to focus on the end-effector, which eases coordinated hand and wrist motions. **In addition to the simultaneous activation of the prosthetic intermediate joints, CCC thus seems to enable grasping while moving the end-effector.**

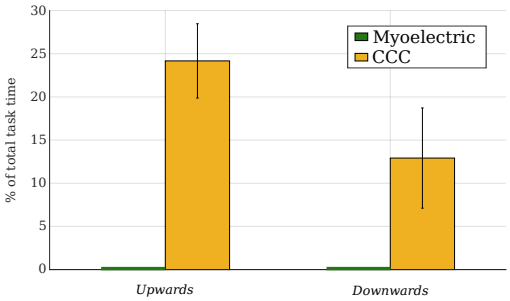

(a) Time of simultaneous activation of wrist and elbow prosthetic joints

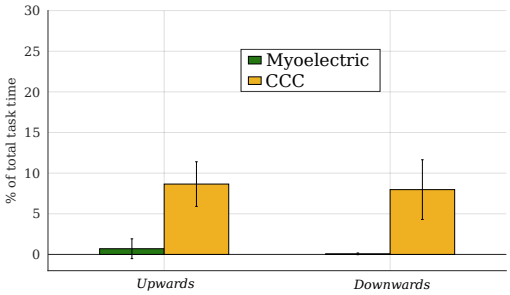

(b) Time of simultaneous activation of prosthetic hand and wrist

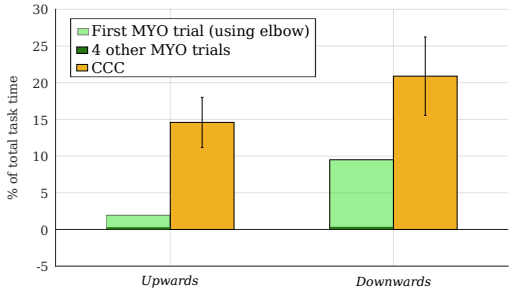

(c) Time of simultaneous activation of elbow prosthetic joint and human shoulder joint

Figure 6.6: Simultaneous activation of arm joints (human and/or prosthetic), in % of total task time. Mean and standard deviation over trials. (a) Prosthetic wrist and elbow. (b) Prosthetic hand and wrist. (c) Prosthetic elbow and human shoulder. For MYO, the first trial –the only one where the elbow was used– is represented in light green, while the other are in deep green

Simultaneity is not only important between prosthetic joints but also between prosthetic and human joints. Indeed, transhumeral myoelectric users often struggle to move the prosthetic arm in coordination with their residual limb, which leads to a global motion in two steps: (i) prosthesis motion followed by (ii) human motion [126], which is inefficient. The natural coordination between joints is missing. The same simultaneity metric as for prosthetic joints is considered, but between prosthetic elbow and human shoulder (see Figure 6.6(c)). For MYO, it is divided into the first trial, in light green, for which the elbow was activated and the four other trial, in deep green, for which the elbow was kept still. For these four last trials, the simultaneity metric is obviously zero, as there was no motion of the elbow. For the MYO trial using the elbow joint, we can observe that the time of simultaneous activation between human shoulder and prosthetic elbow is much smaller than the mean over trials with CCC (1.7% vs 14.6% for upwards motions and 8.1% vs 20.9% for downwards motions). This suggests that **it is easier to recover coordination between human and prosthetic joints with CCC than with MYO.**

Besides the control of two prosthetic joints with the same input (the acromion orientation change), CCC thus allows simultaneity between prosthetic joints and between prosthetic and human joints. It recreates coordinations that were missing, which tends to give a more natural aspect to the prosthesis and its user's motions.

6.2.3 Body compensations

Due to the use of body compensatory motions as controller input, the validation of CCC is not exhaustive without the analysis of the compensations of the participant. As we do not have a natural reference here, CCC upper body motions are compared to the one exhibited with MYO, as in Sections 3.3.3 and 5.3.3.

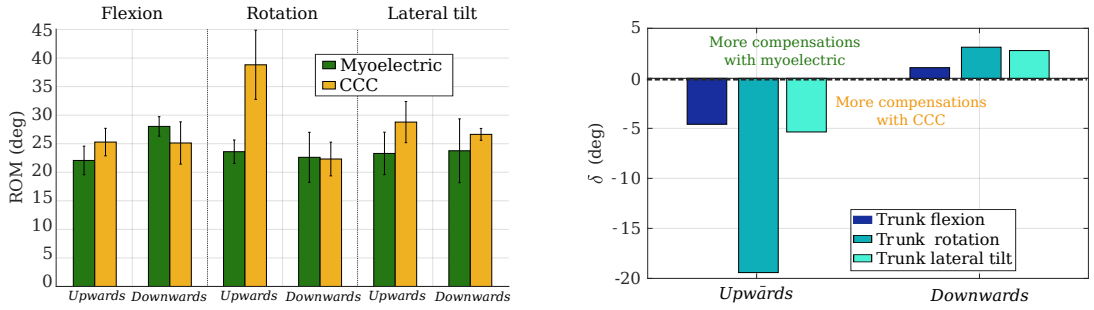

(a) ROM of trunk angles

(b) δ for trunk angles

Figure 6.7: Trunk motions analyzed with (a) the mean of ROM and (b) δ between MYO and CCC

As shoulder is fully functional for the Refined Rolyan Clothespin Test, the only compensatory joint considered here is the trunk (see Figure 6.7). Figure 6.7(a) shows the mean and standard deviation of the ROM of the three trunk angles (flexion, rotation and lateral bending); Figure 6.7(b) shows the metric δ, defined in Section 3.3.3, of these angles. As a reminder, $\delta = max(ROM_{myo}) - max(ROM_{CCC})$. There is no clear difference for trunk flexion and lateral bending (δ is less than 5 deg for both upwards and downwards motions), neither for trunk rotation for downwards motions. Yet, there is much more rotation with CCC for upwards motions ($\delta = -19$ deg). For the Rolyan Clothespin test, rotation is actually not a body compensation since it is not redundant with any prosthetic DOF. It was increased with CCC because of the motor strategy adopted by the participant, which differed with the one adopted with MYO.

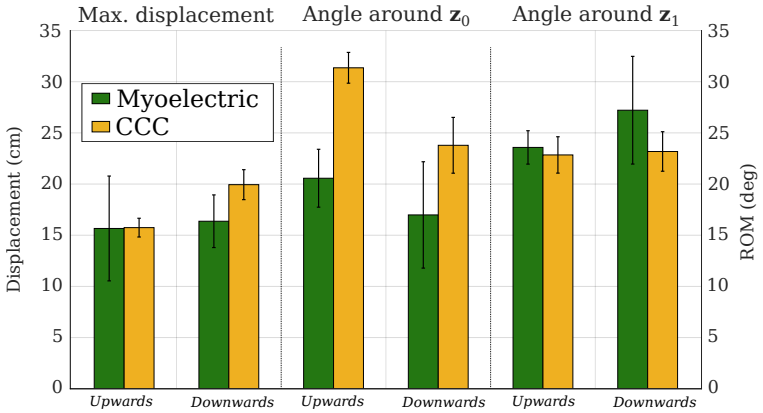

Figure 6.8: Acromion motions. Mean and standard deviation of marker displacement and ROM of angles around $\mathbf{z}_0$ and $\mathbf{z}_1$ axes

As trunk motions are very often simultaneous, studying separately the three anatomical angles is incomplete. To complete the analysis, Figure 6.8 shows some metrics related to the acromion. It captures all trunk motions as well as those of the scapula, which are also exhibited in upper body compensatory motions. That is why its orientation change was chosen to be the controller input. Acromion motion is studied through the displacement of the OptiTrack marker from initial

to current position in hip frame (not to take into account the marker displacement due to potential feet adjustement) and the ROM of orientation changes around $\mathbf{z}_0$ and $\mathbf{z}_1$ axes. We see that there is no clear difference between MYO and CCC for the displacement. For the angle around $\mathbf{z}_0$ axis, responsible for wrist pronosupination, the ROM with CCC is 10 deg and 7 deg higher than the ROM with MYO, for upwards and downwards motions resp. This could be due to MYO settings of the participant which allowed to quickly reach high wrist velocity compared to CCC. To be as fast with MYO as with CCC, the participant thus compensated more with the latter. This might be fixed by increasing the gain λ for CCC. For the angle around $\mathbf{z}_1$ axis, responsible for elbow flexion/extension, there is no difference for upwards motions between the two control modes; for downwards motions, the ROM is higher with MYO. This can be explained by the minimalist use of the elbow joint with this control mode, which was then compensated by upper body motions. This is less visible for upwards motions since elbow was less requested. It can finally be noticed that the compensations used as controller input were good candidates since they were naturally exhibited with MYO and prefered to prosthetic elbow motion.
Body compensations are thus not significantly enhanced with CCC, compared to MYO. Controlling a 2-DOF prosthesis with CCC is not worst than the conventional control approach. Yet, even if trunk angles stayed in an acceptable range to prevent musculoskeletal disorders [187], a comparison with natural motions would be of interest.

6.2.4 Cognitive load

By closing the control loop at the prosthesis level and using motions naturally exhibited by the user – rather than requesting the generation of an independent auxiliary signal – CCC may reduce the cognitive load. To assess this claim, the participant was asked to perform a double task in parallel to the Rolyan during the three last trials of each control mode. Be it with serial 3 or serial 7 subtractions, no major difference was observed between the control modes (see Table 6.2). This was completed by a Raw-TLX[2]; the participant's sub-ratings and the corresponding overall workload, given in Table 6.3, do not clearly discriminate MYO and CCC either.

	Trial 4 (serial 3)	Trial 5 (serial 3)	Trial 6 (serial 7)
CCC	18	17 and 1 error	10
MYO	18	15	12

Table 6.2: Double task assessment: the score is the number of subtractions performed

	Mental Demand	Physical Demand	Temporal Demand	Nonsuccess	Effort	Frustration	Overall Workload
CCC	10%	20%	20%	10%	20%	10%	15%
MYO	15%	5%	10%	5%	10%	5%	8%

Table 6.3: Raw-TLX: sub-ratings and overall workload (mean of the six sub-ratings)

No decrease of cognitive load with CCC is measured. Yet, the participant used only one prosthetic DOF with MYO (the wrist), avoiding co-contractions, which decreases the mental demand. We can assume that, if the subject was forced to use both prosthetic joints with MYO, the cognitive load of the task would increase. It would be even higher with the addition of the hand, third DOF in the myoelectric sequence, which would be the case in real life. **CCC and MYO are thus as demanding for the Refined Rolyan Clothespin Test considered here. MYO was used to control one prosthetic DOF only, which is acknowledged not to require special**

[2]I am not aware of similar use of Raw-TLX for myoelectric prostheses and thus cannot compare with other ratings. This is yet not so relevant since we are only interested in the subjective comparison of MYO and CCC.

attentiveness [77, 79, 80]; more DOF were controlled with CCC but without increasing the cognitive load. This is certified by the small Raw-TLX score.

A low demanding control for simultaneous prosthetic joint motions

The results of this experiment on 2-DOF control with CCC are rich: the task is well performed, with a simultaneous activation of the prosthetic joints, a restored human-prosthesis coordination, and without increased body compensations. The concept of CCC, validated in the previous chapter with one DOF, can thus be extended to two DOF. The cognitive load induced by CCC has now been assessed: it is as low as the one required to control one DOF with myoelectric control for an experienced user.
When completing the same Refined Rolyan Clothespin Test with a conventional myoelectric control, the prosthesis mobility was used at a minimum: only the most useful joint, the wrist, was moved. By allowing simultaneous wrist and elbow motions without more effort, CCC restores a better upper arm mobility. While elbow joint with myoelectric prostheses is usually moved upstream to modify the overall arm posture (lift or lower down forearm) and then locked, it recovers its genuine role and actually participate to arm motions with CCC. We also noticed that, with myoelectric control, the same body compensations as considered for CCC controller input were prefered to prosthetic elbow motions, which confirms that these compensatory motions were good candidates for our controller.
All these trends were obtained for one subject only; more participants are expected to confirm them. Next subjects will be fully naive, contrary to the first participant, to verify in depth the easy-learning character of CCC with 2-DOF.
As it is scalable, CCC could potentially handle n DOF ($n > 2$) simultaneously, which is hardly achievable with myoelectric signals. Simultaneous prosthetic motions are indeed impossible with conventional myoelectric control and their number is quickly limited with pattern recognition (see Section 2.1.2). Moreover, while it is commonly admitted that adding more DOF increases the control complexity and thus the induced cognitive load with myoelectric controls [66, 77, 80], it does not seem to be the case with CCC. The latter could thus be more appropriate for the upcoming UL prostheses, biomimetic and with more than two DOF.
Note that, in the Refined Rolyan Clothespin test set-up, wrist flexion is undoubtedly required when performing the task with a natural arm. As this DOF is not provided on the prosthesis, participants may compensate for this lack. It could be of interest to study the impact of these compensations on the good functioning of CCC.

6.3 Chapter summary

In this Chapter, CCC was tested to control two prosthetic joints, the wrist and the elbow, on the Refined Rolyan Clothespin Test. Preliminary results obtained with one participant validate that the concept proposed in this PhD indeed allows a simultaneous control of two DOF, without any specific training, and with a low cognitive load. The addition of DOF does not increase the control algorithm complexity and does not seem to increase the difficulty for the user, contrary to ASC. This still has to be supported with more participants.

Chapter 7

Perspective

7.1 Conclusion

7.1.1 Summary

UL prosthetics faces various challenges to give back autonomy to amputated people. Cosmetic, body-powered and motorized devices coexist to meet the different users' needs. Particularly addressing mobility, motorized prostheses have nowadays a well advanced mechatronics, with more and more available DOF. Their overall benefit is yet still discussed because of their high price compared to the limited functions to which everyday users really access. As exposed in **Chapter 1**, important issues such as socket, sensory feedback and control remain. The work presented here has focused on the last one, prostheses control.

The numerous existing control approaches all present significant drawbacks, that prevent them to be solidly accepted among the UL amputees population. A broad overview as well as an analysis of their control schemes were drown up in **Chapter 2**. The most common type, named Auxiliary Signal Control in this PhD manuscript, asks the user to generate an auxiliary signal, independent from healthy arm motions, that is directly connected to prosthesis joint motions. This creates a double task for the user: controlling healthy body motions and controlling prosthetic motions. To unburden the user, a partial automation of prosthetic joints can be proposed but this is still in the early stages. Motion Completion Control approaches propose to infer the device motions from the healthy arm motions of the user, through joint synergy models. The user is thus only in charge of one task: controlling his/her body, the prosthesis then follows. Because synergies are not exactly similar between subjects, a personalization of the models shall be required. The versatility is also limited since synergies are task-dependent: a distinct model must then be built for each task, which complexifies the algorithm and weakens its robustness. Even if the adopted approach differs, both Motion Completion Control and Auxiliary Signal Control are open-loop at the prosthesis level: once the prosthetic motion is performed, there is no examination to check whether it corresponded to the user's intent. The only way to detect errors is through the user, who has to send a new signal or trigger a new synergetic motion if a correction is needed. As control algorithms and synergy models are not perfectly accurate, this requires a permanent and high attention from the user for each motion to be performed. The aim of my work was to build a new prosthetic control scheme, that tackles the double task and open-loop issues. The controller input signal must then fulfill two criteria: (i) its generation must not create a double task and (ii) it must allow to estimate the prosthesis position error, to close the control loop at the device level.

Given the nearly impossibility to know in advance the arm motion or the intended target, the only reliable information available in daily life is the user's reaction to the prosthesis motion. When the latter is not the one desired, the user tends to correct it by soliciting his/her healthy joints rather than moving the device through its control path. The idea proposed in **Chapter 3**, developed and validated all along this PhD, is to use these compensatory motions to close the control loop at the prosthesis level. They will define the researched error signal, taken as input of the prosthesis controller. As they are body motions naturally exhibited by the user, their generation does not

create any double task. In this concept, the role of the prosthesis is not to perform a given task but to monitor its wearer's posture; the wearer is in charge of the end-effector task while the prosthesis moves to regulate his/her posture and reduce body compensations. This can be achieved thanks to the creation of a human-robot coupling via the servoing of the prosthesis on user's compensatory movements. A feasibility study with able-bodied and transradial amputated participants was conducted on wrist pronosupination and validates the proof of concept.
Chapter 4 further elaborates the theory of Compensations Cancellation Control (CCC). A general framework, that models the human-prosthesis coupling, allows to write a generic implementation of CCC law. When applying this algorithm to various simulation examples with coupled robotic systems, it appears that the stability of the overall system is sensitive to the tuning of the gain λ. To determine the appropriate value of this parameter, a theoretical stability study was accomplished and confirms what was observed on the simulations: λ has to be largely lower than the cut-off pulse of the proximal robotic part.
This general implementation has then been tested and validated experimentally on human-prosthesis system, with able-bodied and transhumeral amputated participants for elbow flexion/extension control, in **Chapter 5**. First, the influence of λ and its value ensuring stability were verified with a human user in the loop. Then, it was shown that subjects managed to perform slow path tracking tasks with different trajectories but also faster reaching motions with a prosthesis controlled with CCC. No adjustment was required for the amputated participant, the same controller parameters suited.
Chapter 6 finally extends the experimental validation of CCC to the control of two prosthetic DOF (wrist pronosupination and elbow flexion/extension) with one transhumeral amputee. CCC was compared to conventional myoelectric control for the realization of the Refined Rolyan Clothespin test. While the participant minimized effort with myoelectric control and commanded only one DOF, he could benefit from a simultaneous activation of wrist and elbow with CCC, without being distracted from the task. The cognitive load was assessed: CCC was found to be as low demanding as the control of one DOF with myoelectric control for an expert user.

7.1.2 Benefits of Compensations Cancellation Control

Closing the prosthesis control loop with body compensations offers various benefits that ease prosthesis control and shall unburden the user.
First, compensatory motions are strategies naturally employed by the CNS: when the device position is not correct, they are the first motor strategy mobilized by the wearer. No training is thus required for human subjects, since they naturally exhibit the signal used as controller input. CCC is **natural** in the sense that no specific knowledge on the implementation is necessary to make it work. There is also no need for algorithm training since no machine learning techniques are employed. The only parameters to define in CCC are the gain λ and the deadzone threshold q_0. No individual adaptation was required: λ and q_0 were set once and for all for each experiment and kept equal for all participants, able-bodied and amputated, which shows the robustness of CCC. These parameters can potentially be tuned around the values chosen in this work if the user wants a slightly more (or less) reactive device. CCC is also intuitive: there is **no need to learn** new motor strategies or to contract individual muscles.
CCC is simple: besides the very small number of parameters to tune, which are the same for everyone, the **control algorithm is not a black box** for the user. It only uses kinematics models, which are easy to understand, and for which everything is monitored. This could facilitate the prosthesis integration into the user's body image. Moreover, CCC removes the need for the user to be able to reverse-engineer the prosthesis control since the device position does not have to be corrected any more: the end-effector is properly placed by the user while the device is in charge of the user's posture. This also ensures that no unwanted prosthetic motions happen, reducing user's frustration.
In addition, the fact that the device joint positions do not have to be intentionally corrected any

more **decreases the mental burden** of the wearer. The latter does not have to constantly watch out for prosthesis motions but only focuses on the end-effector position. S/he is not even in charge of individual prosthetic joints, which are controlled **simultaneously**, which is less demanding and much closer to natural motions generation. Another natural character restored by CCC is motion continuity: closing the loop not only allows to eliminate the need for the user to take care of prosthesis position correction but also allows to produce **continuous prosthetic motions**. These motions are coordinated with user's ones, **prosthesis and user's body are synchronous**, while they work sequentially with ASC approaches.
Finally, CCC is **scalable**: controlling one, three or more DOF does not modify user's required behavior (compensatory motions to exhibit) or algorithm complexity nor increase the induced cognitive load. This is much more appropriate for the upcoming multi-DOF and biomimetic devices.

7.2 Future directions

This work has set up CCC framework and validated its use to control one and two DOF of UL prostheses. Promising results have been obtained but there is still a long way to go to achieve everyday prosthesis control with CCC.

7.2.1 First upcoming complements

Cognitive load assessment
Because CCC employs natural compensatory strategies, allows the user to focus on the end-effector only and makes simultaneous prosthetic joints control possible, it is claimed that the mental burden of the user is reduced. This has been assessed via Raw TLX and secondary task but on one subject only. To support the preliminary results on this topic, it is planned to involve more subjects but also to assess cognitive burden with EEG activity [196, 197], in order to complete this analysis with more objective and quantitative measures. A long-term study with daily use of CCC compared to daily use of an Auxiliary Signal Control (such as myoelectric) shall also be considered, to evaluate cognitive charge on a regular basis but also muscular fatigue.

Controlling more than two prosthetic degrees of freedom
CCC has been implemented for the control of one DOF and two DOF simultaneously but the general formulation presented Chapter 4 is theoretically valid for much more DOF. A next step will thus be to test the control of more than two prosthetic DOF with CCC. Preliminary tests have been runned on a 3-DOF prosthetic device (elbow flexion/extension, wrist pronosupination and wrist flexion/extension).

7.2.2 Definition of the reference human posture

The prosthesis position error, used to compute the velocity command, is computed from a human posture error, which is defined as a deviation from an objective (or reference) posture (see Chapter 3). This objective has not been studied in details in this work since the first step was to validate the concept of CCC: compensatory motions can be used as controller input to close the prosthesis control loop. Yet, the definition of the objective human posture is crucial to determine whether a body motion is compensatory. CCC does not depend on the task but on this objective, which varies with the context (subject sitting or standing, position of the target with respect to the subject, etc.). Note that the objective human posture can change for a same task and be similar between different tasks.
The experiments performed during this PhD had all a specific setup for which the reference posture could be easily determined; the latter was defined as the initial position of the participants and kept constant during the experiment. This is obviously a simplification; some limitations were already visible in the experiments presented Section 3.3.2 (enhancement of the trunk lateral bending for wrist pronation because shoulder adduction was hardly feasible from certain objective postures)

and Section 5.3 (over-extension of the elbow because the objective posture was not updated). The definition of this reference is a key element for an everyday-life functioning of CCC and is the next fondamental step to explore. Indeed, if the reference posture is not correctly defined, the body motions considered as compensatory will actually not be compensatory, the prosthesis motions will not fulfill its intended purpose – correct the user's posture – and will not be understood by the user; the natural character and the intuitiveness of the control will be totally removed.

To define a correct objective human posture, many ideas can be investigated. The first and simplest one is that the objective would be regularly updated by the user, with a specific signal. Yet, this would induce a double task for the user (positioning the end-effector and defining the reference posture), which is not beneficial at all. The second one is to implement machine learning algorithms which would update the reference posture or recognize in real time whether a body motion is compensatory (see [198] for a pilot study on this topic); but this would raise again the issues of black-box algorithms and accuracy (discussed Chapter 2) we wanted to avoid when building CCC. To tackle that, it could be imagined to implement reinforcement learning algorithms to update the reference, whose reward function would be user's compensatory movements. A third possibility could be to define an evolving objective posture that would follow the user's body motion with a certain delay (with a low-pass filter for instance). Finally, a human model could be built to optimize in real time the posture that allows the current positioning of the end-effector. This posture could be obtained with inverse kinematics methods, with some imposed constraints on joint motions, and would then define the reference human posture. This last suggestion seems the more promising and is the one we have begun to explore. In [199], a null-space optimization approach with a RULA-inspired score [200] has been proposed, for a human upper body model, and validated through a preliminary experimental campaign.

CCC relies on body compensatory motions of the user but its control scheme could be adapted to other continuous metrics that indicate a discomfort linked to a prosthesis position error: metabolic cost, muscular fatigue or balance for example. The objective would be defined accordingly but all of them seem to require a varying objective needed to be regularly updated, depending on the context (physical demand of the task, stable balance to perform the task, etc).

7.2.3 Wearable motion sensors for ecological application

Another essential point for an everyday use of CCC by amputated people, in their home and work environments, is the wearability of the required sensors. A prosthesis control scheme, even excellent, is useless if it is limited to laboratory environment only. In this work, the main sensor employed to measure body compensations was the motion capture system OptiTrack. It was chosen because of the easy body reconstruction and the precise measure of motions it gives. This allows to focus on the proof of CCC concept by bypassing the issue of body motions measurement in ecological situations. However, a motion capture system such as OptiTrack requires markers on the human body and/or the prosthesis, at least four cameras to be sure to capture the markers whatever the subject position, specific light conditions to avoid reflections on untracked objects, as well as a computer that runs the corresponding software. It is thus completely unsuitable to daily living environments. There is an imperious need to replace it with a wearable alternative.
To go incrementally towards a wearable and ecological solution for an every-day use, it is essential to set up a way to employ wearable sensors only. A widespread option is to use IMU, which are low cost, small and light. Many works indeed explore the feasibility to track human motions with IMU [201–203]. In UL prosthetics, these sensors can even be integrated into the socket or the prosthesis, which avoids adding specific tools to be worn by the user (as it can be the case with eye-tracking). For the wrist pronosupination formulation of CCC (described Section 3.3.1), the transfer between OptiTrack and IMU is direct since the data employed to compute body compensations, via the forearm rotation, are quaternions, which can be accessed with both sensors. Fixing an OptiTrack

marker or an IMU on the prosthetic forearm gives the same information. The OptiTrack-IMU transfer is not as easy for the general formulation of CCC. Indeed, recreating a human skeleton with IMU only is not a simple task since IMU provide orientation and rotation but not translation. Measuring the acromion displacement created by trunk motions is thus feasible but measuring the acromion displacement caused by scapula motions is much more difficult. Some solutions are proposed to measure scapula translations with IMU [204, 205] but this would require at least three sensors in the socket; a special attention should be paid to the well-known issues of multiple IMU fusion, with calibration and drift reduction challenges [202, 206]. A complementary alternative could be to use smart textiles to have more information on body motions, without being a burden for the user. There are still in early development though [207]. We finally plan to explore the possibility to use Microsoft HoloLens smartglasses to retrieve hand positions and reconstruct user's posture with prosthesis internal data.
It has to be noticed that a very precise measure of body motions is not necessarily required for a good functioning of CCC, because of the integration part. As the prosthesis is controlled in speed and not in position, the direction of its motion and an approximate velocity amplitude are enough to ensure an adequate control.

7.2.4 Generalization of Compensations Cancellation Control

This PhD focuses on UL prostheses control; CCC has thus been developed for this purpose. Yet, controlling a robotic device via body compensations is a concept that can be extended to other rehabilitation devices or even cobots. The concept of CCC is indeed valid as soon as human and robot work in coordination. The general formulation of CCC can be adapted to different situations; the only essential element required is that the user exhibits body compensations to express device position error.
In many pathologies, like stroke or tetraplegia, compensatory motions of the patients are observed when they want to realize a task, alone [167, 168, 208, 209] or with a rehabilitation robot [210–212]. For able-bodied people, body compensations are also largely observed at work [200, 213]. This thus supports the possible implementation of CCC for rehabilitation robots and cobots. Note that the use of compensatory motions for cobot control is not totally new since it has begun to be explored, in [214, 215] or [216].
The transfer of CCC to robots other than UL prostheses will depend on the type of the device. The easiest one is for UL exoskeletons for which nearly no changes are needed: the human joints guided by the exoskeleton can be considered as the prosthetic joints in the CCC formulation used in this work. The exact same theoretical framework can thus be reemployed. For cobots or other rehabilitation robots (e.g., assistive robotic arms such as Jaco from Kinova [217]), more adaptation will be necessary. The theoretical framework will differ since the end-effector is not an extension of a user's limb; the end-effector motion will not result from a combination of human and robotic movements but from robotic movements only. In these cases, the device does not replace part of a human limb and is not included into the human body but is totally distinct. The coupling still exists because both human and robot focus on a same target but the language of body compensatory motions will be modified compared to the one with prostheses or exoskeletons: a mirrorring effect can be expected. Another point to consider to adapt CCC to cobots and rehabilitation robots is that the relative position of human and robot could be varying if the robot is not worn by the user, which should also require some framework modifications. The transfer will thus not be straightforward but it opens large possibilities for Compensations Cancellation Control.

List of Figures

List of Tables

Appendix A

Few details on some regression and classification algorithms

In Section 2.3.2, two machine learning algorithms were employed to model joints synergies and two to illustrate the difficulty to classify motions. This appendix exposes some details on their theory and implementation.

A.1 Regression algorithms for synergy models

As briefly explained in Section 2.1.2, regression algorithms predict continuous output(s). Prior to the online use of the algorithms, a training process is required to learn the relationship between inputs and (continuous) outputs from example data; the relationship is a function $f : X \rightarrow Y$, which depends on the model employed. This then enables predictions from new inputs.
In the case considered here, the output is the elbow flexion angular velocity (1D) and the input is the shoulder Euler angular velocities (3D). Two different algorithms were implemented: Radial Basis Function Network (RBFN) and Gaussian Mixture Regression (GMR).

A.1.1 Radial Basis Function Network

Theory
RBFN defines the output as a weighted sum of radial functions of the input (see Figure A.1(a))

$$y = f(\mathbf{x}) = \sum_{e=1}^{E} w_e.\phi(\mathbf{x}, \boldsymbol{\theta}_e) \tag{A.1}$$

with ϕ the radial basis functions ($\forall e \in [\![1, E]\!], \phi(\mathbf{x}, \boldsymbol{\theta}_e) = \phi(||\mathbf{x} - \boldsymbol{\theta}_e||)$, E the number of radial functions, $\boldsymbol{\theta}_e \quad (e \in [\![1, E]\!])$ the centers of the basis functions and $w_e \quad (e \in [\![1, E]\!])$ the weights. ϕ are often Gaussian functions; they are here defined as followed:

$$\forall e \in [\![1, E]\!], \phi(x, \boldsymbol{\theta}_e) = e^{-(||\mathbf{x}-\boldsymbol{\theta}_e||)^2} \tag{A.2}$$

E, $\boldsymbol{\theta}_e$ and $w_e \quad (e \in [\![1, E]\!])$ are all determined during the training phase. Different methods are available to set them; in this work, the number of radial basis functions, E, was optimally chosen with cross-validation and set to 5, $\boldsymbol{\theta}_e, e \in [\![1, E]\!]$ were defined with equidistant spacing – results were similar as when defining them with k-means clustering –, and $w_e \quad (e \in [\![1, E]\!])$ were obtained with Linear Least Square.

Implementation
RBFN was implemented on Matlab Mathworks®, be it for the training or the testing phases. Even if some predefined RBFN functions are available on Matlab, the code used for the analysis of Section 2.3.2 was entirely re-written (by a previous PhD student and myself). As the training set came from different subjects, the data were centered and normalized, which thus involves a processing

step at the end of the testing phase to get back unormalized output.

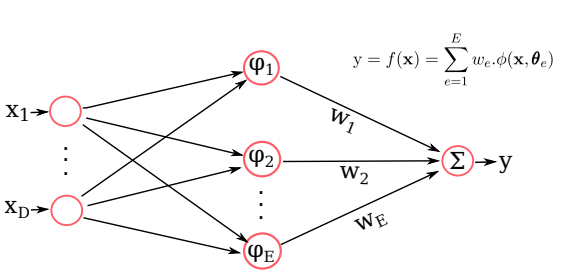

(a) RBFN relationship between inputs and outputs, adapted from [160]. D is the dimension of the inputs, E is the number of radial basis functions.

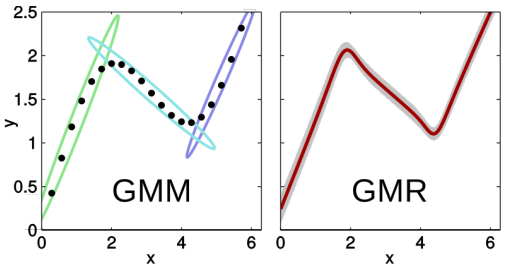

(b) GMM and GMR with 3 Gaussians, from [160].

Figure A.1: RBFN and GMR illustrations.

A.1.2 Gaussian Mixture Regression

Theory

With GMR, it is assumed that the data in the joint input×output space can be represented by a set of Gaussians, the Gaussian Mixture Model (GMM) (see Figure A.1(b)). The training phase is unsupervised, which means that there is no distinction between inputs and outputs, concatenated into one vector. This phase consists in fitting the data with a GMM with the Expectation-Maximization algorithm. A k-means clustering was here applied to initialize the centers of the Gaussians. The GMM gives a model of the density of the concatenated inputs-outputs vectors as a weighted sum of E Gaussian functions:

$$[\mathbf{x}_n^T \quad y_n]^T = \mathbf{z}_n = \sum_{e=1}^{E} \pi_e N(\mathbf{z}_n, \boldsymbol{\mu}_e, \boldsymbol{\Sigma}_e) \tag{A.3}$$

with n the number of samples of the training data set and $\pi_e (e \in [\![1, E]\!])$ the prior probabilities, $\sum_{e=1}^{E} \pi_e = 1$. The Expectation-Maximization algorithm adjusts the prior π_e and the parameters of the Guassians $\boldsymbol{\mu}_e$ and $\boldsymbol{\Sigma}_e$. The number of Gaussians E was determined with the Bayesian Information Criterion [163, 218] and was set to 5.

Once the GMM parameters are determined, a new output can be predicted from a new input, through GMR. To do so, we distinguish the input and output components of $\boldsymbol{\mu}_e$ and $\boldsymbol{\Sigma}_e$:

$$\begin{aligned} \boldsymbol{\mu}_e &= [\boldsymbol{\mu}_{e,X}^T, \boldsymbol{\mu}_{e,Y}^T] \\ \text{and } \boldsymbol{\Sigma}_e &= \begin{pmatrix} \boldsymbol{\Sigma}_{e,X} & \boldsymbol{\Sigma}_{e,XY} \\ \boldsymbol{\Sigma}_{e,YX} & \boldsymbol{\Sigma}_{e,Y} \end{pmatrix} \end{aligned} \tag{A.4}$$

The expected output is then defined as

$$y = \sum_{e=1}^{E} h_e(\mathbf{x}) \left(\boldsymbol{\mu}_{e,Y} + \boldsymbol{\Sigma}_{e,YX} \boldsymbol{\Sigma}_{e,X}^{-1} (\mathbf{x} - \boldsymbol{\mu}_{e,X}) \right) \tag{A.5}$$

$$\text{with } h_e(\mathbf{x}) = \frac{\pi_e N(\mathbf{x}, \boldsymbol{\mu}_{e,X}, \boldsymbol{\Sigma}_{e,X})}{\sum_{l=1}^{E} \pi_l N(\mathbf{x}, \boldsymbol{\mu}_{l,X}, \boldsymbol{\Sigma}_{l,X})} \tag{A.6}$$

and $\mathbf{x}$ the vector of input data.

Implementation

As RBFN, all the steps for GMR were implemented on Matlab Mathworks®, without using the ready-to-use Matlab functions, in order to manage the smallest implementation choice. The inputs and outputs were also centered and normalized for the training phase.

A.2 Classification algorithms for motions recognition

Contrary to regression, classification algorithms give discrete outputs, labels of motions in our case. For the illustrative study of Section 2.3.2, two algorithms were implemented: Bayesian Decision Making (BDM) and Support Vector Machine (SVM).

A.2.1 Bayesian Decision Making

Theory

BDM is one of the simplest classification algorithm. The decision of the class of one input is taken comparing the relation between posterior probabilities. Samples $\mathbf{x}$ are classified belonging to class k if

$$P(C_k|\mathbf{x}) > P(C_j|\mathbf{x}) \quad \forall j \neq k \tag{A.7}$$

Given Bayes theorem, this is equivalent to

$$\begin{aligned} \frac{p(\mathbf{x}|C_k)P(C_k)}{p(\mathbf{x})} &> \frac{p(\mathbf{x}|C_j)P(C_j)}{p(\mathbf{x})} \quad \forall j \neq k \\ \text{or } p(\mathbf{x}|C_k)P(C_k) &> p(\mathbf{x}|C_j)P(C_j) \quad \forall j \neq k \end{aligned} \tag{A.8}$$

with $p(\mathbf{x}|C_k)$ the conditional probability, $P(C_k)$ the prior probability and $p(\mathbf{x})$ the probability density, $p(\mathbf{x}) = \sum_k p(\mathbf{x}|C_k)P(C_k)$; prior probabilities can be estimated from training data. Any monotonic function can also be used to take the decision.

It is assumed, in the case considered in Section 2.3.2, that probabilities are normal distributions, with mean μ_k and arbitrary covariance matrices for each class, $\mathbf{\Sigma}_k$. It gives for a new input $\mathbf{x}$ and a class k

$$p(\mathbf{x}|C_k) = \frac{1}{(2*\pi)^{d/2}|\mathbf{\Sigma}_k|^{1/2}} \exp\left(-\frac{1}{2}(\mathbf{x}-\mu_k)^T\mathbf{\Sigma}_k^{-1}(\mathbf{x}-\mu_k)\right) \tag{A.9}$$

with d the dimension of input vector $\mathbf{x}$.

The training phase of BDM allows to compute the covariance, $\mathbf{\Sigma}_k$, and mean, μ_k of each class, as well as $P(C_k)$:

$$P(C_k) = \frac{N_k}{N} \tag{A.10}$$

with N_k the number of training data belonging to class k and N the total number of training data. During online use, the quantity $p(\mathbf{x}|C_k)P(C_k)$ is computed for all class k ($k = 4$ in our case, the four tasks considered), the highest one gives the class assigned to the input $\mathbf{x}$.

Implementation

This naive Bayesian classifier was also implemented from scratch on Matlab Mathworks®.

A.2.2 Support Vector Machine

Theory

SVM is originally a two-class classifier that separates data with a decision boundary. This boundary, the max-margin hyperplane, is the one for which the smallest distance between the boundary and the samples – called the margin – is maximized [218]. It is determined during the training phase and is completely defined by the support vectors, the training samples that lie nearest to it (see Figure A.2). To determine the hyperplane equation, linear but also non-linear methods with kernel functions can be used; we chose the second one. SVM then deals with new inputs by identifying whose side of the hyperplane they are on.

When the classification problem has more than two classes, various methods are available. The one employed here is the one-versus-one approach, which trains 2-class SVM on all possible pairs of classes and then classifies new inputs in the class which has the highest number of "votes".

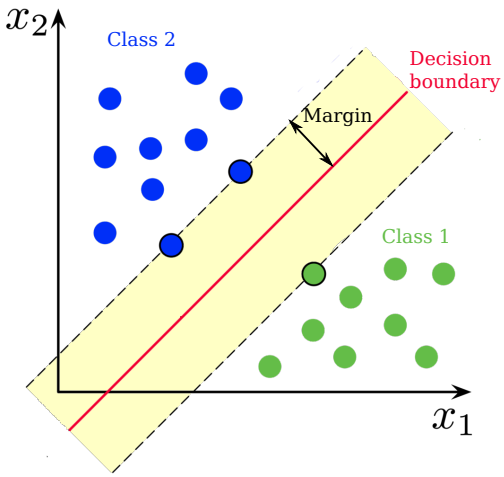

Figure A.2: Illustration of a 2-class SVM classifier functioning, inspired from *wikipedia.org*

Implementation

For the illustrative study of Section 2.3.2, the 4-class SVM classifier was implemented on Matlab Mathworks®, with predefined Matlab functions: *fitcecoc* performs the one-versus-one training of the multi-class SVM, with kernel functions; *predict* then used the trained algorithm to classify samples of the testing data set.

Appendix B

Data collection for movement classification

This appendix describes the data collection, as well as their processing, for the movement classification illustrative study whose results are presented Section 2.3.2.

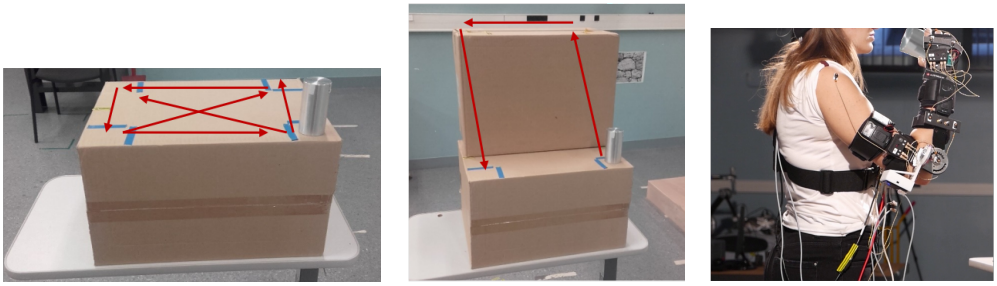

Figure B.1: Set-up of the data collection for the movement classification illustrative study. One able-bodied subject reached an object and moved it to the next position, as indicated by the arrows: reach-and-place at the same height (left), reach-and-place at two different heights (middle). The last task consisted in reaching the object and bringing it to the mouth (right).

The collected data set is from one able-bodied subject performing various tasks: reach-and-place, at nine different heights and positions, and bring-to-mouth (see Figure B.1). Four trials were recorded for each task. Euler angles of the trunk, as well as humerus aperture and elbow flexion angles, were measured with two IMUs and the motion capture system Codamotion®. Four motion classes were defined by hand: reaching, return, change height and bring-to-mouth. Data were segmented with zero-crossings of the elbow marker velocity and classes were manually labeled. The features used as input of the classification algorithms were mean and variance of the trunk Euler angular velocities, trunk rotation and trunk flexion angles. They were computed in a sliding window of 100ms or 500ms, with an increment time of 10ms. Three trials (over four) composed the training set, and the remaining one composed the testing set. In Section 2.3.2, the mean classification accuracy for each algorithm is presented, Table B.1 shows the results for each testing set.

Trial used for testing	trial 1	trial 2	trial 3	trial 4
BDM, $t_w = 100$ms	46.50 %	46.80%	40.10%	47.20%
BDM, $t_w = 500$ms	65.20%	67.90%	54.30%	63.90%
SVM, $t_w = 100$ms	67.70%	58.40%	52.40%	65.80%
SVM, $t_w = 500$ms	65.60%	59.80%	47.60%	67.80%

Table B.1: Classification accuracy of BDM and SVM, with two different sizes of sliding window, t_w, depending on the trial used as testing set.

In addition to the optimization means listed in Section2.3.2, it can also be considered to increase the amount of data, since they are from four trials and one subject only.

Appendix C

Characterization of body compensations with reduced elbow mobility: head and balance metrics

This appendix contains complementary figures of the body compensations characterization study, from Chapter 3.

Experimental set-up reminder
This experiment aims at characterizing the body motions exhibited to compensate a loss in elbow mobility. Ten able-bodied subjects were asked to perform 3D tasks with their right arm, naturally and with their elbow blocked at 90 deg with an orthosis. Eight reaching and object-moving tasks were achieved; the whole sequence was repeated four times.

Complementary figures
Trunk angular trajectories and acromion displacement for the different tasks were analyzed in details, along with representative Figures, in the main text. Head Euler angles and weight repartition have been more briefly discussed, as not considered compensatory since their motions do not directly participate to the task. Below are the corresponding results.

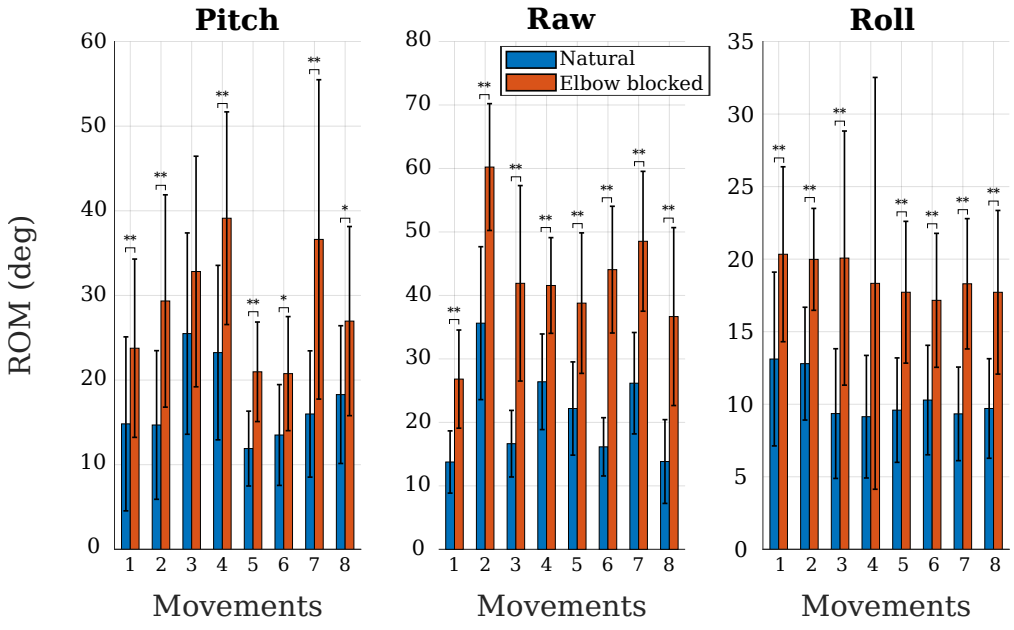

Figure C.1: ROM of head Euler angles, computed in the trunk frame, averaged over subjects, for natural and blocked motions. Numbers indicates the different movements performed during the experiment, illustrated on Figure 3.2

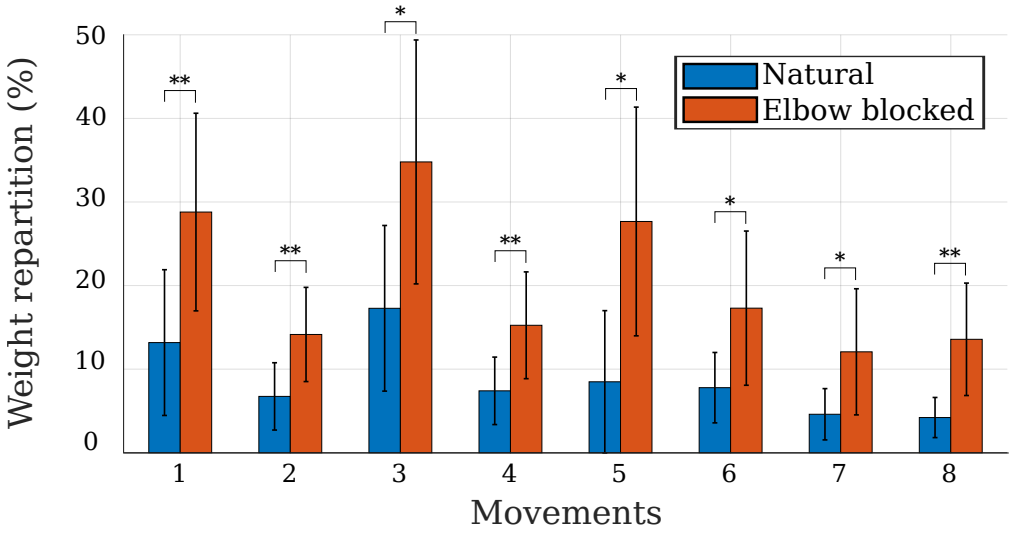

Figure C.2: Weight repartition, defined as $\frac{\text{force on the ipsilateral foot}}{\text{total force applied on the feet}}$, expressed in percent, for natural and blocked motions. Results are averaged over subjects. Numbers indicate the different movements performed during the experiment, illustrated on Figure 3.2

Appendix D

Evaluation of Compensations Cancellation Control for elbow joint control: individual results

This appendix displays the individual results of task performance, body compensations and global joint motions metrics, from the validation experiment with able-bodied participants of Chapter 5.

Experimental set-up reminder
In Section 5.3.2, the general formulation of CCC is tested to control a prosthetic elbow joint. Ten able-bodied subjects, without any previous experience on prosthetic devices, wore an emulated elbow prosthesis attached to their right arm with an orthosis. They were asked to perform path tracking tasks with two different trajecories (rectangular and diagonal) and a 3D reaching task.

Individual results
The results given in the main manuscript are averaged over the ten participants. As mean over participants can hide some inter-subjects variations, the individual results are shown below, for each subject, averaged over trials.

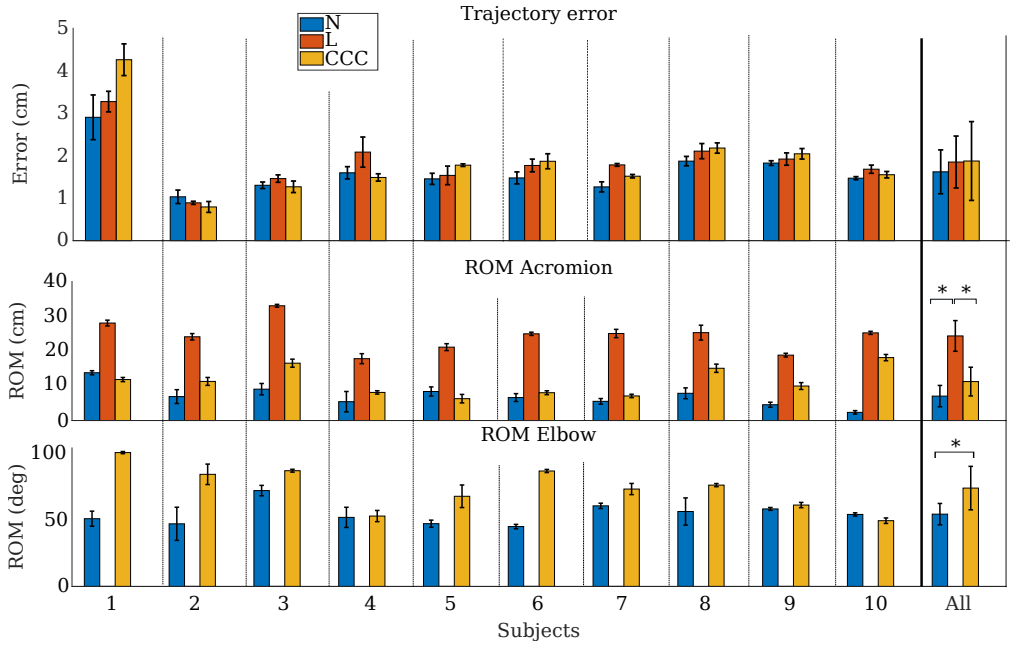

Figure D.1: Individual results for the rectangular path tracking task. Results for each subject are the mean of the metric over the five trials. The last column is the mean over subjects; * indicates $p < 0.05$.

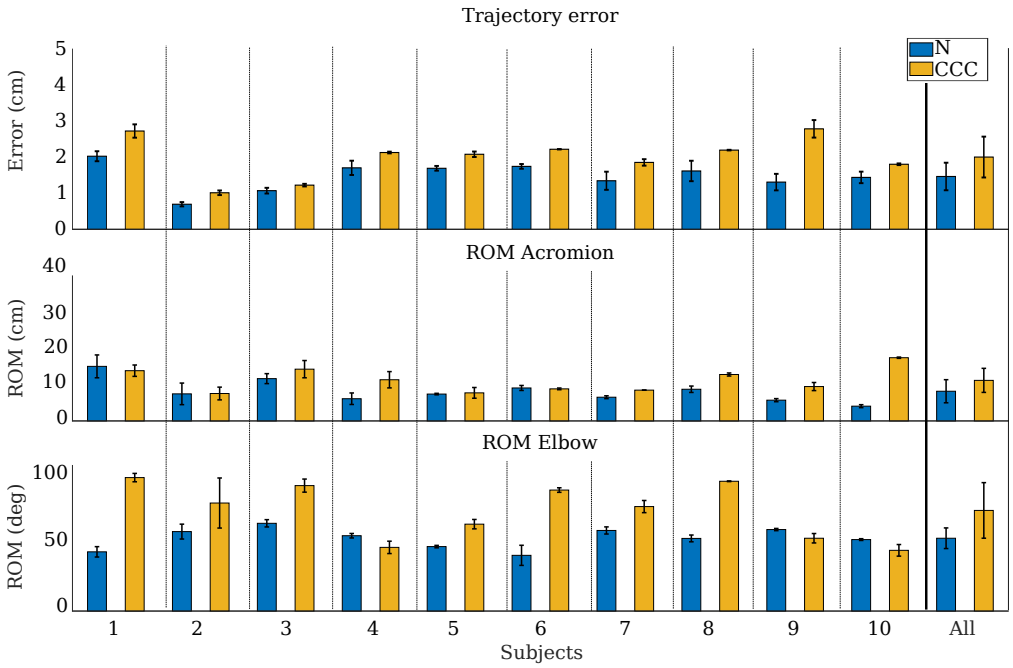

Figure D.2: Individual results for the diagonal path tracking task. Results for each subject are the mean of the metric over the five trials. The last column is the mean over subjects; * indicates $p < 0.05$.

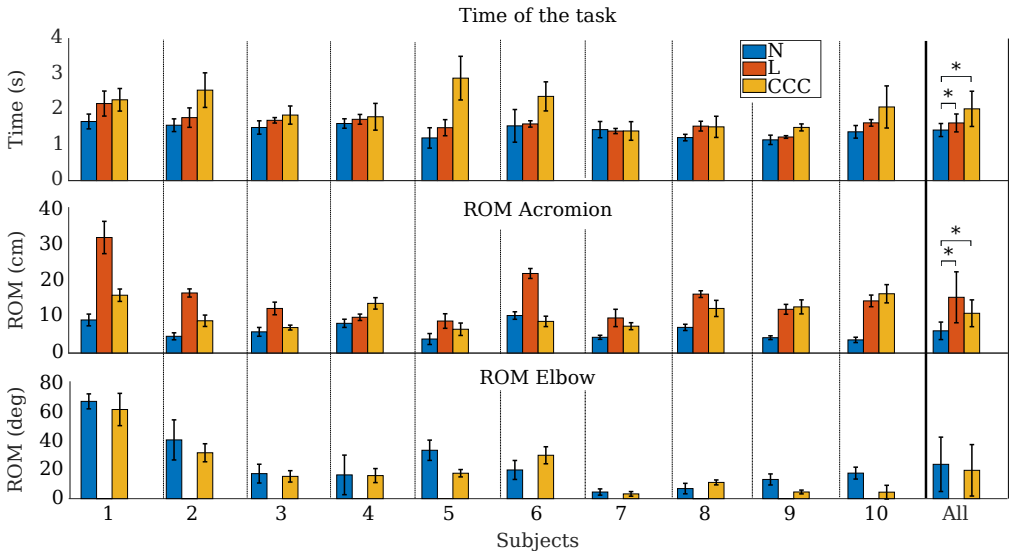

Figure D.3: Individual results for the reaching task, Target 1. Results for each subject are the mean of the metric over the five trials. The last column is the mean over subjects; * indicates $p < 0.05$.

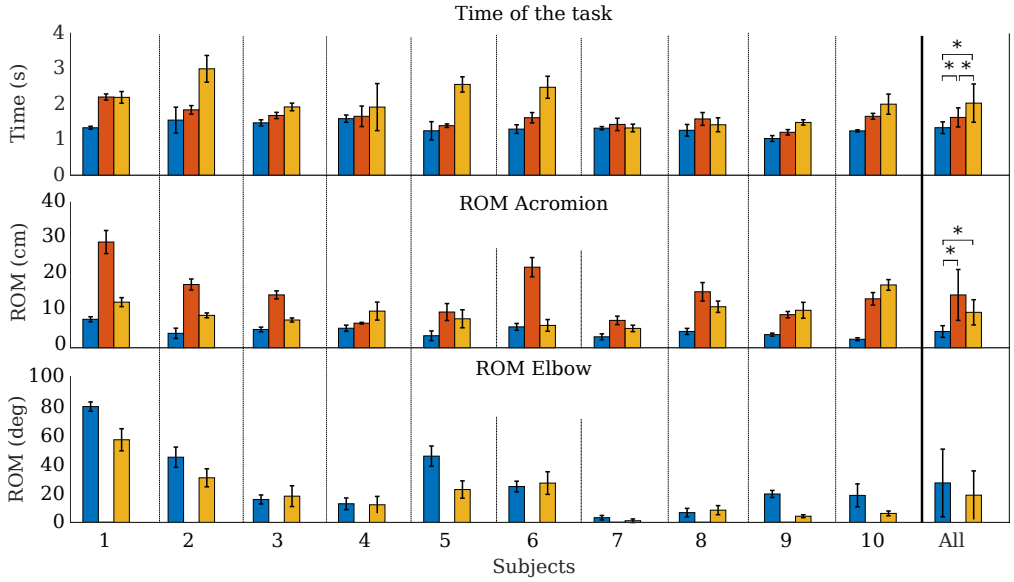

Figure D.4: Individual results for the reaching task, Target 2. Results for each subject are the mean of the metric over the five trials. The last column is the mean over subjects; * indicates $p < 0.05$.

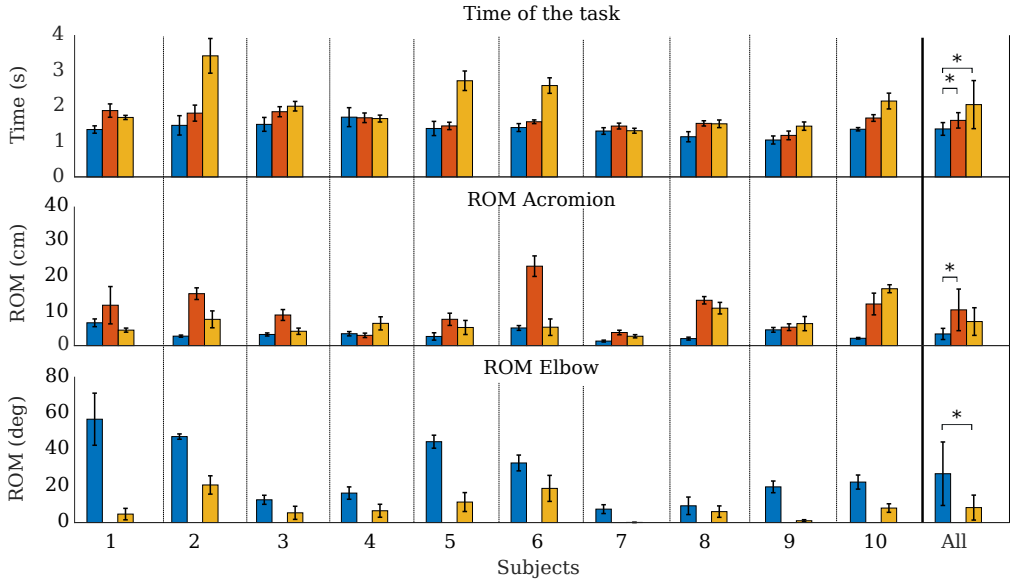

Figure D.5: Individual results for the reaching task, Target 3. Results for each subject are the mean of the metric over the five trials. The last column is the mean over subjects; * indicates $p < 0.05$.

Appendix E

Stability of Compensations Cancellation Control: additional proofs

In Section 4.3, the stability of CCC was studied, in a simplified linear and monovariate case, for a robotic system. Even if the conclusions of this Section have been validated on human-in-the-loop experiments, a more detailed analysis has been conducted by Alexis Poignant; some elements are presented in this Appendix. Figure E.1 reminds the diagram and the notations employed for the analysis. The kinematics of the robotic system is still considered as linear.

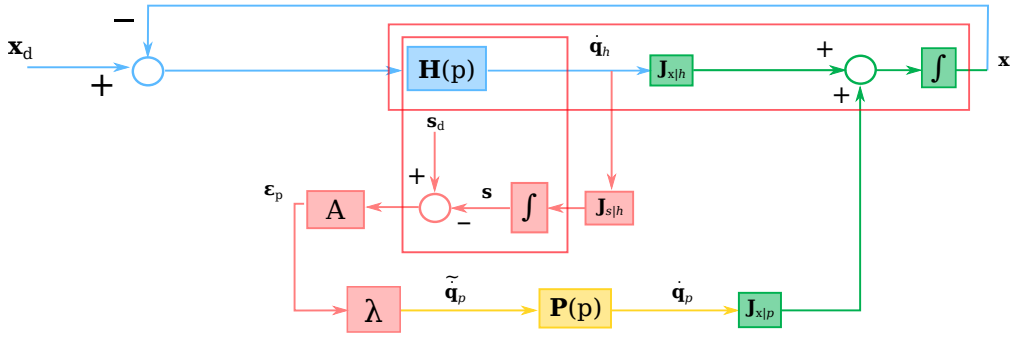

Figure E.1: Block diagram of the simplified case of a robotic system with distal joints controlled with CCC. $\mathbf{H}(p)$ is the closed-loop transfer function of the proximal part, $\mathbf{P}(p)$ is the transfer function of the distal part, $\mathbf{A}$ is the mapping matrix between the error measured by the sensors and the error of the distal joints, $\mathbf{J}_{x|h}$, $\mathbf{J}_{x|p}$, $\mathbf{J}_{s|h}$ and λ are defined in the equations developped Section 4.1. The red rectangles help to visualize the double integrator in the proximal robotic part.

E.1 Addition of a deadzone

To avoid unwanted motions of the distal part when the proximal part is around the objective posture, a deadzone is added on $\boldsymbol{\epsilon}_p$. This is similar to the addition of a deadzone before $\mathbf{H}(p)$. Considering an harmonic input, $X\sin(\omega t)$, the deadzone can be represented as a complex gain $N(X)$, assuming that it is followed by a low pass filter ($\mathbf{H}(p)$). N is defined by

$$N(X) = \frac{U + jV}{X} \tag{E.1}$$

with $U = \frac{2}{T}\int_0^T w(t)\sin(\omega t)dt$ and $V = \frac{2}{T}\int_0^T w(t)\cos(\omega t)dt$, $w(t)$ being the non-linearity of input $X\sin(\omega t)$. In the case analyzed here, N is real

$$N(X) = \begin{cases} 0 \text{ if } X < X_t \\ \frac{2}{\pi}\arcsin(\frac{X_m}{X} + \frac{2X_m}{\pi X}\sqrt{1 - \left(\frac{X_m}{X}\right)^2} \text{ if } X_t < X < X_m \\ 1 \text{ if } X > X_m \end{cases} \tag{E.2}$$

where X_t and X_m are the threshold and saturation values respectively. The open-loop transfer function becomes

$$\left[\frac{X}{X_d}\right]_{OL} = \frac{\mathbf{H}(p)}{p}\mathbf{J}_{x|h}\left(1 + F(p,\lambda)\right)N(X) \tag{E.3}$$

In free regime, studying this non-linearity is equivalent to studying stable oscillations and analyzing the closed-loop denominator:

$$1 + \frac{\mathbf{H}(p)}{p}\mathbf{J}_{x|h}\left(1 + F(p,\lambda)\right)N(X) = 0 \tag{E.4}$$

or

$$\frac{\mathbf{H}(p)}{p}\mathbf{J}_{x|h}\left(1 + F(p,\lambda)\right) = \frac{-1}{N(X)} \tag{E.5}$$

According to Loeb's criteria, as $N(X)$ is at the left of the critical point (-1,0), the system stays stable.
To analyze the deadzone in forced regime, we lack information on $\mathbf{H}(p)$.

E.2 Imperfect internal prosthesis command

In Section 4.3, it was assumed that $\mathbf{P}(p) = 1$, i.e. the response time of the distal part's internal command (the control of prostesis' motors in real life application) was very short compared to the response time of the proximal part (playing the role of the human user). To be more exact, $\mathbf{P}$ can be written as a closed-loop transfer function

$$\mathbf{P}(p) = \frac{B(p)}{1 + B(p)} \tag{E.6}$$

and we presume that the open-loop transfer function $B(p)$ has good enough phase and gain margins. The open-loop transfer function of the entire system becomes

$$\begin{aligned}\left[\frac{X}{X_d}\right]_{OL} &= \frac{\mathbf{H}(p)}{p}\mathbf{J}_{x|h}\left(\frac{p + \mathbf{P}(p)\lambda}{p}\right) \\ &= \frac{\mathbf{H}(p)}{p}\mathbf{J}_{x|h}\left(\frac{p + pB(p) + \lambda B(p)}{p + pB(p)}\right)\end{aligned} \tag{E.7}$$

For high-frequencies, we have

$$\left[\frac{X}{X_d}\right]_{OL} \approx \frac{\mathbf{H}(p)}{p}\mathbf{J}_{x|h} \tag{E.8}$$

and for low frequencies

$$\left[\frac{X}{X_d}\right]_{OL} \approx \frac{\mathbf{H}(p)}{p}\mathbf{J}_{x|h}\frac{p + \lambda}{p} \tag{E.9}$$

This thus corresponds to the ideal case studied in Section 4.3, where the entire system behaves as the proximal part in high frequencies and as the proximal part multiplied by a proportional-integrator in low frequencies. The only case for which the stability is at risk is around the critical point between p and $B(p)$. Assuming the static gain of $pB(p)$ or $\lambda B(p)$ is relatively low, this critical point will always be at low frequencies, where the entire system is far from critical points. It can thus be considered that stability is still ensured.

E.3 Multivariate case

Until now, the analysis was performed on a monovariate case. Considering now a multivariate case (which is of great interest for CCC), where proximal and distal robotic parts have two DOF each,

$$\dot{\mathbf{q}}_h = \begin{pmatrix} q_{h1} \\ q_{h2} \end{pmatrix} \in \mathbb{R}^{2\times 1}$$
$$\dot{\mathbf{q}}_p = \begin{pmatrix} q_{p1} \\ q_{p2} \end{pmatrix} \in \mathbb{R}^{2\times 1}$$

and thus

$$\mathbf{J}_{x|h} \in \mathbb{R}^{2\times 2}$$
$$\mathbf{J}_{x|p} \in \mathbb{R}^{2\times 2}$$
$$\mathbf{J}_{s|h} \in \mathbb{R}^{2\times 2}$$
$$\mathbf{A} \in \mathbb{R}^{2\times 2}$$

We still assume that $\mathbf{M}$, the mapping between sensor and prosthesis error signal, can be written as

$$\mathbf{M} = -\mathbf{J}_{s|h}\mathbf{J}^{+}_{x|h}\mathbf{J}_{x|p} \tag{E.10}$$

Thus,

$$\begin{aligned} \mathbf{A} = \mathbf{M}^{+} = -\left(\mathbf{J}_{s|h}\mathbf{J}^{+}_{x|h}\mathbf{J}_{x|p}\right)^{+} \\ \text{and} \quad \mathbf{J}_{x|h} = -\mathbf{J}_{x|p}\mathbf{A}\mathbf{J}_{s|h} \end{aligned} \tag{E.11}$$

In this case, the open-loop transfer function of the system is

$$\left[\frac{X}{X_d}\right]_{OL} = \frac{\mathbf{H}(p)}{p}\mathbf{J}_{x|h}\left(1 + \frac{\lambda}{p}\right) \tag{E.12}$$

with four transfer functions similar to the one of the monovariate case. The condition for stability is thus the same as the one found in Section 4.3:

$$\lambda \ll \omega_c \tag{E.13}$$

with ω_c the cut-off pulse of the proximal robotic part.

Appendix F

Raw-TLX questionnaire

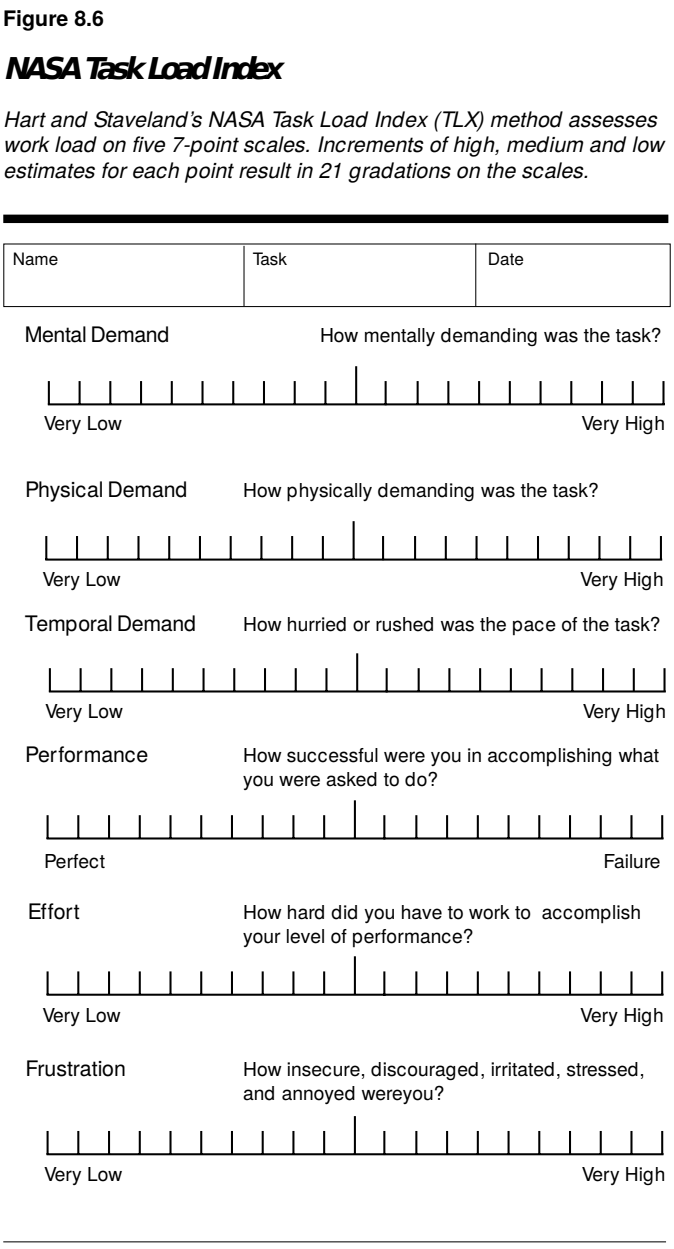

Figure 8.6

NASA Task Load Index

Hart and Staveland's NASA Task Load Index (TLX) method assesses work load on five 7-point scales. Increments of high, medium and low estimates for each point result in 21 gradations on the scales.

Name	Task	Date

Mental Demand — How mentally demanding was the task?
Very Low — Very High

Physical Demand — How physically demanding was the task?
Very Low — Very High

Temporal Demand — How hurried or rushed was the pace of the task?
Very Low — Very High

Performance — How successful were you in accomplishing what you were asked to do?
Perfect — Failure

Effort — How hard did you have to work to accomplish your level of performance?
Very Low — Very High

Frustration — How insecure, discouraged, irritated, stressed, and annoyed wereyou?
Very Low — Very High

Figure F.1: TLX scale.
Available at http://humansystems.arc.nasa.gov/groups/TLX/downloads/TLXScale.pdf

References

[1] K. Ziegler-Graham, E. J. MacKenzie, P. L. Ephraim, T. G. Travison, and R. Brookmeyer, "Estimating the Prevalence of Limb Loss in the United States: 2005 to 2050," *Archives of Physical Medicine and Rehabilitation*, vol. 89, no. 3, pp. 422–429, 2008.

[2] G. Bastas, *Essentials of Physical Medicine and Rehabilitation (Fourth Edition)*, 2020, ch. Lower Limb Amputations, pp. 658–663.

[3] G. K. Kumar, C. D. Souza, and E. Diaz, "Incidence and causes of lower-limb amputations in a tertiary care center: Evaluation of the medical records in a period of 2 years," *International Journal of Surgery Science*, vol. 2, no. 3, pp. 16–19, 2018.

[4] N. Unwin, "Epidemiology of lower extremity amputation in centres in Europe, North America and East Asia," *British Journal of Surgery*, vol. 87, no. 3, pp. 328–337, 2000.

[5] Association de Défense et d'Etude des Personnes Amputées, (ADEPA). [Online]. Available: https://www.adepa.fr/

[6] T. R. Dillingham, L. E. Pezzin, and E. J. MacKenzie, "Limb amputation and limb deficiency: epidemiology and recent trends in the United States," *Southern medical journal*, vol. 95, no. 8, pp. 875–884, 2002.

[7] F. Cordella *et al.*, "Literature Review on Needs of Upper Limb Prosthesis Users," *Frontiers in Neuroscience*, vol. 10, 2016.

[8] K. Østlie, R. J. Franklin, O. H. Skjeldal, A. Skrondal, and P. Magnus, "Musculoskeletal Pain and Overuse Syndromes in Adult Acquired Major Upper-Limb Amputees," *Archives of Physical Medicine and Rehabilitation*, vol. 92, no. 12, pp. 1967–1973, 2011.

[9] H. Autorité de Santé, "Evaluation des prothèses externes du membre supérieur," 2010.

[10] S. Watve, G. Dodd, R. MacDonald, and E. R. Stoppard, "Upper limb prosthetic rehabilitation," *Orthopaedics and Trauma*, vol. 25, no. 2, pp. 135–142, 2011.

[11] O. Horgan and M. MacLachlan, "Psychosocial adjustment to lower-limb amputation: A review," *Disability and Rehabilitation*, vol. 26, no. 14-15, pp. 837–850, 2004.

[12] J. Jacques, E. Verbraeken, and J.-M. Vanmarsenille, "L'appareillage de l'amputé du membre supérieur," *Louvain Medecine*, vol. 138, no. 4, pp. 193–198, 2019.

[13] E. Biddiss and T. Chau, "Upper-Limb Prosthetics: Critical Factors in Device Abandonment," *American Journal of Physical Medicine and Rehabilitation*, vol. 86, no. 12, pp. 977–987, 2007.

[14] K. Østlie *et al.*, "Prosthesis use in adult acquired major upper-limb amputees: patterns of wear, prosthetic skills and the actual use of prostheses in activities of daily life," *Disability and Rehabilitation: Assistive Technology*, vol. 7, no. 6, pp. 479–493, 2012.

[15] C. Castellini, "Design Principles of a Light, Wearable Upper Limb Interface for Prosthetics and Teleoperation," in *Wearable Robotics*, 2020, pp. 377–391.

[16] R. F. Weir, *Standard handbook of biomedical engineering and design*, New York, 2003, ch. Design of Artificial Arms and Hands for Prosthetic Applications, pp. 32.1–32.61.

[17] E. A. Biddiss and T. T. Chau, "Upper limb prosthesis use and abandonment: A survey of the last 25 years," *Prosthetics and Orthotics International*, vol. 31, no. 3, pp. 236–257, 2007.

[18] J. Ribeiro *et al.*, "Analysis of Man-Machine Interfaces in Upper-Limb Prosthesis: A Review," *Robotics*, vol. 8, no. 1, p. 16, 2019.

[19] Steeper Group. [Online]. Available: https://www.steepergroup.com/prosthetics/

[20] L. Capestany and W. Esparza, "Transhumeral Recreational Prosthesis," *Journal of Prosthetics and Orthotics*, vol. 23, no. 3, pp. 165–167, 2011.

[21] Ottobock. [Online]. Available: https://www.ottobockus.com/

[22] W. Selpho, "Construction of artificial hands," US Patent US18 021A, 1857.

[23] J. N. Billock, "Upper Limb Prosthetic Terminal Devices: Hands Versus Hooks," *Clinical Prosthetics and Orthotics*, vol. 10, no. 2, pp. 57–65, 1986.

[24] Le Tourneau prosthetics. [Online]. Available: https://www.llop.com/upper-limb-prosthetics-prosthetic-arms/

[25] L. Resnik, M. Borgia, A. W. Heinemann, and M. A. Clark, "Prosthesis satisfaction in a national sample of veterans with upper limb amputation," *Prosthetics and Orthotics International*, pp. 1–11, 2020.

[26] The O&P Edge. [Online]. Available: https://www.oandp.com/

[27] C. D. Metcalf *et al.*, "Changes in Hand Function with Age and Normative Unimpaired Scores when Measured with the Southampton Hand Assessment Procedure," *The British Journal of Hand Therapy*, vol. 13, no. 3, pp. 79–83, 2008.

[28] Össur. [Online]. Available: https://www.ossur.com/en-us/prosthetics/touch-solutions

[29] C. Cipriani, M. Controzzi, and M. C. Carrozza, "Objectives, criteria and methods for the design of the SmartHand transradial prosthesis," *Robotica*, vol. 28, no. 6, pp. 919–927, 2009.

[30] D. A. Zlotolow and S. H. Kozin, "Advances in Upper Extremity Prosthetics," *Hand Clinics*, vol. 28, no. 4, pp. 587–593, 2012.

[31] P. J. Kyberd *et al.*, "Two-degree-of-freedom powered prosthetic wrist," *The Journal of Rehabilitation Research and Development*, vol. 48, no. 6, p. 609, 2011.

[32] N. M. Bajaj, A. J. Spiers, and A. M. Dollar, "State of the art in prosthetic wrists: Commercial and research devices," in *Proceedings of the IEEE International Conference on Rehabilitation Robotics*, 2015.

[33] S. C. Jacobson, D. F. Knutti, R. T. Johnson, and H. H. Sears, "Development of the Utah Artificial Arm," *IEEE Transactions on Biomedical Engineering*, vol. 9, no. 4, pp. 249–269, 1982.

[34] H. H. Sears, "Advances in Arm Prosthetics," *Motion Control Inc*, 1999.

[35] M. S. Johannes *et al.*, "An overview of the developmental process for the modular prosthetic limb," *Johns Hopkins APL Technical Digest*, vol. 30, no. 3, pp. 207–216, 2011.

[36] L. Resnik, S. L. Klinger, K. Etter, and C. Fantini, "Controlling a multi-degree of freedom upper limb prosthesis using foot controls: user experience," *Disability and Rehabilitation: Assistive Technology*, vol. 9, no. 4, pp. 318–329, 2013.

[37] Mobius Bionics. [Online]. Available: https://www.mobiusbionics.com/luke-arm/

[38] Texas prosthetics. [Online]. Available: http://www.txprostheticcenter.com/utah-arm

[39] The London Prosthetics. [Online]. Available: www.thelondonprosthetics.com

[40] J. Ten Kate, G. Smit, and P. Breedveld, "3D-printed upper limb prostheses: a review," *Disability and Rehabilitation: Assistive Technology*, vol. 12, no. 3, pp. 300–314, 2017.

[41] C. Piazza *et al.*, "The SoftHand Pro-H: A Hybrid Body-Controlled, Electrically Powered Hand Prosthesis for Daily Living and Working," *IEEE Robotics and Automation Magazine*, vol. 24, no. 4, pp. 87–101, 2017.

[42] M. Catalano *et al.*, "Adaptive synergies for the design and control of the Pisa/IIT SoftHand," *The International Journal of Robotics Research*, vol. 33, no. 5, pp. 768–782, 2014.

[43] G. Kanitz, F. Montagnani, M. Controzzi, and C. Cipriani, "Compliant Prosthetic Wrists Entail More Natural Use Than Stiff Wrists During Reaching, Not (Necessarily) During Manipulation," *IEEE Transactions on Neural Systems and Rehabilitation Engineering*, vol. 26, no. 7, pp. 1407–1413, 2018.

[44] S. M. Engdahl *et al.*, "Surveying the interest of individuals with upper limb loss in novel prosthetic control techniques," *Journal of NeuroEngineering and Rehabilitation*, vol. 12, no. 1, 2015.

[45] D. K. Blough *et al.*, "Prosthetic cost projections for servicemembers with major limb loss from vietnam and OIF/OEF," *The Journal of Rehabilitation Research and Development*, vol. 47, no. 4, pp. 387–402, 2010.

[46] G. McGimpsey and T. C. Bradford, "Limb Prosthetics Services and Devices; Critical Unmet Need: Market Analysis," Bioengineering Institute Center for Neuroprosthetics, Worcester Polytechnic Institution, Tech. Rep.

[47] I. Vujaklija and D. Farina, "3D printed upper limb prosthetics," *Expert Review of Medical Devices*, vol. 15, no. 7, pp. 505–512, 2018.

[48] Cybathlon, ETH Zürich. [Online]. Available: https://cybathlon.ethz.ch/

[49] C. Lake, "The Evolution of Upper Limb Prosthetic Socket Design," *Journal of Prosthetics and Orthotics*, vol. 20, no. 3, pp. 85–92, 2008.

[50] E. Biddiss, D. Beaton, and T. Chau, "Consumer design priorities for upper limb prosthetics," *Disability and Rehabilitation: Assistive Technology*, vol. 2, no. 6, pp. 346–357, 2007.

[51] C. Shallal *et al.*, "An Adaptive Socket Attaches onto Residual Limb Using Smart Polymers for Upper Limb Prosthesis," in *Proceedings of the IEEE 16th International Conference on Rehabilitation Robotics*, 2019.

[52] L. Paterno, M. Ibrahimi, E. Gruppioni, A. Menciassi, and L. Ricotti, "Sockets for Limb Prostheses: A Review of Existing Technologies and Open Challenges," *IEEE Transactions on Biomedical Engineering*, vol. 65, no. 9, pp. 1996–2010, 2018.

[53] D. Farina and S. Amsüss, "Reflections on the present and future of upper limb prostheses," *Expert Review of Medical Devices*, vol. 13, no. 4, pp. 321–324, 2016.

[54] Y. Sang, X. Li, Y. Gan, D. Su, and Y. Luo, "A novel socket design for upper-limb prosthesis," *International Journal of Applied Electromagnetics and Mechanics*, vol. 45, no. 1-4, pp. 881–886, 2014.

[55] S. Jönsson, K. Caine-Winterberger, and R. Brånemark, "Osseointegration amputation prostheses on the upper limbs: methods, prosthetics and rehabilitation," *Prosthetics and Orthotics International*, vol. 35, no. 2, pp. 190–200, 2011.

[56] K. Hagberg, E. Häggstrm, S. Jönsson, B. Rydevik, and R. Brånemark, "Osseoperception and Osseointegrated Prosthetic Limbs," in *Psychoprosthetics*, 2008, pp. 131–140.

[57] G. Lundborg, A. Waites, A. Björkman, B. Rosén, and E.-M. Larsson, "Functional magnetic resonance imaging shows cortical activation on sensory stimulation of an osseointegrated prosthetic thumb," *Scandinavian Journal of Plastic and Reconstructive Surgery and Hand Surgery*, vol. 40, no. 4, pp. 234–239, 2006.

[58] C. Antfolk *et al.*, "Sensory feedback in upper limb prosthetics," *Expert Review of Medical Devices*, vol. 10, no. 1, pp. 45–54, 2013.

[59] H. P. Saal and S. J. Bensmaia, "Biomimetic approaches to bionic touch through a peripheral nerve interface," *Neuropsychologia*, vol. 79, pp. 344–353, 2015.

[60] E. Battaglia *et al.*, "The Rice Haptic Rocker: Skin stretch haptic feedback with the Pisa/IIT SoftHand," in *Proceedings of the IEEE World Haptics Conference*, 2017.

[61] G. S. Dhillon and K. W. Horch, "Direct Neural Sensory Feedback and Control of a Prosthetic Arm," *IEEE Transactions on Neural Systems and Rehabilitation Engineering*, vol. 13, no. 4, pp. 468–472, 2005.

[62] M. Ortiz-Catalan, B. Hakansson, and R. Brånemark, "An osseointegrated human-machine gateway for long-term sensory feedback and motor control of artificial limbs," *Science Translational Medicine*, vol. 6, no. 257, 2014.

[63] S. Raspopovic *et al.*, "Restoring Natural Sensory Feedback in Real-Time Bidirectional Hand Prostheses," *Science Translational Medicine*, vol. 6, no. 222, 2014.

[64] F. M. Petrini *et al.*, "Sensory feedback restoration in leg amputees improves walking speed, metabolic cost and phantom pain," *Nature Medicine*, vol. 25, no. 9, pp. 1356–1363, 2019.

[65] B. Stephens-Fripp, G. Alici, and R. Mutlu, "A Review of Non-Invasive Sensory Feedback Methods for Transradial Prosthetic Hands," *IEEE Access*, vol. 6, pp. 6878–6899, 2018.

[66] C. Castellini *et al.*, "Proceedings of the first workshop on peripheral machine interfaces: Going beyond traditional surface electromyography," *Frontiers in Neurorobotics*, vol. 8, no. 22, pp. 1–17, 2014.

[67] A. D. Roche, H. Rehbaum, D. Farina, and O. C. Aszmann, "Prosthetic Myoelectric Control Strategies: A Clinical Perspective," *Current Surgery Reports*, vol. 2, no. 3, 2014.

[68] M. Markovic, M. A. Schweisfurth, L. F. Engels, D. Farina, and S. Došen, "Myocontrol is closed-loop control: incidental feedback is sufficient for scaling the prosthesis force in routine grasping," *Journal of NeuroEngineering and Rehabilitation*, vol. 15, no. 1, 2018.

[69] I. Saunders and S. Vijayakumar, "The role of feed-forward and feedback processes for closed-loop prosthesis control," *Journal of NeuroEngineering and Rehabilitation*, vol. 8, no. 1, p. 60, 2011.

[70] J. D. Brown *et al.*, "An exploration of grip force regulation with a low-impedance myoelectric prosthesis featuring referred haptic feedback," *Journal of NeuroEngineering and Rehabilitation*, vol. 12, no. 1, 2015.

[71] S. L. Carey, M. J. Highsmith, M. E. Maitland, and R. V. Dubey, "Compensatory movements of transradial prosthesis users during common tasks," *Clinical Biomechanics*, vol. 23, no. 9, pp. 1128–1135, 2008.

[72] C. R. Gambrell, "Overuse Syndrome and the Unilateral Upper Limb Amputee: Consequences and Prevention," *Journal of Prosthetics and Orthotics*, vol. 20, no. 3, pp. 126–132, 2008.

[73] A. Fougner, O. Stavdahl, P. J. Kyberd, Y. G. Losier, and P. A. Parker, "Control of Upper Limb Prostheses: Terminology and Proportional Myoelectric Control—A Review," *IEEE Transactions on Neural Systems and Rehabilitation Engineering*, vol. 20, no. 5, pp. 663–677, 2012.

[74] A. W. Shehata, E. J. Scheme, and J. W. Sensinger, "Evaluating Internal Model Strength and Performance of Myoelectric Prosthesis Control Strategies," *IEEE Transactions on Neural Systems and Rehabilitation Engineering*, vol. 26, no. 5, pp. 1046–1055, 2018.

[75] S. Mick, D. Cattaert, F. Paclet, P.-Y. Oudeyer, and A. de Rugy, "Performance and Usability of Various Robotic Arm Control Modes from Human Force Signals," *Frontiers in Neurorobotics*, vol. 11, 2017.

[76] A. Chadwell, L. Kenney, S. Thies, A. Galpin, and J. Head, "The Reality of Myoelectric Prostheses: Understanding What Makes These Devices Difficult for Some Users to Control," *Frontiers in Neurorobotics*, vol. 10, 2016.

[77] D. Farina *et al.*, "The Extraction of Neural Information from the Surface EMG for the Control of Upper-Limb Prostheses: Emerging Avenues and Challenges," *IEEE Transactions on Neural Systems and Rehabilitation Engineering*, vol. 22, no. 4, pp. 797–809, 2014.

[78] B. Popov, "The bio-electrically controller prosthesis," *Journal of Bone and Joint Surgery*, vol. 47, pp. 421–424, 1965.

[79] P. Parker, K. Englehart, and B. Hudgins, *Electromyography*, 2004, ch. Control of Powered Upper Limb Prosthesis.

[80] G. Li, *Advances in Applied Electromyography*, 2011, ch. Electromyography Pattern-Recognition-Based Control of Powered Multifunctional Upper-Limb Prostheses, pp. 99–116.

[81] M. A. Oskoei and H. Hu, "Myoelectric control systems—A survey," *Biomedical Signal Processing and Control*, vol. 2, no. 4, pp. 275–294, 2007.

[82] L. Vodovnik *et al.*, "Some topics on myoelectric control of orthotic-prosthetic systems," *Report no EDC 4-67-17, Case Western Reserve University*, 1967.

[83] G. N. Saridis and T. P. Gootee, "EMG Pattern Analysis and Classification for a Prosthetic Arm," *IEEE Transactions on Biomedical Engineering*, vol. 29, no. 6, pp. 403–412, 1982.

[84] R. W. Wirta, D. R. Taylor, and R. Finley, "Pattern-recognition arm prosthesis: a historical perspective-a final report," *Bulletin of Prosthetics Research*, vol. 10, no. 30, pp. 10–35, 1978.

[85] J. M. Hahne, M. A. Schweisfurth, M. Koppe, and D. Farina, "Simultaneous control of multiple functions of bionic hand prostheses: Performance and robustness in end users," *Science Robotics*, vol. 3, no. 19, 2018.

[86] S. Amsuess, P. Goebel, B. Graimann, and D. Farina, "A Multi-Class Proportional Myocontrol Algorithm for Upper Limb Prosthesis Control: Validation in Real-Life Scenarios on Amputees," *IEEE Transactions on Neural Systems and Rehabilitation Engineering*, vol. 23, no. 5, pp. 827–836, 2015.

[87] D. Blana, T. Kyriacou, J. M. Lambrecht, and E. K. Chadwick, "Feasibility of using combined EMG and kinematic signals for prosthesis control: A simulation study using a virtual reality environment," *Journal of Electromyography and Kinesiology*, vol. 29, pp. 21–27, 2016.

[88] T. Kuiken, G. Dumanian, R. Lipschutz, L. Miller, and K. Stubblefield, "The use of targeted muscle reinnervation for improved myoelectric prosthesis control in a bilateral shoulder disarticulation amputee," *Prosthetics and Orthotics International*, vol. 28, pp. 245–253, 2004.

[89] P. Zhou *et al.*, "Decoding a New Neural-Machine Interface for Control of Artificial Limbs," *Journal of Neurophysiology*, vol. 98, no. 5, pp. 2974–2982, 2007.

[90] C. W. Antuvan and L. Masia, "An LDA-Based Approach for Real-Time Simultaneous Classification of Movements Using Surface Electromyography," *IEEE Transactions on Neural Systems and Rehabilitation Engineering*, vol. 27, no. 3, pp. 552–561, 2019.

[91] X. Yang, J. Yan, Y. Fang, D. Zhou, and H. Liu, "Simultaneous Prediction of Wrist/Hand Motion via Wearable Ultrasound Sensing," *IEEE Transactions on Neural Systems and Rehabilitation Engineering*, vol. 28, no. 4, pp. 970–977, 2020.

[92] P. Herberts, C. Almström, R. Kadefors, and P. D. Lawrence, "Hand Prosthesis Control Via Myoelectric Patterns," *Acta Orthopaedica Scandinavica*, vol. 44, no. 4-5, pp. 389–409, 1973.

[93] CoApt engineering, CoApt GEN2. [Online]. Available: https://coaptgen2.com/

[94] N. Jiang, S. Došen, K.-R. Müller, and D. Farina, "Myoelectric Control of Artificial Limbs: Is There a Need to Change Focus?" *IEEE Signal Processing Magazine*, vol. 29, no. 5, pp. 150–152, 2012.

[95] I. Kyranou, S. Vijayakumar, and M. S. Erden, "Causes of Performance Degradation in Non-invasive Electromyographic Pattern Recognition in Upper Limb Prostheses," *Frontiers in Neurorobotics*, vol. 12, 2018.

[96] A. Ameri, M. A. Akhaee, E. Scheme, and K. Englehart, "A Deep Transfer Learning Approach to Reducing the Effect of Electrode Shift in EMG Pattern Recognition-Based Control," *IEEE Transactions on Neural Systems and Rehabilitation Engineering*, vol. 28, no. 2, pp. 370–379, 2019.

[97] J. L. Betthauser *et al.*, "Limb Position Tolerant Pattern Recognition for Myoelectric Prosthesis Control with Adaptive Sparse Representations From Extreme Learning," *IEEE Transactions on Biomedical Engineering*, vol. 65, no. 4, pp. 770–778, 2018.

[98] P. M. Pilarski *et al.*, "Online Human Training of a Myoelectric Prosthesis Controller via Actor-Critic Reinforcement Learning," in *Proceedings of the IEEE International Conference on Rehabilitation Robotics*, 2011.

[99] M. A. Toosi, A. Maleki, and A. Fallah, "Estimation and anticipation of elbow joint angle from shoulder data during planar movements," in *Proceedings of the 2nd International Conference on Control, Instrumentation and Automation*, 2011.

[100] A. Krasoulis, I. Kyranou, M. S. Erden, K. Nazarpour, and S. Vijayakumar, "Improved prosthetic hand control with concurrent use of myoelectric and inertial measurements," *Journal of NeuroEngineering and Rehabilitation*, vol. 14, no. 1, 2017.

[101] A. Krasoulis, S. Vijayakumar, and K. Nazarpour, "Multi-Grip Classification-Based Prosthesis Control With Two EMG-IMU Sensors," *IEEE Transactions on Neural Systems and Rehabilitation Engineering*, vol. 28, no. 2, pp. 508–518, 2020.

[102] A. A. Adewuyi, L. J. Hargrove, and T. A. Kuiken, "Resolving the effect of wrist position on myoelectric pattern recognition control," *Journal of NeuroEngineering and Rehabilitation*, vol. 14, no. 1, 2017.

[103] A. Akhtar, N. Aghasadeghi, L. Hargrove, and T. Bretl, "Estimation of distal arm joint angles from EMG and shoulder orientation for transhumeral prostheses," *Journal of Electromyography and Kinesiology*, vol. 35, pp. 86–94, 2017.

[104] A. Gigli, V. Gregori, M. Cognolato, M. Atzori, and A. Gijsberts, "Visual Cues to Improve Myoelectric Control of Upper Limb Prostheses," in *Proceedings of the 7th IEEE International Conference on Biomedical Robotics and Biomechatronics*, 2018.

[105] X. Li *et al.*, "A motion-classification strategy based on sEMG-EEG signal combination for upper-limb amputees," *Journal of NeuroEngineering and Rehabilitation*, vol. 14, no. 1, 2017.

[106] D. G. K. Madusanka, L. N. S. Wijayasingha, R. A. R. C. Gopura, Y. W. R. Amarasinghe, and G. K. I. Mann, "A review on hybrid myoelectric control systems for upper limb prosthesis," in *Proceedings of the Moratuwa Engineering Research Conference*, 2015.

[107] S. Salminger *et al.*, "Long-term implant of intramuscular sensors and nerve transfers for wireless control of robotic arms in above-elbow amputees," *Science Robotics*, vol. 4, no. 32, 2019.

[108] L. Kenney, I. Lisitsa, P. Bowker, G. Heath, and D. Howard, "Dimensional change in muscle as a control signal for powered upper limb prostheses: a pilot study," *Medical Engineering and Physics*, vol. 21, no. 8, pp. 589–597, 1999.

[109] R. Abboudi, C. Glass, N. Newby, J. Flint, and W. Craelius, "A biomimetic controller for a multifinger prosthesis," *IEEE Transactions on Rehabilitation Engineering*, vol. 7, no. 2, pp. 121–129, 1999.

[110] G. Heath and P. Bowker, "Myokinemetric control of a prosthetic prehensor from residual forearm musculature," in *Proceedings of the International Conference on Informatics and Control*, 1997, pp. 866–870.

[111] N. Li, D. Yang, L. Jiang, H. Liu, and H. Cai, "Combined use of FSR sensorarray and svm classifier for finger motion recognition based on pressure distribution map," *Journal of Bionic Engineering*, vol. 1, no. 9, pp. 39–47, 2012.

[112] E. Cho *et al.*, "Force myography to control robotic upper extremity prostheses: a feasibility study," *Frontiers in Bioengineering and Biotechnology*, 2016.

[113] V. Ravindra and C. Castellini, "A Comparative Analysis of Three Non-Invasive Human-Machine Interfaces for the Disabled," *Frontiers in Neurorobotics*, vol. 8, 2014.

[114] J. Silva, T. Chau, and A. Goldenberg, "MMG-based multisensor data fusion for prosthesis control," in *Proceedings of the 25th Annual International Conference of the IEEE Engineering in Medicine and Biology Society*, 2003.

[115] C. Orizio, *Electromyography*, 2004, ch. Surface Mechanomyogram.

[116] Z. F. Yang, D. Kumar, and S. Arjunan, "Mechanomyogram for identifying muscle activity and fatigue," in *Proceedings of the Annual International Conference of the IEEE Engineering in Medicine and Biology Society*, 2009.

[117] O. S. Alkhafaf, M. K. Wali, and A. H. Al-Timemy, "Improved Prosthetic Hand Control with Synchronous Use of Voice Recognition and Inertial Measurements," *IOP Conference Series: Materials Science and Engineering*, vol. 745, 2020.

[118] M. Velliste, S. Perel, M. C. Spalding, A. S. Whitford, and A. B. Schwartz, "Cortical control of a prosthetic arm for self-feeding," *Nature*, vol. 453, no. 7198, pp. 1098–1101, 2008.

[119] H. Kim *et al.*, "Continuous Shared Control for Stabilizing Reaching and Grasping With Brain-Machine Interfaces," *IEEE Transactions on Biomedical Engineering*, vol. 53, no. 6, pp. 1164–1173, 2006.

[120] J. Wessberg *et al.*, "Real-time prediction of hand trajectory by ensembles of cortical neurons in primates," *Nature*, vol. 408, pp. 361–365, 2000.

[121] B. Mahmoudi, E. A. Pohlmeyer, N. W. Prins, S. Geng, and J. C. Sanchez, "Towards autonomous neuroprosthetic control using hebbian reinforcement learning," *Journal of Neural Engineering*, vol. 10, no. 6, 2013.

[122] D. P. McMullen *et al.*, "Demonstration of a Semi-Autonomous Hybrid Brain–Machine Interface Using Human Intracranial EEG, Eye Tracking, and Computer Vision to Control a Robotic Upper Limb Prosthetic," *IEEE Transactions on Neural Systems and Rehabilitation Engineering*, vol. 22, no. 4, pp. 784–796, 2014.

[123] K. R. Lyons and S. S. Joshi, "Upper Limb Prosthesis Control for High-Level Amputees via Myoelectric Recognition of Leg Gestures," *IEEE Transactions on Neural Systems and Rehabilitation Engineering*, vol. 26, no. 5, pp. 1056–1066, 2018.

[124] A. Jackowski, M. Gebhard, and R. Thietje, "Head Motion and Head Gesture-Based Robot Control: A Usability Study," *IEEE Transactions on Neural Systems and Rehabilitation Engineering*, vol. 26, no. 1, pp. 161–170, 2018.

[125] D. Reinkensmeyer, O. Akoner, D. Ferris, and K. Gordon, "Slacking by the human motor system: Computational models and implications for robotic orthoses," in *Proceedings of the Annual International Conference of the IEEE Engineering in Medicine and Biology Society*, 2009.

[126] M. Merad *et al.*, "Assessment of an Automatic Prosthetic Elbow Control Strategy Using Residual Limb Motion for Transhumeral Amputated Individuals With Socket or Osseointegrated Prostheses," *IEEE Transactions on Medical Robotics and Bionics*, vol. 2, no. 1, pp. 38–49, 2020.

[127] A. J. Metzger, A. W. Dromerick, R. J. Holley, and P. S. Lum, "Characterization of Compensatory Trunk Movements During Prosthetic Upper Limb Reaching Tasks," *Archives of Physical Medicine and Rehabilitation*, vol. 93, no. 11, pp. 2029–2034, 2012.

[128] M. Gardner, R. Woodward, R. Vaidyanathan, E. Burdet, and B. C. Khoo, "An unobtrusive vision system to reduce the cognitive burden of hand prosthesis control," in *Proceedings of the 13th International Conference on Control Automation Robotics and Vision*, 2014.

[129] G. Ghazaei, A. Alameer, P. Degenaar, G. Morgan, and K. Nazarpour, "Deep learning-based artificial vision for grasp classification in myoelectric hands," *Journal of Neural Engineering*, vol. 14, no. 3, 2017.

[130] F. Ficuciello, A. Migliozzi, G. Laudante, P. Falco, and B. Siciliano, "Vision-based grasp learning of an anthropomorphic hand-arm system in a synergy-based control framework," *Science Robotics*, vol. 4, no. 26, 2019.

[131] M. Markovic, S. Došen, D. Popović, B. Graimann, and D. Farina, "Sensor fusion and computer vision for context-aware control of a multi degree-of-freedom prosthesis," *Journal of Neural Engineering*, vol. 12, no. 6, 2015.

[132] D. G. K. Madusanka, R. A. R. C. Gopura, Y. W. R. Amarasinghe, and G. K. I. Mann, "Hybrid Vision Based Reach-to-Grasp Task Planning Method for Trans-Humeral Prostheses," *IEEE Access*, vol. 5, pp. 16 149–16 161, 2017.

[133] S. Došen and D. B. Popović, "Transradial Prosthesis: Artificial Vision for Control of Prehension," *Artificial Organs*, vol. 35, no. 1, pp. 37–48, 2010.

[134] M. R. Maymo, A. Shafti, and A. A. Faisal, "Fast orient: lightweight computer vision for wrist control in assistive robotic grasping," in *Proceedings of the 7th IEEE International Conference on Biomedical Robotics and Biomechatronics*, 2018.

[135] A. Kar and P. Corcoran, "Towards the development of a standardized performance evaluation framework for eye gaze estimation systems in consumer platforms," in *Proceedings of the IEEE International Conference on Systems, Man, and Cybernetics*, 2016.

[136] D. Whitney, "Resolved Motion Rate Control of Manipulators and Human Prostheses," *IEEE Transactions on Man-Machine systems*, vol. 10, no. 2, pp. 47–53, 1969.

[137] A. Davalli and R. Sacchetti, "Mini joystick for upper limb prosthesis," in *Proceedings of the MyoElectric Controls/Powered Prosthetics Symposium*, 2002.

[138] R. D. Lipschutz, B. Lock, J. Sensinger, A. E. Schultz, and T. A. Kuiken, "Use of a Two-Axis Joystick for Control of Externally Powered, Shoulder Disarticulation Prostheses," *Journal of rehabilitation research and development*, vol. 48, no. 6, pp. 661–667, 2011.

[139] R. O. Maimon-Mor *et al.*, "Towards free 3D end-point control for robotic-assisted human reaching using binocular eye tracking," in *Proceedings of the International Conference on Rehabilitation Robotics*, 2017.

[140] I. Boni, J. Millenaar, M. Controzzi, and M. Ortiz-Catalan, "Restoring Natural Forearm Rotation in Transradial Osseointegrated Amputees," *IEEE Transactions on Neural Systems and Rehabilitation Engineering*, vol. 26, no. 12, pp. 2333–2341, 2018.

[141] G. Li and T. Kuiken, "Modeling of Prosthetic Limb Rotation Control by Sensing Rotation of Residual Arm Bone," *IEEE Transactions on Biomedical Engineering*, vol. 55, no. 9, pp. 2134–2142, 2008.

[142] Z. Li, K. Gray, J. R. Roldan, D. Milutinovi, and J. Rosen, "The joint coordination in reach-to-grasp movements," in *Proceedings of the IEEE/RSJ International Conference on Intelligent Robots and Systems*, 2014.

[143] J. Soechting and F. Lacquaniti, "Invariant characteristics of a pointing movement in man," *The Journal of Neuroscience*, vol. 1, no. 7, pp. 710–720, 1981.

[144] F. Lacquaniti and J. Soechting, "Coordination of arm and wrist motion during a reaching task," *The Journal of Neuroscience*, vol. 2, no. 4, pp. 399–408, 1982.

[145] T. Bockemühl, N. F. Troje, and V. Dürr, "Inter-joint coupling and joint angle synergies of human catching movements," *Human Movement Science*, vol. 29, no. 1, pp. 73–93, 2010.

[146] D. Popović, M. Popović, and T. Sinkjaer, "Life-like Control for Neural Prostheses: "Proximal Controls Distal"," in *Proceedings of the IEEE Engineering in Medicine and Biology 27th Annual Conference*, 2005.

[147] F. Lacquaniti, J. Soechting, and C. Terzuolo, "Some factors pertinent to the organization and control of arm movements," *Brain Research*, vol. 252, no. 2, pp. 394–397, 1982.

[148] M. Merad, E. de Montalivet, A. Roby-Brami, and N. Jarrassé, "Intuitive prosthetic control using upper limb inter-joint coordinations and imu-based shoulder angles measurement : a pilot study," in *Proceedings of the IEEE/RSJ International Conference on Intelligent Robots and Systems*, 2016.

[149] N. A. Alshammary, D. A. Bennett, and M. Goldfarb, "Synergistic Elbow Control for a Myoelectric Transhumeral Prosthesis," *IEEE Transactions on Neural Systems and Rehabilitation Engineering*, vol. 26, no. 2, pp. 468–476, 2017.

[150] D. A. Bennett and M. Goldfarb, "IMU-Based Wrist Rotation Control of a Transradial Myoelectric Prosthesis," *IEEE Transactions on Neural Systems and Rehabilitation Engineering*, vol. 26, no. 2, pp. 419–427, 2016.

[151] R. Kaliki, R. Davoodi, and G. Loeb, "Prediction of Distal Arm Posture in 3-D Space From Shoulder Movements for Control of Upper Limb Prostheses," *Proceedings of the IEEE*, vol. 96, no. 7, pp. 1217–1225, 2008.

[152] R. R. Kaliki, R. Davoodi, and G. E. Loeb, "Prediction of elbow trajectory from shoulder angles using neural networks," *International Journal of Computational Intelligence and Applications*, vol. 7, no. 3, pp. 333–349, 2008.

[153] S. D. Iftime, L. L. Egsgaard, and M. B. Popović, "Automatic determination of synergies by radial basis function artificial neural networks for the control of a neural prosthesis," *IEEE Transactions on Neural Systems and Rehabilitation Engineering*, vol. 13, no. 4, pp. 482–489, 2005.

[154] M. Merad, "Investigations on upper limb prosthesis control with an active elbow," Ph.D. dissertation, Sorbonne University, 2017.

[155] M. Merad *et al.*, "Can We Achieve Intuitive Prosthetic Elbow Control Based on Healthy Upper Limb Motor Strategies?" *Frontiers in Neurorobotics*, vol. 12, 2018.

[156] R. L. Sainburg and D. Kalakanis, "Differences in Control of Limb Dynamics During Dominant and Nondominant Arm Reaching," *Journal of Neurophysiology*, vol. 83, no. 5, pp. 2661–2675, 2000.

[157] J. E. Schaffer and R. L. Sainburg, "Interlimb differences in coordination of unsupported reaching movements," *Neuroscience*, vol. 350, pp. 54–64, 2017.

[158] R. Garcia-Rosas, Y. Tan, D. Oetomo, and C. Manzie, "On-line Synergy Identification for Personalized Active Arm Prosthesis: a Feasibility Study," in *Proceedings of the Annual American Control Conference*, 2018.

[159] R. Garcia-Rosas, Y. Tan, D. Oetomo, C. Manzie, and P. Choong, "Personalized Online Adaptation of Kinematic Synergies for Human-Prosthesis Interfaces," *IEEE Transactions on Cybernetics*, pp. 1–15, 2019.

[160] F. Stulp and O. Sigaud, "Many Regression Algorithms, One Unified Model – A Review," *Neural Networks*, vol. 69, pp. 60–79, 2015.

[161] M. Farokhzadi, A. Maleki, A. Fallah, and S. Rashidi, "Online Estimation of Elbow Joint Angle Using Upper Arm Acceleration: A Movement Partitioning Approach," *Journal of Biomedical Physics and Engineering*, vol. 7, pp. 305–314, 2016.

[162] L. Cenciotti, S. Micera, M. Carrozza, P. Dario, and M. Popović, "A hybrid system for the prediction of upper arm articular synergies using statistical and soft-computing techniques," in *Proceedings of the Sixth Annual IFESS*, 2001, pp. 235–255.

[163] J. Friedman, T. Hastie, and R. Tibshirani, *The elements of statistical learning*, 2nd ed., 2008.

[164] S. J. Preece *et al.*, "Activity identification using body-mounted sensors—a review of classification techniques," *Physiological Measurement*, vol. 30, no. 4, 2009.

[165] M. S. Totty and E. Wade, "Muscle Activation and Inertial Motion Data for Non-Invasive Classification of Activities of Daily Living," *IEEE Transactions on Biomedical Engineering*, vol. 65, no. 5, pp. 1069–1076, 2018.

[166] A. Bulling, U. Blanke, and B. Schiele, "A tutorial on human activity recognition using body-worn inertial sensors," *ACM Computing Surveys*, vol. 46, no. 3, pp. 1–33, 2014.

[167] M. C. Cirstea and M. F. Levin, "Compensatory strategies for reaching in stroke," *Brain*, vol. 123, no. 5, pp. 940–953, 2000.

[168] M. Casadio *et al.*, "Functional reorganization of upper-body movement after spinal cord injury," *Experimental Brain Research*, vol. 207, no. 3-4, pp. 233–247, 2010.

[169] K. L. Kontson, I. P. Marcus, B. M. Myklebust, and E. F. Civillico, "An Integrated Movement Analysis Framework to Study Upper Limb Function: A Pilot Study," *IEEE Transactions on Neural Systems and Rehabilitation Engineering*, vol. 25, no. 10, pp. 1874–1883, 2017.

[170] M. Deijs, R. Bongers, N. R. van Leusen, and C. K. van der Sluis, "Flexible and static wrist units in upper limb prosthesis users: functionality scores, user satisfaction and compensatory movements," *Journal of NeuroEngineering and Rehabilitation*, vol. 13, no. 1, 2016.

[171] A. Hussaini, A. Zinck, and P. Kyberd, "Categorization of compensatory motions in transradial myoelectric prosthesis users," *Prosthetics and Orthotics International*, vol. 41, no. 3, pp. 286–293, 2016.

[172] F. Montagnani, M. Controzzi, and C. Cipriani, "Exploiting arm posture synergies in activities of daily living to control the wrist rotation in upper limb prostheses: A feasibility study," in *Proceedings of the 37th Annual International Conference of the IEEE Engineering in Medicine and Biology Society*, 2015.

[173] A. Mengarelli *et al.*, "Validity of the Nintendo Wii Balance Board for the Assessment of Balance Measures in the Functional Reach Test," *IEEE Transactions on Neural Systems and Rehabilitation Engineering*, vol. 26, no. 7, pp. 1400–1406, 2018.

[174] H. Abdi and P. Molin, "Lilliefors/Van Soests test of normality," *Encyclopedia of measurement and statistics*, pp. 540–544, 2007.

[175] V. Bewick, L. Cheek, and J. Ball, "Statistics review 10: Further nonparametric methods," *Critical Care*, vol. 8, no. 3, p. 196, 2004.

[176] S. Oyama *et al.*, "Biomechanical Reconstruction Using the Tacit Learning System: Intuitive Control of Prosthetic Hand Rotation," *Frontiers in Neurorobotics*, vol. 10, 2016.

[177] M. Legrand, N. Jarrassé, F. Richer, and G. Morel, "A closed-loop and ergonomic control for prosthetic wrist rotation," in *Proceedings of the IEEE International Conference on Robotics and Automation*, 2020.

[178] *Race Task Description Cybathlon 2020*, ETH Zürich, 2020.

[179] J. Ho, T. Tumkaya, S. Aryal, H. Choi, and A. Claridge-Chang, "Moving beyond P values: data analysis with estimation graphics," *Nature Methods*, vol. 16, no. 7, pp. 565–566, 2019.

[180] T. J. Sejnowski, "Making smooth moves," *Nature*, vol. 394, no. 6695, pp. 725–726, 1998.

[181] J. Cowley, L. Resnik, J. Wilken, L. S. Walters, and D. Gates, "Movement quality of conventional prostheses and the DEKA arm during everyday tasks," *Prosthetics and Orthotics International*, vol. 41, no. 1, pp. 33–40, 2016.

[182] S. Balasubramanian, A. Melendez-Calderon, and E. Burdet, "A Robust and Sensitive Metric for Quantifying Movement Smoothness," *IEEE Transactions on Biomedical Engineering*, vol. 59, no. 8, pp. 2126–2136, 2012.

[183] M. Legrand *et al.*, "Controlling upper-limb prostheses with body compensations," in *Proceedings of the 5th International Symposium on Wearable Robotics*, 2020.

[184] A. Hussaini and P. Kyberd, "Refined clothespin relocation test and assessment of motion," *Prosthetics and Orthotics International*, vol. 41, no. 3, pp. 294–302, 2016.

[185] A. Hussaini, W. Hill, and P. Kyberd, "Clinical evaluation of the refined clothespin relocation test: A pilot study," *Prosthetics and Orthotics International*, vol. 43, no. 5, pp. 485–491, 2019.

[186] S. Balasubramanian, A. Melendez-Calderon, A. Roby-Brami, and E. Burdet, "On the analysis of movement smoothness," *Journal of NeuroEngineering and Rehabilitation*, vol. 12, no. 1, 2015.

[187] D. Kee and W. Karwowski, "LUBA: An assessment technique for postural loading on the upper body based on joint motion discomfort and maximum holding time," *Applied Ergonomics*, vol. 32, pp. 357–366, 2001.

[188] L. Herda, P. Fua, R. Plänkers, R. Boulic, and D. Thalmann, "Using skeleton-based tracking to increase the reliability of optical motion capture," *Human Movement Science*, vol. 20, no. 3, pp. 313–341, 2001.

[189] J. Meyer, M. Kuderer, J. Muller, and W. Burgard, "Online marker labeling for fully automatic skeleton tracking in optical motion capture," in *Proceedings of the IEEE International Conference on Robotics and Automation (ICRA)*, 2014.

[190] J. C. Perry, J. Rosen, and S. Burns, "Upper-Limb Powered Exoskeleton Design," *IEEE/ASME Transactions on Mechatronics*, vol. 12, no. 4, pp. 408–417, 2007.

[191] M. Legrand, N. Jarrassé, E. de Montalivet, F. Richer, and G. Morel, "Closing the loop between body compensations and upper-limb prosthetic movements: a feasibility study," *IEEE Transactions on Medical Robotics and Bionics*, 2020.

[192] S. Hignett and L. McAtamney, "Rapid Entire Body Assessment (REBA)," *Applied Ergonomics*, vol. 31, no. 2, pp. 201–205, 2000.

[193] R. M. Williams *et al.*, "Does Having a Computerized Prosthetic Knee Influence Cognitive Performance During Amputee Walking?" *Archives of Physical Medicine and Rehabilitation*, vol. 87, no. 7, pp. 989–994, 2006.

[194] S. G. Hart, "Nasa-Task Load Index (NASA-TLX); 20 Years Later," *Proceedings of the Human Factors and Ergonomics Society Annual Meeting*, vol. 50, no. 9, pp. 904–908, 2006.

[195] S. Said *et al.*, "Validation of the Raw National Aeronautics and Space Administration Task Load Index (NASA-TLX) Questionnaire to Assess Perceived Workload in Patient Monitoring Tasks: Pooled Analysis Study Using Mixed Models," *Journal of Medical Internet Research*, 2020.

[196] J. V. V. Parr, "Evaluating and alleviating the cognitive burden associated with myoelectric prosthetic hand control," Ph.D. dissertation, Liverpool Hope University, 2018.

[197] S. Deeny, C. Chicoine, L. Hargrove, T. Parrish, and A. Jayaraman, "A simple ERP method for quantitative analysis of cognitive workload in myoelectric prosthesis control and human-machine interaction," *PloS one*, vol. 9, no. 11, 2014.

[198] S. Cai, G. Li, S. Huang, H. Zheng, and L. Xie, "Automatic Detection of Compensatory Movement Patterns by a Pressure Distribution Mattress Using Machine Learning Methods: A Pilot Study," *IEEE Access*, vol. 7, pp. 80 300–80 309, 2019.

[199] A. Poignant, M. Legrand, N. Jarrassé, and G. Morel, "Computing the positioning error of an upper-arm robotic prosthesis from the observation of its wearers posture," *submitted to IEEE International Conference on Robotics and Automation*, 2020.

[200] L. McAtamney and E. N. Corlett, "RULA: a survey method for the investigation of work-related upper limb disorders," *Applied Ergonomics*, vol. 24, no. 2, pp. 91–99, 1993.

[201] M. Sierotowicz, M. Connan, and C. Castellini, "Human-In-The-Loop Assessment of an Ultralight, Low-Cost Body Posture Tracking Device," *Sensors*, vol. 20, no. 3, p. 890, 2020.

[202] I. H. Lopez-Nava and A. Munoz-Melendez, "Wearable Inertial Sensors for Human Motion Analysis: A Review," *IEEE Sensors Journal*, vol. 16, no. 22, pp. 7821–7834, 2016.

[203] A. Filippeschi *et al.*, "Survey of Motion Tracking Methods Based on Inertial Sensors: A Focus on Upper Limb Human Motion," *Sensors*, vol. 17, no. 6, p. 1257, 2017.

[204] A. G. Cutti, A. Giovanardi, L. Rocchi, A. Davalli, and R. Sacchetti, "Ambulatory measurement of shoulder and elbow kinematics through inertial and magnetic sensors," *Medical and Biological Engineering and Computing*, vol. 46, no. 2, pp. 169–178, 2007.

[205] L. Peppoloni, A. Filippeschi, E. Ruffaldi, and C. A. Avizzano, "A novel 7 degrees of freedom model for upper limb kinematic reconstruction based on wearable sensors," in *Proceedings of the 11th IEEE International Symposium on Intelligent Systems and Informatics*, 2013.

[206] P. Muller, M.-A. Begin, T. Schauer, and T. Seel, "Alignment-Free, Self-Calibrating Elbow Angles Measurement Using Inertial Sensors," *IEEE Journal of Biomedical and Health Informatics*, vol. 21, no. 2, pp. 312–319, 2017.

[207] M. Stoppa and A. Chiolerio, "Wearable Electronics and Smart Textiles: A Critical Review," *Sensors*, vol. 14, no. 7, pp. 11 957–11 992, 2014.

[208] S. Messier, D. Bourbonnais, J. Desrosiers, and Y. Roy, "Kinematic Analysis of Upper Limbs and Trunk Movement During Bilateral Movement After Stroke," *Archives of Physical Medicine and Rehabilitation*, vol. 87, no. 11, pp. 1463–1470, 2006.

[209] S. M. Michaelsen, S. Jacobs, A. Roby-Brami, and M. Levin, "Compensation for distal impairments of grasping in adults with hemiparesis," *Experimental Brain Research*, vol. 157, no. 2, 2004.

[210] Y. X. Zhi *et al.*, "Automatic Detection of Compensation During Robotic Stroke Rehabilitation Therapy," *IEEE Journal of Translational Engineering in Health and Medicine*, vol. 6, pp. 1–7, 2018.

[211] N. Nordin, S. Xie, and B. Wünsche, "Assessment of movement quality in robot- assisted upper limb rehabilitation after stroke: a review," *Journal of NeuroEngineering and Rehabilitation*, vol. 11, no. 1, p. 137, 2014.

[212] R. L. Harvey *et al.*, *Stroke recovery and rehabilitation*, 2008.

[213] J. S. Moore and A. Garg, "The Strain Index: A Proposed Method to Analyze Jobs For Risk of Distal Upper Extremity Disorders," *American Industrial Hygiene Association Journal*, vol. 56, no. 5, pp. 443–458, 1995.

[214] A. Shafti *et al.*, "Real-time Robot-assisted Ergonomics," in *Proceedings of the IEEE International Conference on Robotics and Automation*, 2019.

[215] L. Peternel, W. Kim, J. Babic, and A. Ajoudani, "Towards ergonomic control of human-robot co-manipulation and handover," in *Proceedings of the 17th IEEE-RAS International Conference on Humanoid Robotics*, 2017.

[216] A. M. Zanchettin, E. Lotano, and P. Rocco, "Collaborative Robot Assistant for the Ergonomic Manipulation of Cumbersome Objects," in *Proceedings of the IEEE/RSJ International Conference on Intelligent Robots and Systems*, 2019.

[217] Jaco assistive robotic arm, from Kinova. [Online]. Available: https://www.kinovarobotics.com/en/products/assistive-technologies/kinova-jaco-assistive-robotic-arm

[218] C. M. Bishop, *Pattern Recognition and Machine Learning*, 2006.

Mathilde Legrand – Thèse de doctorat – 2021

Titre: Contrôle de prothèses de bras à partir des mouvements de compensation de l'utilisateur

Mots clés: Contrôle de prothèses, Mouvements de compensation, Interaction Physique Homme-Robot

Résumé: Les récents progrès de la mécatronique pour les prothèses de bras ont permis divers avancées, comme un plus grand nombre de degrés de liberté contrôlables ou un meilleur système de fixation de la prothèse au corps de la personne via lostéointégration. Assurer un contrôle naturel et efficace de ces dispositifs de pointe reste néanmoins un défi majeur.
Les approches actuelles présentent toutes des limites qui conduisent souvent les porteurs de prothèse à abandonner la dimension active de lappareil. Ils vont lutiliser comme un outil rigide et réaliser la tche avec des mouvements compensatoires. Pour éviter cela, nous proposons dutiliser ces mouvements comme un signal derreur pour contrôler la prothèse. Lhumain est alors responsable de la réalisation de la tche pendant que la prothèse est responsable de la posture de son porteur.
Cette proposition est implémentée pour contrôler un poignet et un coude, individuellement puis simultanément. Les expériences confirment que lutilisation des mouvements compensatoires en entrée du contrôleur prothétique ne les accrot pas. Elles montrent aussi la facilité de la prise en main, la polyvalence et la scalabilité du mode de contrôle proposé. Une étude théorique complète ce travail et analyse en détails le couplage homme-robot ainsi créé. Les résultats obtenus ouvrent dintéressantes perspectives pour un contrôle intuitif de prothèse.

Title: Upper limb prostheses control based on user's body compensations

Keywords: Prostheses control, Body compensations, Physical Human-Robot Interaction

Abstract: In recent years, the development of advanced mechatronics for upper-limb prostheses has led to technological improvements such as a better fixation system to the body with osseointegration or a larger number of degrees of freedom. However, providing these devices with a natural and efficient control is still a major challenge.
Current approaches, such as myoelectric control, all show limitations, that can lead prosthetic users to abandon the active dimension of the device, use it as a rigid tool and perform the desired task with body compensations. To avoid such a behavior, we propose in this PhD thesis to employ body compensatory motions as an error signal to control the prosthetic device. With this concept, the human subject is in charge of the end-effector task, while the prosthesis is in charge of its users posture.
This proposition is implemented and tested to control prosthetic wrist and elbow joints, first individually and then simultaneously. A theoretical study completes this work and analyzes in details the human-robot coupling created. The presented experiments first confirm that using body compensations as controller input does not enhance them. They then show the easy learning of the control scheme by naive subjects, its task-versatility and its scalability. The foundations thus laid open exciting perspectives for a natural prosthesis control.